Preparation and Characterization of $BiFeO_3$ Films by Using Magnetic-Field-Assisted Pulsed Laser Deposition

JungMin Park

MARCH 2013

Preparation and Characterization of $BiFeO_3$ Films by Using Magnetic-Field-Assisted Pulsed Laser Deposition

A dissertation submitted to
THE GRADUATE SCHOOL OF ENGINEERING SCIENCE
OSAKA UNIVERSITY
in partial fulfillment of the requirements for the degree of
DOCTOR OF PHILOSOPHY IN ENGINEERING

BY

JungMin Park

MARCH 2013

ABSTRACT

Bismuth ferrite ($BiFeO_3$) exhibits both ferroelectric and anti-ferromagnetic orderings at room temperature (RT). In particular, polycrystalline $BiFeO_3$ films have attracted a lot of attention, because they have large polarization values and environment-friendly materials which can replace Pb-based materials. In order to prepare polycrystalline $BiFeO_3$ films, various deposition methods have been used, such as pulsed laser deposition (PLD), chemical solution deposition (CSD), and sputtering. So far, the research has focused on polycrystalline $BiFeO_3$ films less than 600 nm which can be used in memory devices. On the other hand, thick polycrystalline $BiFeO_3$ films above or near 2.0 μm are required for a wide range of practical applications such as actuators and sensors. However, little or no study has been conducted concerning thick polycrystalline $BiFeO_3$ films, and the understanding of their characteristics is insufficient. The obstacle for the preparation of thick films is the significant loss of Bi and Bi_2O_3 during the preparation of $BiFeO_3$ films, and the cracking arising from the mismatch of thermal stresses between the film and the substrate.

In this study, the preparation and the characterization of polycrystalline thick $BiFeO_3$ films and epitaxial $BiFeO_3$ films have been performed using the magnetic-field-assisted pulsed laser deposition.

Firstly, the behavior of the plume and the evolution of microstructures under a magnetic field have been investigated through a simulation. The trajectory of the plume under a magnetic field was modified and confined to the substrate, as opposed to that without a magnetic field. Under the modified trajectory of the plume, the flux of the evaporated species became conical and as a result, the formation of dynamical microstructures such as columnar structures was predicted.

Secondly, in experiments, polycrystalline $BiFeO_3$ films on $Pt/TiO_2/SiO_2/Si$ substrate were prepared using magnetic-field-assisted pulsed laser deposition. The film thickness and

the deposition rate depended on the magnetic field. The polycrystalline $BiFeO_3$ films prepared under a magnetic field showed significant difference, displaying columnar structures and changes in the orientation. 1.8 μm-thick $BiFeO_3$ films with columnar structure were successfully obtained for a magnetic field of 0.4 T and a deposition time of 30 min. For thick $BiFeO_3$ films with columnar structure, the polarization value (P_r) and the coercive field (E_c) were 62 $\mu C/cm^2$ and 198 kV/cm at 20 kHz and room temperature (RT), respectively. The piezoelectric coefficient (d_{33}) was ~ 50 pm/V. In addition, polycrystalline $BiFeO_3$ films were prepared by 90° off-axis deposition under a magnetic field. Droplets-free polycrystalline $BiFeO_3$ films were successfully obtained, because the charge species were deflected towards the substrate by Lorenz force, whereas the neutral species and large particles do not affected by the magnetic field.

Finally, epitaxial $BiFeO_3$ films on a La-doped $SrTiO_3$ (001) substrate were prepared successfully by controlling the magnetic field. The epitaxial $BiFeO_3$ films prepared under magnetic fields of 0 T, 0.1 T and 0.4 T showed a rhomhedral structure including two spots, (103) and (-103) with stress-relaxation. The increase in the magnetic field caused a high deposition rate during a film growth, and the epitaxial growth mode was changed from layer-by-layer to island mode. For the epitaxial $BiFeO_3$ films prepared under a magnetic field of 0.1 T, the polarization (P_r) was 46 $\mu C/cm^2$ at 80 K, and a saturated ferroelectric polarization versus electric field (*P-E*) hysteresis loop was obtained.

Magnetic-field-assisted pulsed laser deposition will likely prove to be useful in the preparation of films of Bi-, Na-and K-based materials which have been difficult to prepare due to their volatility. Also, it will enable for the fabrication of thick films with a dynamic microstructure in short deposition times with this method, droplet-free films can be obtained as the deflected charge species reach onto the substrate by 90° off-axis deposition.

ACKNOWLEDGEMENT

"I am with you and will watch over you wherever you go, and I will bring you back to this land. I will not leave you until I have done what I have promised you."

(GENESIS 28 : 15)

First of all, I would like to express my sincere gratitude to Professor Masashi Shiraishi of Osaka University, the head of our lab, for his advices, constant support, and encouragement throughout the course of my study. Also, I would like to express my great appreciation to Associate Professor Takeshi Kanashima of Osaka University for his support and encouragement, which helped me shaped my study into a reality. In particular, I would like to express my greatest gratitude to Professor Masanori Okuyama of Osaka University, my mentor, for his guidance, and encouragement during the course of my study. I also would like to thank Professor Mikio Takai and Professor Akira Sakai of Osaka University, for their valuable and effective advices and suggestions in preparing this thesis. I greatly thank my sincere appreciation to Dr. Eiji Shikoh, Dr. Masayuki Sohgawa, and Dr. Yuichiro Ando of Osaka University, for their continuous support during course of Ph. D candidate. I deeply thank Dr. Seiji Nakashima of Hyogo University, for his valuable advice and fruitful discussions. I would like to express my sincere acknowledgements to Dr. Dan Richinshi of Tokyo Institute of Technology, Professor Hiroaki Okamoto, and Dr. Yasushi Sobajima of Osaka University, for their continuous support. I also would like to express my respectful thanks to Mr. Chitose Sada of Osaka University. His advices and helps were usual effective and professional. I am also grateful Professor Hideo Itozaki and Associate Professor Tetsuya Takeuchi of Osaka University, for their helps of streak camera and magnetic hysteresis loop measurement. I would like to acknowledge Dr. Michel Delmo of Osaka University for his kindness and support. I am deeply grateful Dr. Hyun. Lee (LG co. ltd), Dr. Dong Hun Lee

(Hynixs co. ltd), Mr. Fumiya Gotoda (Denso co. ltd), Mr. Yu Katsura (Mitsubishi co. ltd) of the former Okuyama lab, Okamoto lab's members, and Shiraishi lab's members.

I am deeply grateful Professor Hee Young Lee, Professor Jai Yeoul Lee, and Professor Dang Hyok Yoon of Yeungnam University, for sincere advices not only for the research but also my life with their continuous support. I also heartily acknowledge Dr. Ji Yeon Kwon (Osaka University), Dr. Sun Min Lee (POSTECH), Dr. Jong Suck Jung (Samsung EM co. ltd), Dr. Su Jin Kang (Osaka University) for their support during the period of my study. I would not forget to thank to Mr. Dong Chan Woo, Dr. Chang Young Koo for Yeungnam University and Dr. Seung Hyun. Kim of Brawn University, Dr. Chi Sung Park (LG Chem. co. ltd), Dr. Jong Ho Ryu (KIME), and Dr. No Keun Park (Kyoto University) who have helped me overcome these tough times.

I give my kind greetings to Yuki's family, Miss. Chieko Ogawa, Mrs. Emiko Tasaka, Kim's family, Rikio Matsuzawa, and Michiko Matsuzawa. I heartily appreciate fellowship supports granted by Kato Asao International Scholarship Foundation.

Finally, I would like to thank my best friend, Mr. Seong Yoon Shin, for his constant supports and encouragements. I would like to give my special thanks to my loving sister, Mrs. Hee Jung Park, and her husband, Mr. Sang Hwa Shin, for their mental encouragements and constant supports all through my life. Especially to my parents whose positive advice, encouragement, and endless love, gave me strength, patience, benevolence, and a lot of hope to finish this work. Without their love, prayer, and support, I cannot be here finishing up this study. Thank you for being there!

JungMin Park

March 2013

CONTENTS

LIST OF FIGURES

LIST OF TABLES

CHAPTER 1

INTRODUCTION

Bismuth ferrite ($BiFeO_3$) is a very interesting material. $BiFeO_3$, as multiferroics material exhibits ferroelectric and anti-ferromagnetic properties at room temperature (RT). In addition, the $BiFeO_3$ film has attracted a lot of attention, because it has a giant polarization value. In this chapter, the fundamentals for $BiFeO_3$ are explained, and the purpose of this study is introduced.

1.1 Fundamentals

1.1.1 Ferroelectricity in perovskite materials

Ferroelectricity was first discovered in Rochelle salt in 1921. [1] After the discovery of simple mixed oxides which exhibit a perovskite structure, the study of the ferroelectricity accelerated rapidly fundamental understanding and exploring the practical applications of ferroelectric materials, which have attracted a lot of attention. [2] Ferroelectric materials can be used in such as nonvolatile ferroelectric random access memories (FeRAM), sensors and transducers. [3]

Ferroelectricity possesses polar axes in the orientation which can be altered by an external field. The paraelectric materials with a non-polar phase are reflected by a single

potential, but ferroelectric materials exhibit double potential wells as shown in Fig.1.1. In the presence of an electric field, two potential wells do not have the same position or energy and are deformed by an electric field. [4] Moreover, ferroelectrics materials exhibit a spontaneous polarization in the absence of an electric field. The spontaneous polarization can be switched by applying an external electric field. When repeating the polarization reversal (or switching) by an electric field in a ferroelectric material, the ferroelectric hysteresis loop is represented as shown in Fig. 1.2. The coercive field (E_c), remnant polarization (P_r) and saturation polarization (P_s) in the ferroelectric hysteresis loop are important parameters for characterizing ferroelectric properties.

Among all the ferroelectric materials, the perovskite-ferroelectric materials have been studied extensively and used widely. The perovskite structure has the general stoichiometry ABO_3, where "A" and "B" are the cations and "O" is the anion. [5, 7] The structure of an ideal cubic perovskite is shown in Figs.1.3 (a) and (b). The A cations are located at the corner of the unit cell, and the B cations in the centre are located in an octahedra consisting of oxygens. The perovskite structures in ferroelectric materials undergo a structural phase transition from a paraelectric phase to a ferroelectric phase through the Curie temperature (T_c). For example, barium titanate ($BaTiO_3$, BTO) is a well-known perovskite-ferroelectric material. [8] Above T_c, BTO has a centrosymmetric structure and no spontaneous polarization, such as a paraelectric phase. Below T_c, BTO has a ferroelectric phase, including the displacement of the B site ion in the unit cell, as shown in Fig. 1.4. Consequently, perovskite-ferroelectric materials depend on the Curie temperature and transform to non-cetrosymmetric structures below T_c.

1.1.2 Multiferroic materials

Both ferroelectricity and ferromagnetism exhibit that spontaneous electric and magnetic polarizations exist in the absence of an electric field and magnetic field. Also, a hysteresis loop is obtained, with the switching from one state to the other by either external electric field or magnetic field. According to H. Schmid, some materials show two or three

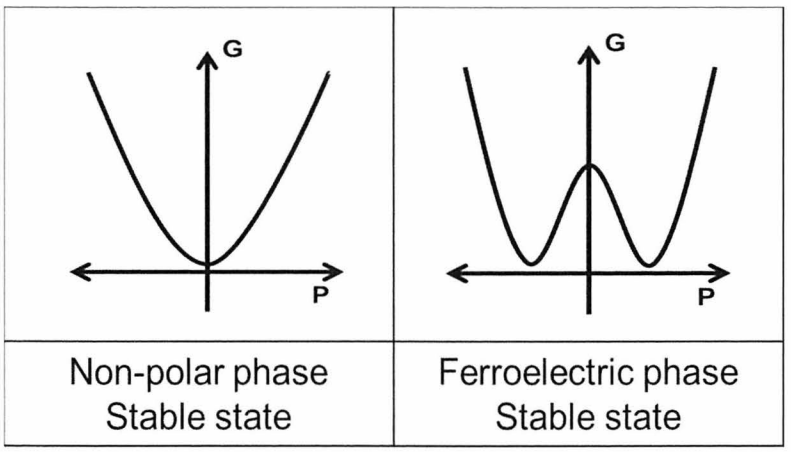

Figure 1.1. Gibbs free energies versus polarization in a non-polar phase and a ferroelectric phase. [5]

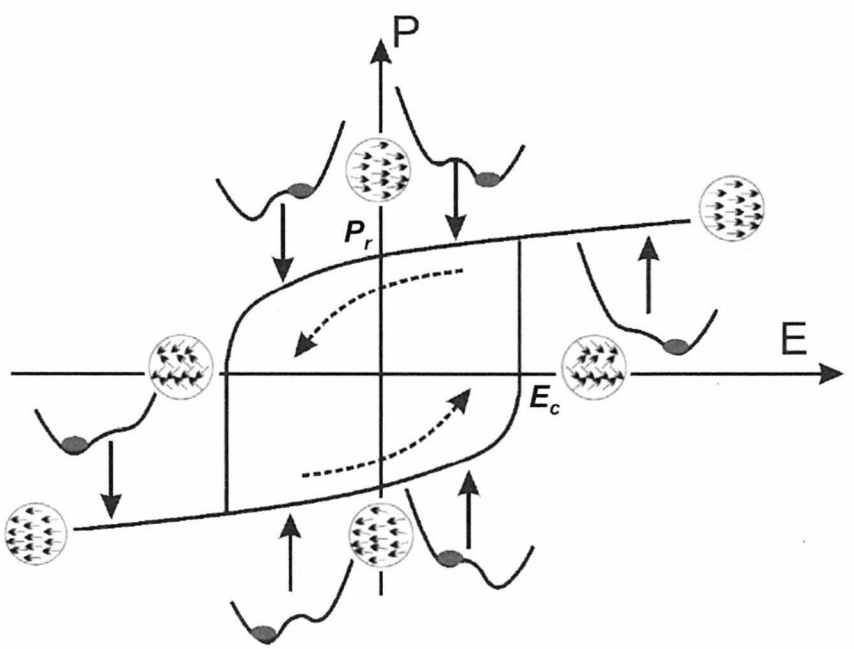

Figure 1.2. Ferroelectric polarization versus electric field (*P-E*) hysteresis loop and polarization switching. [6]

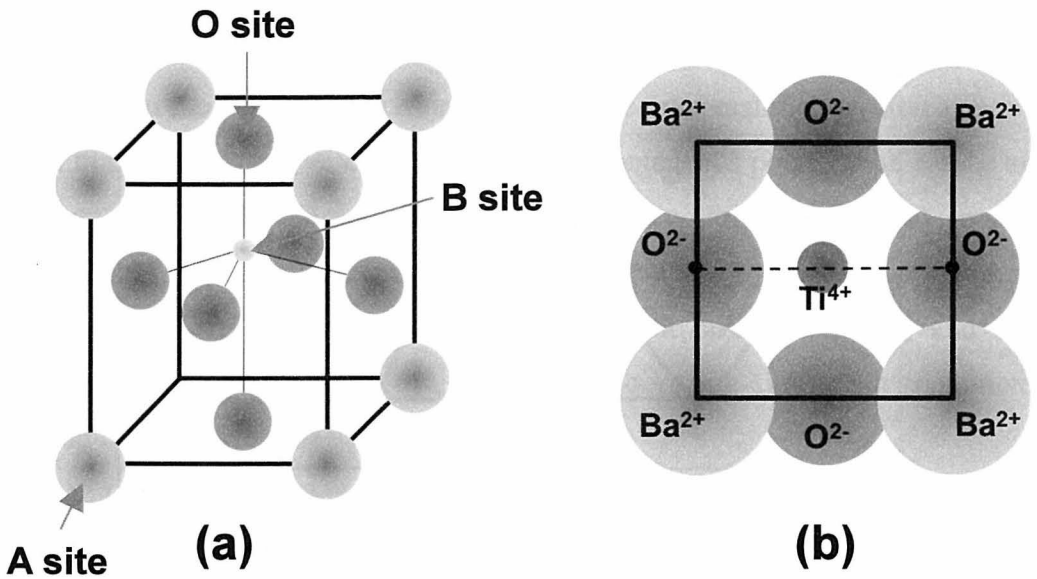

Figure 1.3. (a) Perovskite structure with ABO_3 formula, and (b) atomic position in for cubic $BaTiO_3$.

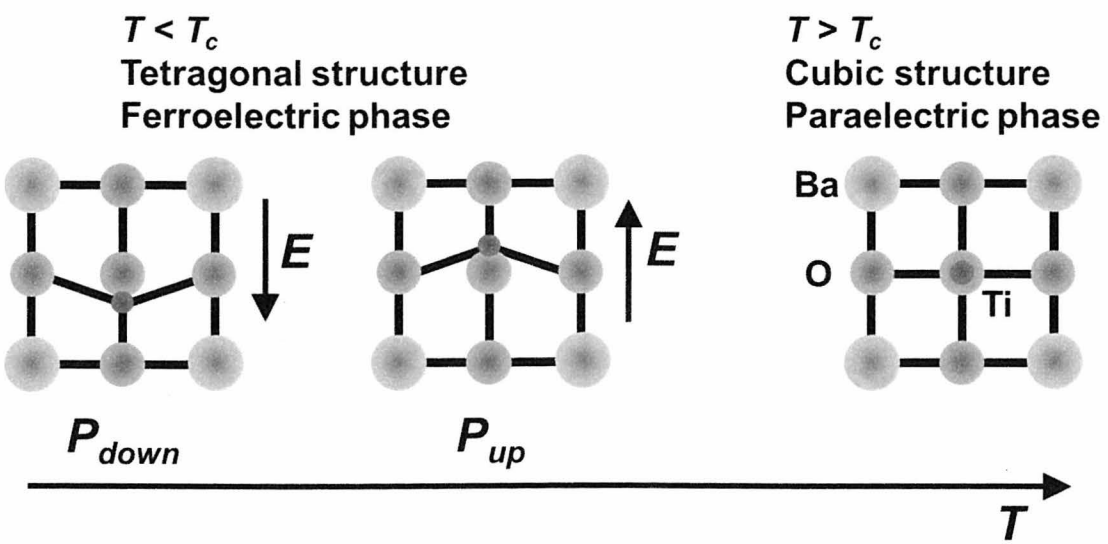

Figure 1.4. State of ferroelectric structure illustrating the phase transition at $T > T_c$ (paraelectric phase) and $T < T_c$ (ferroelectric phase) for $BaTiO_3$.

orderings of ferroic properties such as ferroelectricity, ferromagnetism and ferroelasticity simultaneously. These materials are called multiferroics. [9] Among multiferroic materials, some materials, called magnetoelectrics, have a coupling between the electric and magnetic orderings as shown in Fig. 1.5. [10] In a magnetoelectric material, the ferroelectric ordering can be controlled by a magnetic field, and the magnetic ordering can be controlled by an electric field. The physical phenomena arising from the coexistence of several orderings offer possibilities for various applications, such as multi-functional memory devices different from the ferroelectric random access memory (FeRAM) and magnetic random access memory (MRAM), which are driven only by electric field and magnetic field. [11] As multiferroic materials with a single phase, $BiFeO_3$, $YMnO_3$, $HoMnO_3$, and $TbMnO_3$ have attracted a lot of attention and their physical properties have been investigated. Their basic properties are summarized in Table 1.1.

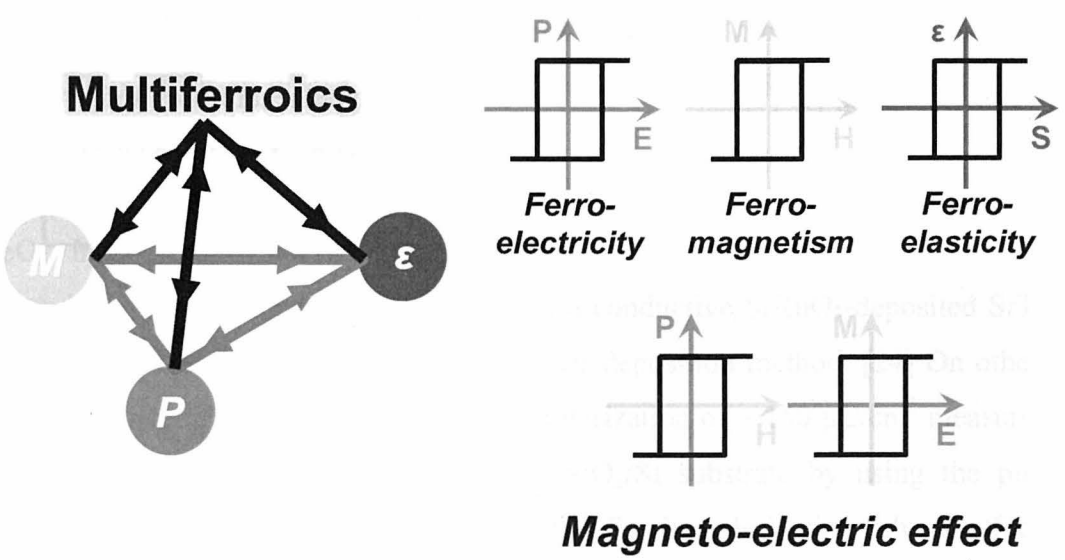

Figure 1.5. Definition and conception of multiferroics, exhibiting simultaneously ferroelectric, ferromagnetic and ferroelastic properties. Mutual control inducing magnetization (M) by an electric field (E) or polarization (P) by magnetic field (H) is represented in matter. [12]

Table 1.1. Basic properties of reported multiferroic materials.

Materials	T_C	T_N	Characteristics
$TbMnO_3$ [13]		~ 41 K	polarization induced by magnetic field below 30 K
$YMnO_3$ [14]	~ 950 K	~ 77 K	6 $\mu C/cm^2$
$BiFeO_3$ [15]	~ 1100 K	~ 640 K	$P_{[001]}$ ~ 75 $\mu C/cm^2$
$DyFeO_3$ [16]	~ 3.5 K	~ 645 K	0.4 $\mu C/cm^2$ under 90kOe
$BiMnO_3$ [17]	~ 800 K	~ 100 K	~ 20 $\mu C/cm^2$
$HoMnO_3$ [18]	~ 875 K	~ 76 K	~ 5.6 $\mu C/cm^2$
$Sr_3Co_2Fe_{24}O_{41}$ [19]			Z-type hexaferrites and a low-field magnetoelectric effect at room temperature.

1.1.3 Bismuth ferrite ($BiFeO_3$)

Bismuth ferrite ($BiFeO_3$) has been the focus of more attention than other multiferroic materials, because it has a high transition temperature, such as the Curie temperature (T_C ~ 1100 K) and Neel temperature (T_N ~ 640 K). [20] In addition, its multiferroic characteristics can be realized at room temperature (RT) and can be used in multifunctional devices. [11]

Bulk $BiFeO_3$ has been early reported on the crystal structure, ferroelectric properties and magnetic properties as shown in Figs. 1.6. The crystal structure of bulk $BiFeO_3$ is a rhombohedrally distorted perovskite structure with a space group of *R3c*, and a lattice parameter of a = 0.562 nm, α = 59.35°. [21] Although the characterization on electrical properties of bulk $BiFeO_3$ has been difficult, due to the high leakage current arising from lower resistivity of the sample, the ferroelectric properties of bulk $BiFeO_3$ revealed a small spontaneous polarization (P_s) of ~ 3.5 $\mu C/cm^2$ and 6.1 $\mu C/cm^2$ along the [001] and [111] directions, measured at 77 K. [22] The magnetic properties of bulk $BiFeO_3$ has a G-type antiferromagnetic ordering, where the spin direction of each Fe^{3+} is antiparallel to that of the nearest Fe^{3+}, but the weak ferromagnetism exists, due to the spin canting. It has a long-wavelength modulation whose the period of the spin cycloid is ~ 62 nm with a wave-vector along the [110] direction. [23]

However, $BiFeO_3$ films show excellent ferroelectric properties in contrast to bulk $BiFeO_3$. In 2003, R. Ramesh's group reported a larger polarization value of ~ 50 $\mu C/cm^2$ measured at RT for epitaxial $BiFeO_3$ films on a conductive $SrRuO_3$-deposited $SrTiO_3$ (001) single crystal substrate by using the pulsed laser deposition method. [24] On other hand, in 2004, M. Okuyama's group reported a giant polarization of ~ 150 $\mu C/cm^2$ measured at 80 K for polycrystalline $BiFeO_3$ films on $Pt/TiO_2/SiO_2/Si$ substrate by using the pulsed laser deposition as shown in Fig. 1.7(b). [25] Theoretically, the polarization value is affected by the crystal symmetry, and the spontaneous polarization is expected to be ~ 100 $\mu C/cm^2$ along the [111] direction and ~ 150 $\mu C/cm^2$ along the [001] direction for rhombohedral and tetragonal structures in $BiFeO_3$ films as shown in Fig. 1.7(c). [26] The theoretical result calculated by the first calculation principle is almost consistent with the experimental results mentioned above.

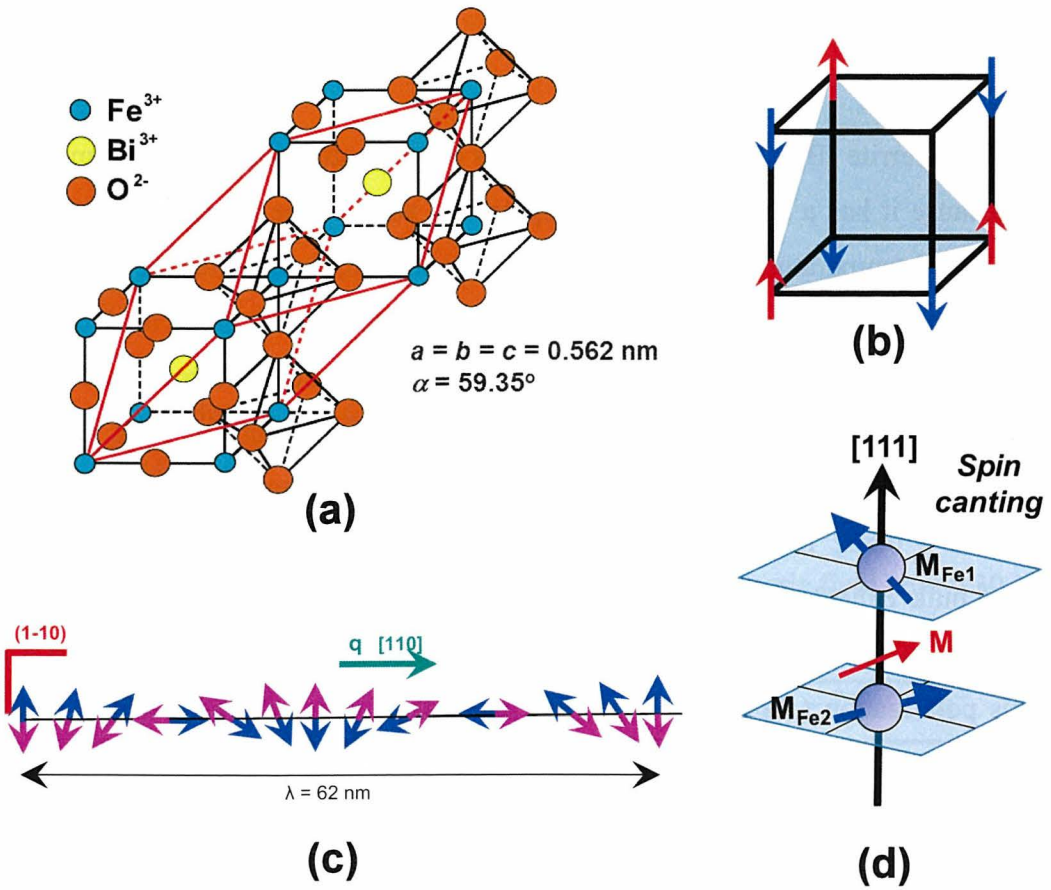

Figure 1.6. (a) Crystal structure, (b) magnetic structure, (c) long range cycloidal spin ordering, and (d) weak ferromagnetism, due to spin canting for $BiFeO_3$. [27, 28]

Table 1.2. Basic properties of $BiFeO_3$.

Phase	I	II	III
State	Ferroelectric Antiferromagnetic or Weak ferromagnetic (due to spin canting)	Ferroelectric Paramagnetic	Paraelectric Paramagnetic
T_N & T_C	370°C (T_N)	850°C (T_C)	

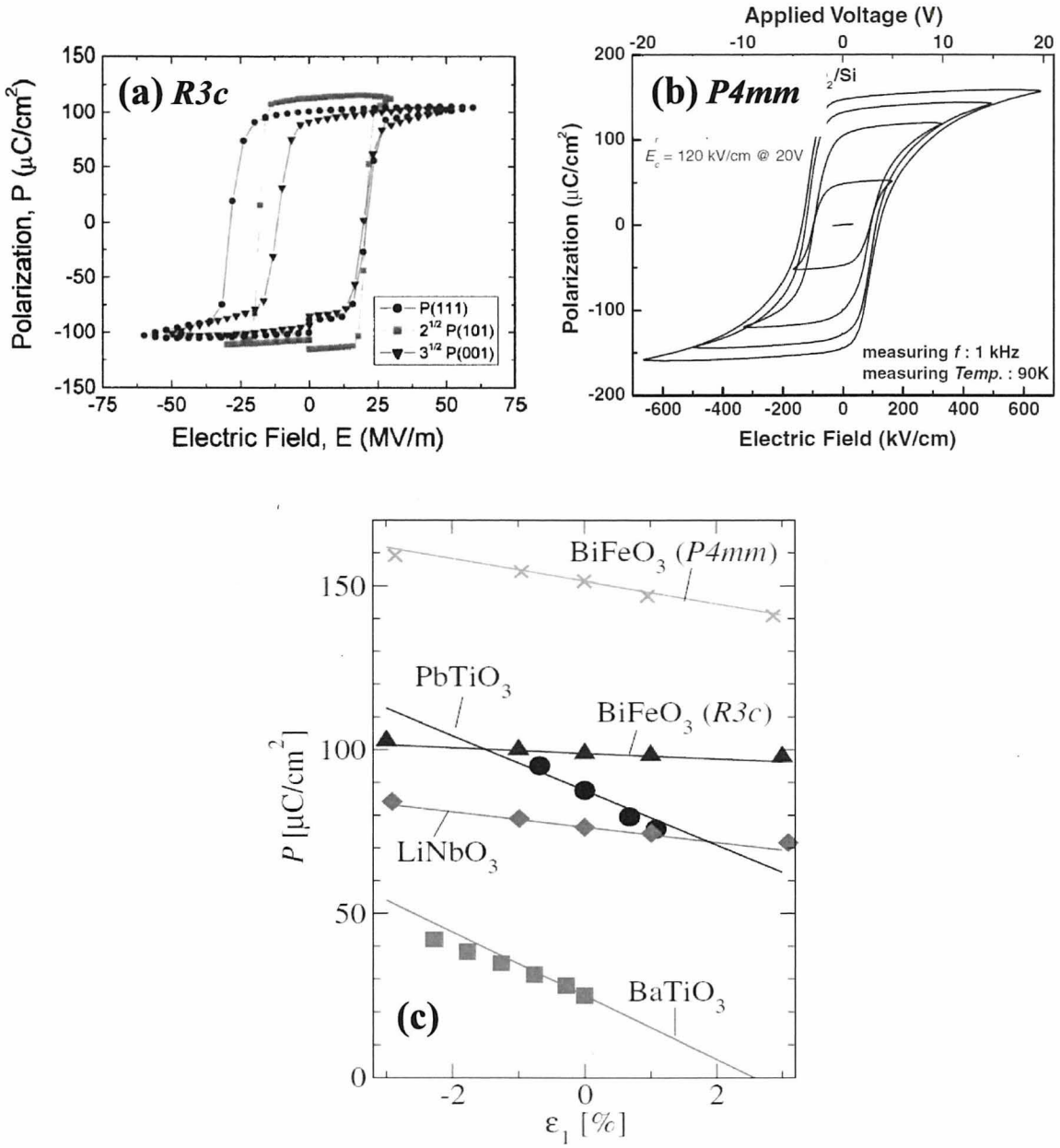

Figure 1.7. *P-E* hysteresis loops indicating the ferroelectric property in (a) epitaxial $BiFeO_3$ films on $SrTiO_3$ (001), (101), and (111) single crystal substrate and (b) polycrystalline $BiFeO_3$ film on $Pt/TiO_2/SiO_2/Si$ substrate. (c) Estimated polarization values by first principle calculation on $BiFeO_3$ films. [25, 26, 29]

1.2 Purpose of This Study

Among other multiferroic materials as mentioned in chapter 1.1.2, $BiFeO_3$ has attracted a lot of attention, because of its ferroelectric and anti-ferroelectric (weak ferromagnetism due to spin canting) orderings at room temperature (RT). In particular, the polycrystalline $BiFeO_3$ film on $Pt/TiO_2/SiO_2/Si$ substrate has giant polarization values. Further, as the Bi-based ferroelectric material, it is environment-friendly, have low processing temperatures, making them better than Pb-based ferroelectric materials. So far, the preparation of polycrystalline $BiFeO_3$ films has been tried by various deposition methods, and considerable experimental progress has been made on understanding the physical properties of $BiFeO_3$ films.

On the other hand, polycrystalline $BiFeO_3$ films grown on $Pt/TiO_2/SiO_2/Si$ substrate have one major problem which is the poor ferroelectric properties with a leaky ferroelectric polarization versus electric field (*P-E*) hysteresis loop, due to the leakage current arising from the Bi and Bi_2O_3 loss. This problem is an obstacle to using polycrystalline $BiFeO_3$ films in more applications. For example, in order to use it in sensors and actuators, the polycrystalline $BiFeO_3$ film has to be at least 2 μm thick, while for manufacturing memory devices, it needs to be below 600 nm. Recently, most experiments have focused on $BiFeO_3$ films with less than 600 nm in thickness. The limitation of the film thickness is due to the difficulty in controlling Bi and Bi_2O_3 loss in $BiFeO_3$ films during a deposition.

The aim of this study is to prepare and characterize polycrystalline $BiFeO_3$ films which overcome the limitation of the thickness, and make the first step towards using them in a wide range of practical applications. To attain the aim of this study, a magnetic-field-assisted pulsed laser deposition method is employed as a new deposition method. Nothing has been reported so far on the preparation of $BiFeO_3$ films using this deposition method. The preparation of $BiFeO_3$ films under various magnetic fields is a starting point. In next chapters, the features of the magnetic-field-assisted pulsed laser deposition are clarified in comparison with a conventional pulsed laser deposition, and the preparation of polycrystalline $BiFeO_3$ films with a thickness of at least 2 μm is conducted.

The outline of this thesis is introduced in Fig. 1.8.

In chapter 1, fundamental terms are explained and the purpose of this study is introduced.

In chapter 2, in order to clarify the features of the magnetic-field-assisted pulsed laser deposition in comparison with the conventional pulsed laser deposition, the behavior of the plume and the evolution of the microstructures under a magnetic field are simulated.

In chapter 3, the deposition method and measurement tools for the preparation and the characterization of $BiFeO_3$ films are introduced. Their simple principles are described.

In chapter 4, polycrystalline $BiFeO_3$ films are prepared on $Pt/TiO_2/SiO_2/Si$ substrate by using the magnetic-field-assisted pulsed laser deposition method. The microstructure of polycrystalline $BiFeO_3$ films prepared under various magnetic fields is compared with that of polycrystalline $BiFeO_3$ films prepared by the conventional pulsed laser deposition, and the dependence of the ferroelectric properties of polycrystalline $BiFeO_3$ films on film thickness is discussed. In addition, polycrystalline $BiFeO_3$ films prepared by 90^o off-axis deposition are characterized.

In chapter 5, epitaxial $BiFeO_3$ films on La-doped $SrTiO_3$ (001) single crystal substrate are prepared under various magnetic fields by using the magnetic-field-assisted pulsed laser deposition method. The lattice parameter of epitaxial $BiFeO_3$ films is discussed in detail. The growth mode of epitaxial $BiFeO_3$ films on a La doped $SrTiO_3$ (001) single crystal substrate prepared under various magnetic fields is compared with that of the conventional pulsed laser deposition. Ferroelectric properties of the epitaxial $BiFeO_3$ films are measured at room temperature and low temperature.

In chapter 6, finally, conclusions of this study are summarized.

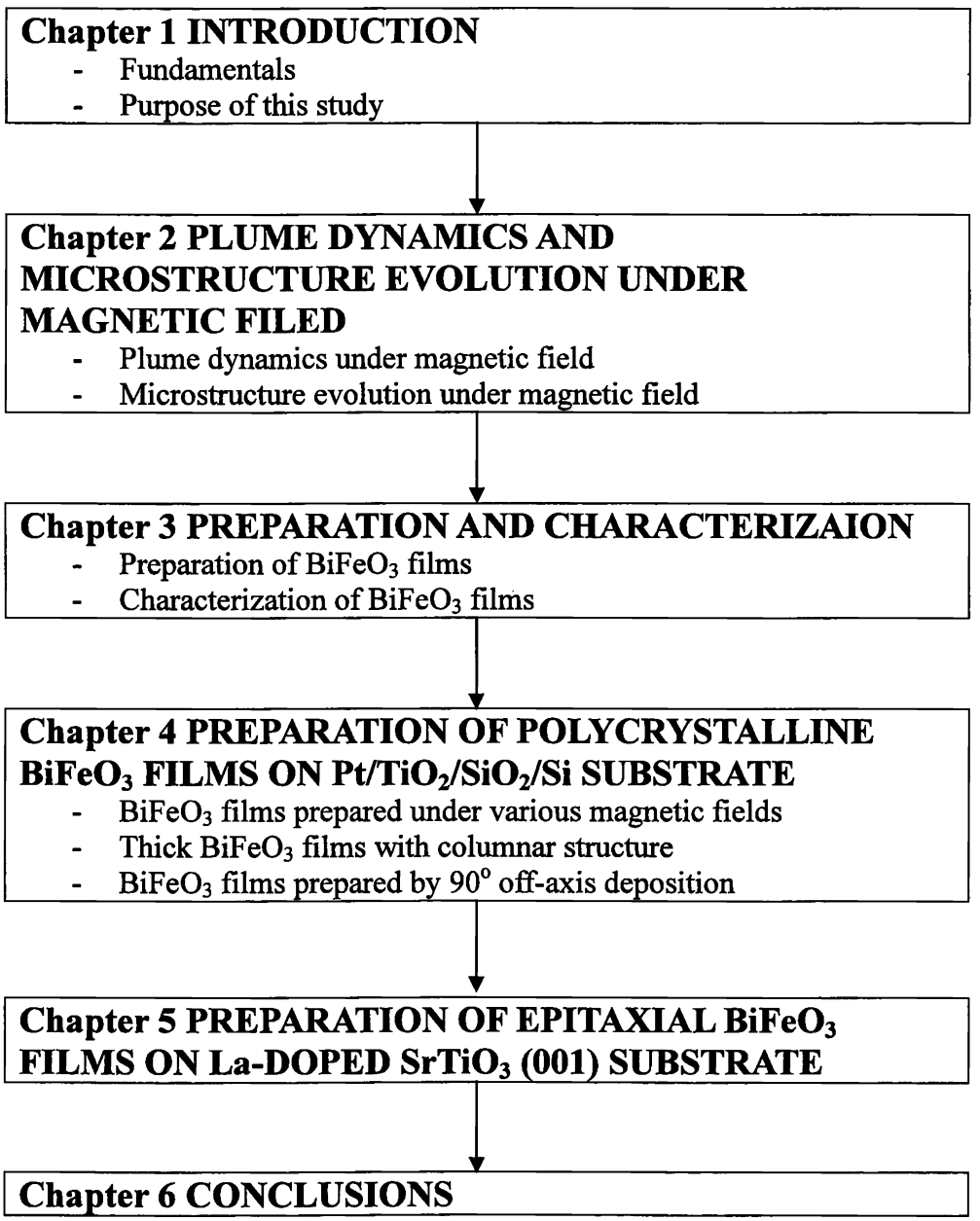

Figure 1.8. Outline of this thesis.

References

[1] J. Valasek, *Phys. Rev.* **17**, 475 (1921).

[2] L.E. Cross and R. E. Newnham, *History of Ferroelectrics, vol. III, Westerville*, 1987.

[3] K. Uchino, *Ferroelectric devices*, (2000).

[4] D. Damjanovic, *Rep. Prof. Rhys.* **61**, 1267 (1998).

[5] M. E. Lines and A. Glass, *"Principle and Application of Ferroelectric and Related Materials"*, Oxford University Press, Oxford, 2001.

[6] H. Wijshoff, *Physics Reports*, **491**, 77 (2010).

[7] J. F. Scott, *"Ferroelectric Memories"*, Springer, Berlin, 2000.

[8] A. V. Hippel, *Rev. Mod. Phys.* **22**, 221 (1950).

[9] H. Schmid, *Ferroelectrics* **162**, 317 (1994).

[10] P. Curie, *J. Phys.***3** *(Ser. III)*: 393-415, (1984).

[11] W. Eerebstein, N. D. Murther, and J. F. Scott, *Nature* **442**, 759 (2006).

[12] K. F. Wang, J. M. Liu, and Z. F. Ren, *Advances in Physics*, **58**, 321 (2009).

[13] T. Kimura, T. Goto, H. Shintani, K. Ishizaka, T. Arima, and Y. Tokura, *Nature* **426**, 55 (2003).

[14] B. V. Aken, T. T. M. Palstra, A. Filippetti, and N. A. Spaldin, *Nature Mater.* **3**, 164 (2004).

[15] V. V. Shvartsman, W. Kleemann, R. Haumont, and J. Kreisel. *Appl. Phys. Lett.* **90**, 172115 (2007).

[16] Y. Tokunaga, S. Iguchi, T. Arima, and Y. Tokura, *Phys. Rev. Lett.* **101**, 097205 (2008).

[17] R. Seshadri and N.A. Hill, *Chem. Mater.* **13**, 2892 (2001).

[18] B. Lorenz, A. P. Litvionchuk, M. M. Gospodinov, and C. W. Chu, *Phy. Rev. Lett.* **92**, 087204 (2004).

[19] Y. Kitagawa, Y. Hiraoka, T. Honda, T. Ishikura, H. Nakamura, and T. Kimura, *Nature Materials* **9**, 797 (2010).

[20] G. A. Smolenskii and I. Chupis, *Sov. Phys. Usp.* **26**, 475 (1982).

[21] F. Kubel and H. Schmid, *Acta Crystallogr.* **46**, 698 (1990).

[22] J. R. Teague, R. Gerson, and W. J. James, *Solid State Commun.* **8**, 1073 (1970).

[23] D. Lebeugle, D. Colson, A. Forget, M. Viret, P. Bonville, J. F. Marucco, and S. Fusil, *Phys. Rev. B* **76**, 024116 (2007).

[24] J. Wang, J.B. Neaton, H. Zheng, V. Nagarajan, S.B. Ogale, B. Liu, D. Viehland, V. Vaithyanathan, D.G. Schlom, U.V. Waghmare, N.A. Spaldin, K.M. Rabe, M. Wuttig, and R. Ramesh, *Science* **299**, 1719 (2003).

[25] K. Y. Yun, D. Ricinschi, T. Kanashima, M. Noda, and M. Okuyama, *Jpn. J. Appl. Phys.* **43**, L647 (2004).

[26] C. Ederer and N. Spaldin, *Phys. Rev. Lett.* **95**, 257601 (2005).

[27] F. Zavaliche, S. Y. Yang, T. Zhao, Y. H. Chu, M. P. Cruz, C. B. Eom, and R. Ramash, *Phase Transit.* **79**, 997 (2006).

[28] D. Lebeugle, D. Colson, A. Forget, M. Viret, P. Bonville, J. F. Marucco, and S. Fusil, *Rhys. Rev. B* **76**, 024116 (2007).

[29] J. Li, J. Wang, M. Wutting, R. Ramesh, N. Wang, B. Ruette, A. P. Pyatakov, A. K. Zvezdin, and D. Viehland, *Appl. Phys. Lett.* **84**, 5261 (2004).

CHAPTER 2

PLUME DYNAMICS AND MICROSTRUCTRE EVOLUTION UNDER MAGNETIC FIELD

The plume produced by a laser ablation plays an important role in the pulsed laser deposition. In this chapter, the behavior of the plume under a magnetic field is investigated, and the evolution of the microstructures caused by the plume under a magnetic field is clarified based on simulations.

2.1 Introduction

In the conventional pulsed laser deposition method, the focused laser irradiates the target, which is set in a vacuum chamber. A plume is formed as the interaction takes place between the laser and the target. The evaporated species including atoms, molecules, electrons, ions, cluster and particulates in the plume transfer onto the substrate. [1] This deposition method can be divided into the following four steps [1]:

1. Formation of plume produced by a laser ablation.
2. Dynamics of the evaporated species in the plume.
3. Deposition of the evaporated species onto the substrate.

4. Nucleation and growth of the film on the substrate surface.

In this study, the magnetic-field-assisted pulsed laser deposition, consisting of the application of a magnetic field during laser ablation is proposed as a new deposition method. As mentioned above, the plume is an important factor in the pulsed laser deposition and contributes to the evolution of microstructures. Further, the plume produced by the laser ablation under a magnetic field might cause the dynamic phenomena and modification. Understanding the plume dynamics under a magnetic field is regarded as a prerequisite for understanding of the evolution of microstructures if films are prepared by using the magnetic-field-assisted pulsed laser deposition.

In chapter 2, to clarify the behavior of the plume under a magnetic field, the trajectory of the plume under a magnetic field and without a magnetic field is simulated. Based on the assumed trajectory of the plume obtained by a simulation, the evolution of microstructures is estimated.

2.2 Plume Dynamics under Magnetic Field

To estimate the behavior of the plume under a magnetic field and without magnetic field, the trajectory of the plume in a given space (5 cm x 3 cm) was simulated based on the following equation:

$$m\frac{d^2\boldsymbol{r}}{dt^2} = q\boldsymbol{v} \times \boldsymbol{B}, \tag{2.1}$$

where m, $\boldsymbol{r}$, t, q, $\boldsymbol{v}$, and $\boldsymbol{B}$ represent mass, position, time, charge, velocity, and magnetic field of flux density, respectively. The estimation was considered for only charge species in the plume. In most previous research, it has reported the fact that charge species are the majority in the plume. [2-4] Of course, neutral species that typically include heavy and large particulates exist in the plume, but they are not affected by the magnetic field and travel along a straight path. The presence of the magnetic field promotes the ionization of the evaporated

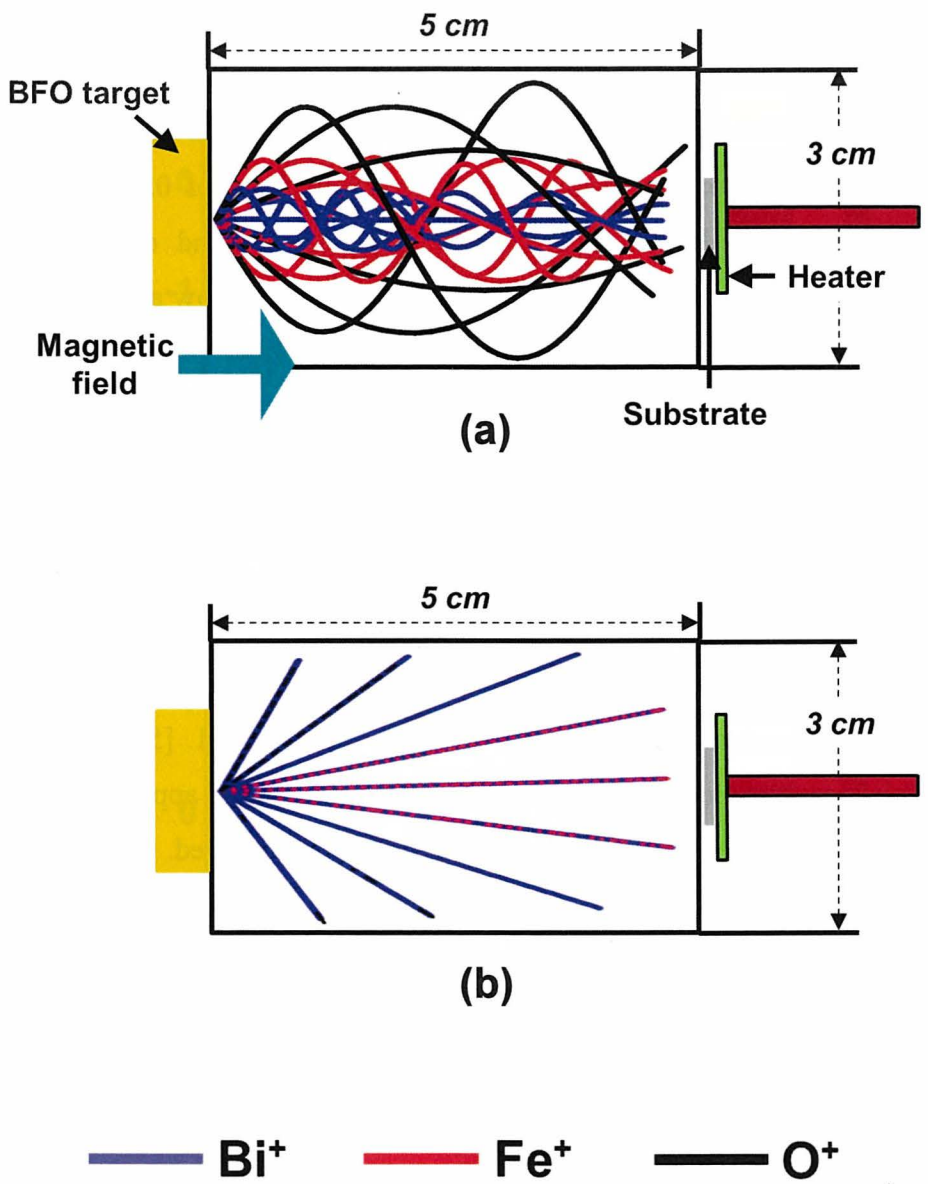

Figure 2.1. Trajectories of plume under magnetic fields of (a) 0.4 T and (b) 0 T, estimated by simulation, under an oxygen pressure of 0.05 Torr, in a given space (5 cm x 3 cm).

species in the plume, because the accelerated electrons caused by the magnetic field collide with atoms and molecules. Therefore, in this simulation, the charge species were regarded as majority species in the plume under a magnetic field, but the neutral species were negligible.

In simulation, the atomic masses were Bi (208.98), Fe (55.85) and O (16), respectively. Atoms are assumed to be traveling toward the substrate with a little collision under an oxygen pressure of 0.1 Torr, while the particle energy is 50 eV and time step is 10^{-9} s. The magnetic field was set to 0 T and 0.4 T. The simulated results are shown in Figs. 2.1(a) and (b). The trajectories of the plume under a magnetic field of 0.4 T and 0 T show a significant difference, while the trajectories of each ion depend on atomic mass. The trajectories of the plume are modified by a magnetic field and show a helical movement, as opposed to the straight path observed under a magnetic field of 0 T. These results are predictable. The magnetic field exerts Lorenz force, and the ions species are affected according to the $\boldsymbol{v} \times \boldsymbol{B}$. As shown in Figs. 2.1(a) and (b), the magnetic field deflects the ions species away from the primary path of the plume responsible for the loss of evaporated species, and this can result in confining the plume to the substrate. The angular distribution of the plume is generally dominated by cos θ function. From the simulated trajectory of the plume under a magnetic field, it is considered that the angular distribution of the plume under a magnetic field is dominated by the $\cos^n \theta$ function, where $n > 1$. [5-7] The n is associate with a film thickness and a deposition rate. When n is increased by applying a magnetic field, the film thickness is increased and a high deposition rate is achieved. Consequently, the ions species deflected by a magnetic field predict the possibility of the high deposition rate derived from the confined plume, with an effective deposition, unlike the loss of evaporated species along the primary path. To simply prove this prediction, the distribution of stacking was investigated in a given space (2 cm x 2 cm) indicating the real size of Pt substrate, while 10000 atoms of Fe ion species travel along the trajectory of the plume as shown in Figs. 2.1(a) and (b).

Figures 2.2(a) and (b) show the distribution of the stacking for the Fe ion species which travel along the trajectories of the plume under magnetic fields of 0.4 T and 0 T. It can be seen that the distribution of the stacking along each trajectory of the plume is different. The distribution of stacked species under a magnetic field of 0 T is broad, likely depending

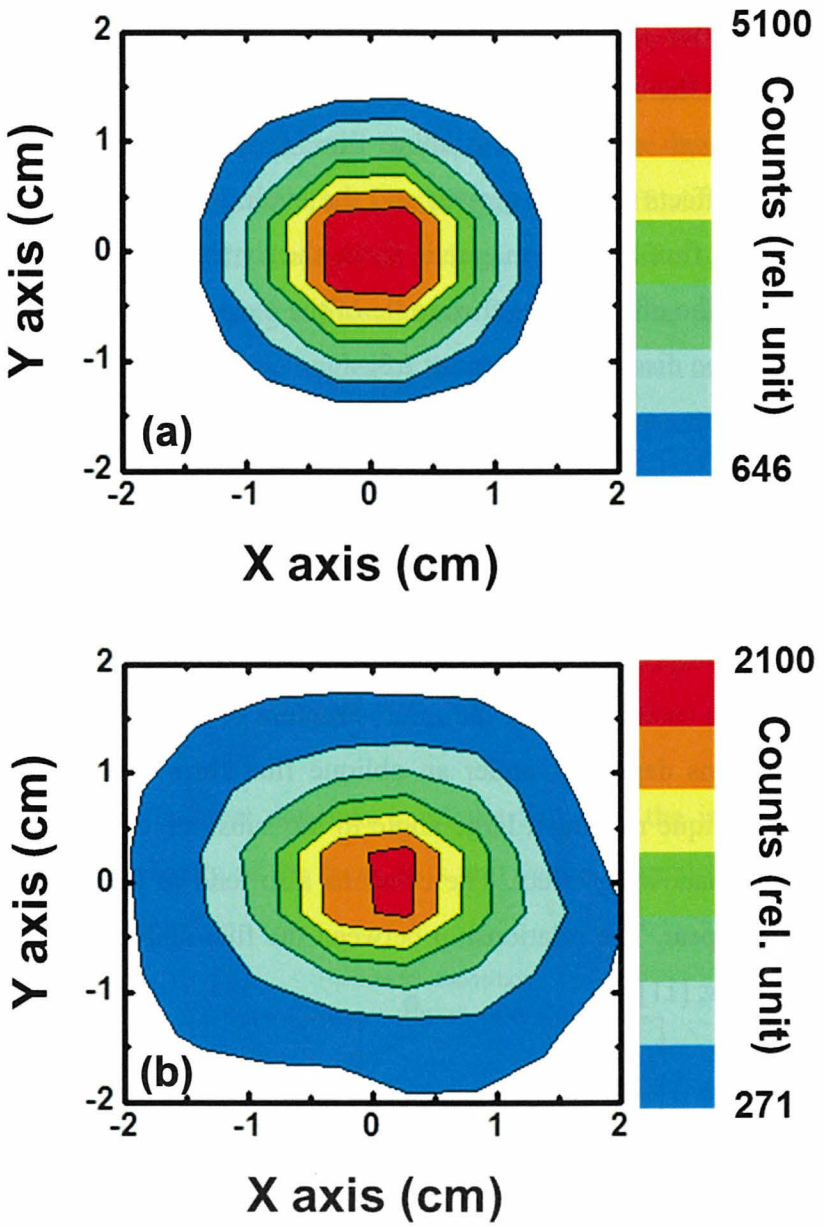

Figure 2.2. Distribution of stacked atoms in a given space (2 cm x 2 cm). The atoms traveled along the trajectory of the plume under (a) a magnetic field and (b) without a magnetic field, according to the simulated results shown in Fig. 2.1.

on the cos θ function. However, the distribution of stacked species under a magnetic field is sharper, and concentrated in the given space, likely depending on the $\cos^n \theta$ function. This result strongly supports the fact that high deposition rate is caused due to the magnetic field. In addition, the deflected ions species arising from the modified trajectory reach the substrate conically. This shows the conical flux of evaporated species until reaching the surface of the substrate. In the growth of a polycrystalline film, it is well known that the flux of the evaporated species affects the film growth and the evolution of microstructures in the film. [8-10] In the conical flux under a magnetic field, the dynamic evolution of microstructures might be predicted. The effect of the flux angle of the evaporated species on the evolution of microstructures will be discussed in chapter 2.3.

2.3 Microstructure Evolution under Magnetic Field

The flux of evaporated species significantly affects the evolution of microstructures. When the flux has an incident angle, the microstructure of films dynamically develops. It is well known that films deposited under an oblique flux form a columnar structure. [5, 6] When the flux is oblique making a large angle to the substrate or film normal, columns are formed due to the shadowing effect. The columns also tend to tilt away from the substrate normal and voids appear. The relationship between the flux and the column is explained by the tangent law below, [11]

$$\tan\beta = 1/2 \tan\alpha, \tag{2.2}$$

where β and α represent the angle of orientation of these columns and the deposition angle.

However, this law is applicable only for the oblique angle from one side. In chapter 2.1.1, it was confirmed that the deflected ion species arising from the modified trajectory reach the substrate conically. The evolution of microstructures depends on the incident angle of the flux. If the modified trajectory of the plume under a magnetic field causes the dynamic flux of evaporated species, having various incident angles, a dynamic evolution of the

microstructures might take place onto the substrate. Thus, to investigate the effect of the flux angle on the evolution of microstructures, a simulation was carried out, and the evolutions of microstructures for both oblique and conical fluxes were compared.

In the simulation, the two-dimensional periodic boundary condition is assumed. A uniform grid mesh of 100x100 was used for the calculation, as shown in Fig. 2.3. The surface of the substrate assumed the existence of facets, indicating pre-coalescence. Each mesh corresponds to a micro-facet in a grain. This model ignores the diffusion interactions between grains or islands on the surface. In the case of polycrystalline $BiFeO_3$ films deposited on a (111) Pt-coated Si substrate by using a pulsed laser deposition, the preferred orientation is (100) and (110) planes. Therefore, the angles of the facet are chosen as 0°, ±45°, and ±45°/2 degrees, which correspond to (100) and (110) of these planes, respectively. The facets of the initial nuclei are randomly distributed and each facet has a distinctive color. Surface migration is ignored, and all surfaces have the same sticking coefficient (= 1) calculated as in the following equation,

$$v = n \cdot J \tag{2.3}$$

The growth velocity of each facet depends upon the flux and the incident angle. In this equation, v is the growth velocity of the facet, $\boldsymbol{n}$ is unit vector normal to the facet, and $\boldsymbol{J}$ is a vector parallel to the flux direction.

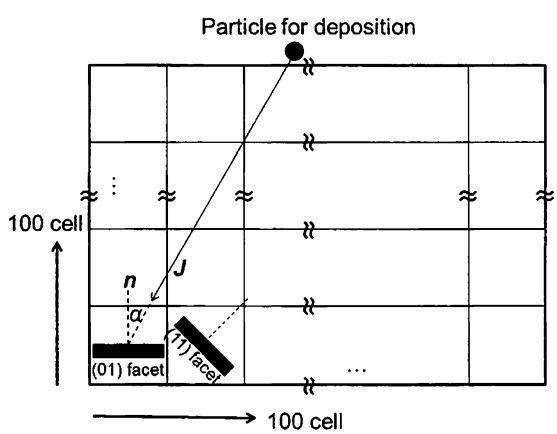

Figure 2.3. Schematic of the two-dimensional periodic boundary. The grid mesh consists of 100x100 cells.

A large number of species (10000) are irradiated, and the development of facets is calculated. The objective of the simulation is to estimate the evolution of microstructures on flux angle of evaporated species. However, the physical effects are negligible.

Figures 2.4(a)-(c) show the evolution of microstructures for oblique angles of 0^{o}, 30^{o}, and 60^{o} from the one side. For a normal angle of 0^{o}, the microstructure was densely packed without any voids. On the other hand, the microstructures were columnar at oblique angles of 30^{o} and 60^{o}. They displayed porosity with voids, and the columns were tilted in the direction of the incident species. This result is consistent with results about the microstructures in obliquely deposited films reported by other authors. In their results, the shadowing effect gave rise to the voids between the columns, and the evolution of microstructures under the oblique angle of the incident species from one side has been only reported. [12-14] For the plume produced by a laser ablation, even though the trajectory of the plume is a straight path, as shown in Fig. 2.1(b), the trajectory of the plume under a magnetic field is modified, and the incident species have an oblique angles from both sides as shown in Fig. 2.1(a). Thus, the evolution of microstructures for an oblique angle from both sides is considered.

Figures 2.5(a)-(f) show the evolution of microstructures for oblique angles from both sides assumed for a plume modified under a magnetic field. It can be seen that the evolution of microstructures for the same oblique angle from both sides significantly differs from that for an oblique angle from one side. In the case of both sides, while the columnar structure is formed due to the oblique angle, the columns are grown normal to the substrate, regardless of the oblique angle of species. In the case of the oblique angle of 60^{o}, the columnar structure is not present, and the growth on 0^{o} facet becomes dominant. The evolution of microstructures under an oblique incidence angle greater than 60^{o} could not be achieved in this simulation. If the conical flux causes the modified trajectory of the plume under a magnetic field, the case of a different oblique angle with respect to both sides should be also considered. Figures 2.5(e) and (f) show the evolution of microstructures for different oblique angles with respect to both sides. The evolution of microstructures for different oblique angles from both sides shows a similar trend to that for the oblique angle from one side. Even though the microstructure is dense, the columns are tilted in one direction, having a large incident angle. As a result, the growth in the direction having a large incident angle is dominant.

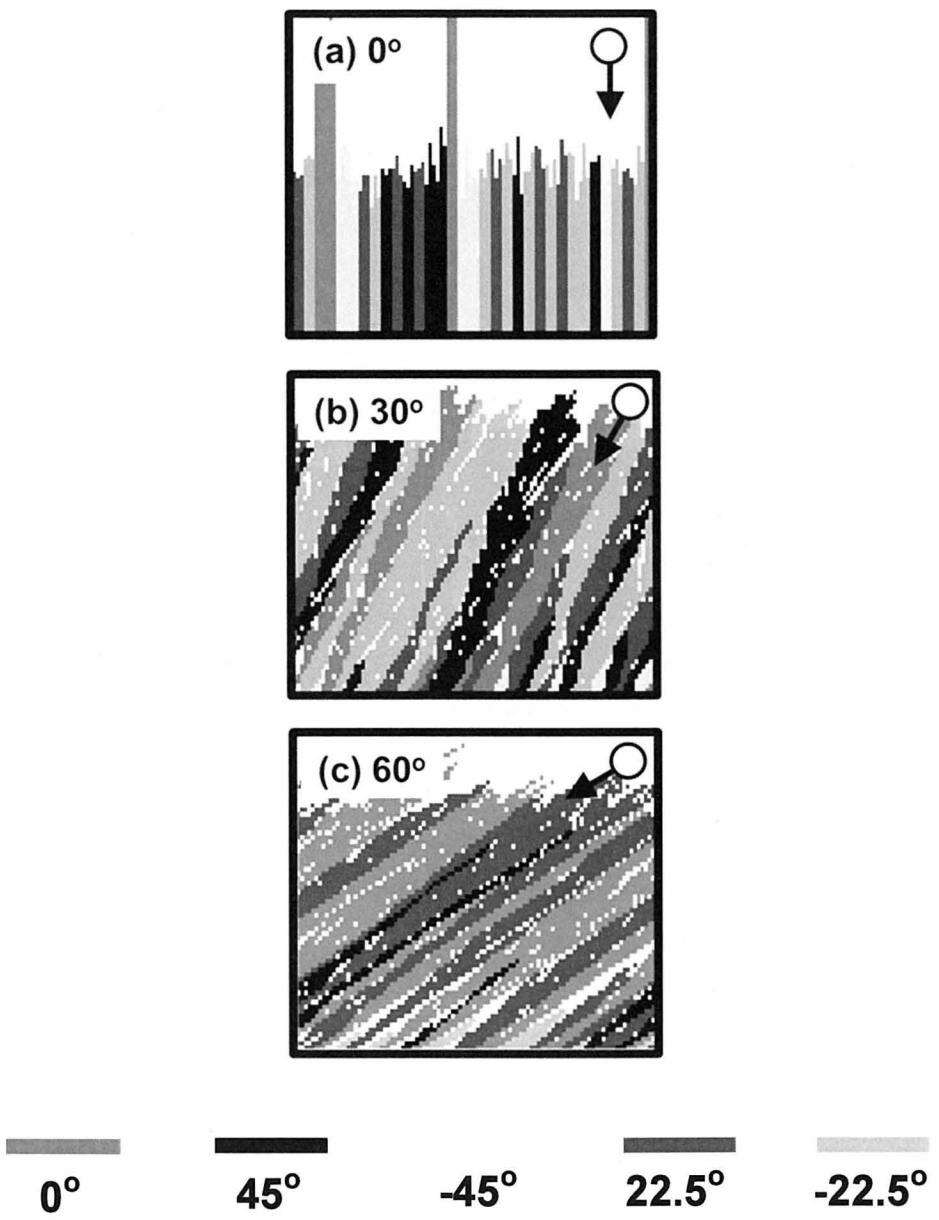

Figure 2.4. Evolution of microstructures for oblique angles of (a) 0°, (b) 30°, and (c) 60° from one side.

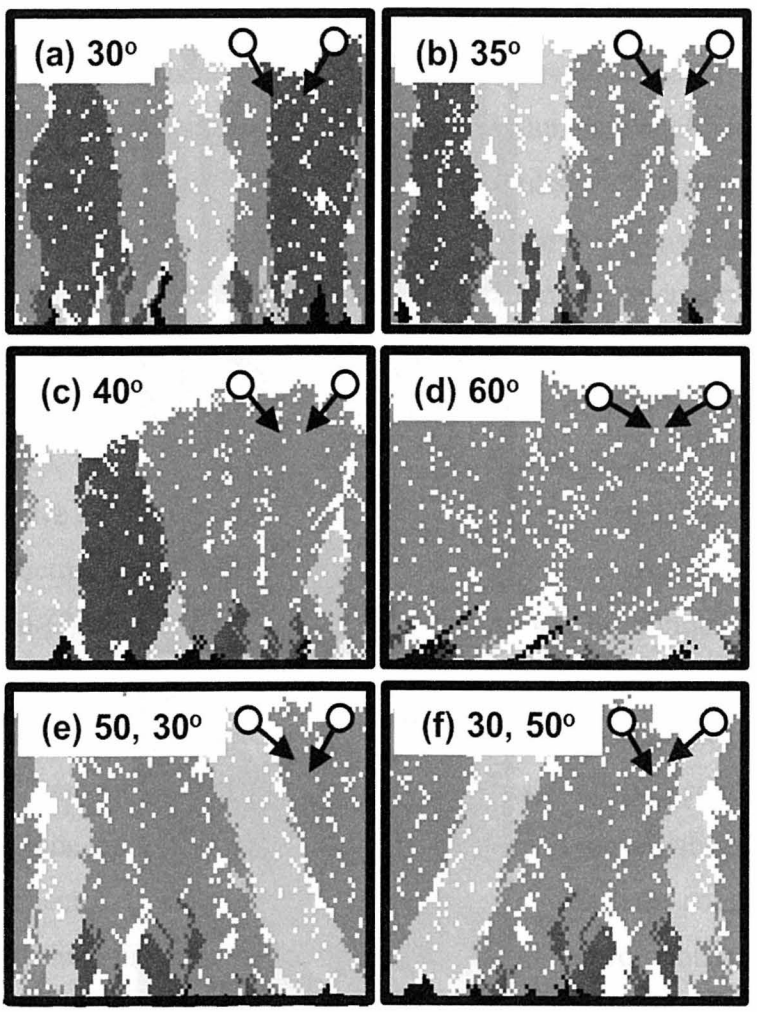

Figure 2.5. Evolution of microstructures for oblique angles of (a) 30°, (b) 35°, (c) 40°, and (d) 60°, and for different oblique angles of (e) 50°, 30° and (f) 30°, 50° from both sides.

In chapter 2.2, it was suggested that the charge species are the majority in the plume under a magnetic field, and the neutral species were neglected in the observation of the trajectory of the plume under a magnetic field. Nevertheless, neutral species exist in the plume, while they are not affected by the magnetic field and travel along a straight path.

Therefore, the evolution of microstructures was estimated under the assumption on real circumstances of a deposition, including both charge and neutral species. The 0^{o}, representing the normal incidence for neutral species, and the oblique angles of 40^{o} and 30^{o} from both sides were considered. Figures 2.6(a)-(c) show the evolution of microstructures under various ratios of the incident angles of 40^{o}, 30^{o}, and 0^{o}. In the case of 10 : 10 : 1 as shown in Fig. 2.6(a), a columnar structure was observed, when the ratio of the normal incidence was smaller than that of the oblique incidence. However, when the ratio of the normal incidence is close to that of the oblique incidence, the columnar structure is not present, because the normal incidence is dominant in the evolution of microstructures, as shown in Figs 2.6(b) and (c). These results demonstrate that the normal incidence derived from neutral species does not affect the formation of columnar structure, and leads to the formation of the granular structure. This is supported by the fact that under magnetic field, the charge species are the majority in the plume. It can also be predicted that, if the columnar structure is obtained by a laser ablation under a magnetic field, the charge species will play a more important role than the neutral species. Consequently, the incidence angle of the species contributes to the evolution of microstructures, and the conical flux of the charge species influences the formation of columnar structures.

2.4 Summary

In this chapter, simulations were carried out to investigate the plume dynamics and the evolution of microstructures under a magnetic field. Under a magnetic field, the plume was dynamically modified and confined. Also, the magnetic field deflected the trajectory of the plume away from its primary path of the plume without a magnetic field.

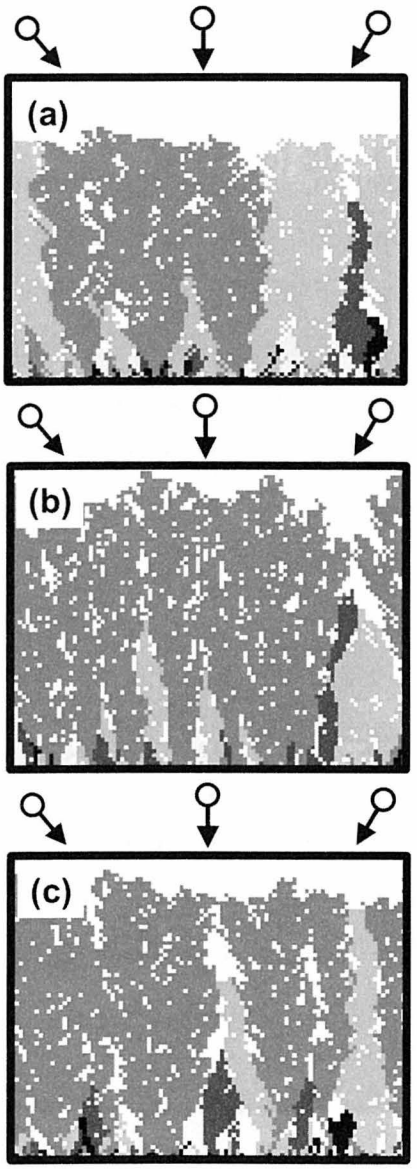

Figure 2.6. Evolution of microstructure under various ratios of incident angles of 40°, 30° and 0°. (a) 10 : 10 : 1, (b) 2 : 2 : 1, and (c) 1 : 1 : 1.

From those results, the high deposition rate is predicted due to the suppression of species loss, induced by the primary path without a magnetic field. In addition, the conical flux is caused by the modified trajectory of the plume under a magnetic field. The oblique incidence from both sides formed columnar structures with columns normal to the substrate. In the case of a different incidence angle to the normal substrate, the columns grew predominantly tilted in the direction having the larger incidence angle. The neutral species resulting in the normal flux did not affect the formation of columnar structures. Consequently, it can be considered that the dynamic plume under a magnetic field significantly contributes to the deposition rate and the evolution of microstructures.

References

[1] D. B. Chrisey and G. K. Hubler, "*Pulsed Laser Deposition of Thin Films*" Wiley, New York, 1994.

[2] S. S. Harial, M. S. Tillack, B. O'Shay, C. V. Bindhu, and F. Najmabadi, *Phys. Rev E* **69**, 026413 (2004).

[3] L. Drinberger, P. E. Dyer, S. R. Farrar, and P. H. Key, *Appl. Phys. A* **59**, 311 (1994).

[4] T. Kobayashi, H. Akiyoshi, and M. Tachiki, *Appl. Surf. Sci.* **197-198**, 294 (2002).

[5] I. Noorbatcha, R. R. Lucchese, and Y. Zeiri, *J. Chem. Phys.* **86**, 5816 (1987).

[6] R. K. Singh and J. Narayan, *Rhys, Rev. B* **41**, 8843 (1990).

[7] S. I. Anisimov, D. Bauerle, and B. S. Luk'yanchuk, *Rhys, Rev. B* **48**, 12076 (1993).

[8] M. M. Hawkeye and M. J. Brett, *J. Vac. Sci. Technol. A* **25**, 1317 (2007).

[9] K. Robbie, J. C. Sit, and M. J. Brett, *J. Vac. Sci. Technol. B* **16**, 1115 (1998).

[10] H. Konig and G. Helwig, Optic (Stuttgart) **6**, 111 (1950).

[11] J. M. Nieuwenhuizen and H. B. Haanstra, *Philips Tech. Rev.* **27**, 87 (1966).

[12] Parithosh and D. J. Srolovitz, *J. Appl. Phys.* **91**, 1963 (2002).

[13] A. G. Dirks and H. J. Leamy, *Thin Solid Films* **47**, 219 (1977).

[14] K. Muller, *J. Appl. Phys.* **58**, 2573 (1985).

CHAPTER 3

PREPARATION AND CHARACTERIZATION

In this study, magnetic-field-assisted pulsed laser deposition is employed as a new deposition method. The preparation of $BiFeO_3$ films is attempted, using the new deposition method. In this chapter, the magnetic-field-assisted pulsed laser deposition method is introduced, and characterization methods are described.

3.1 Preparation of $BiFeO_3$ Films

3.1.1 Pulsed laser deposition (PLD)

Film growth is very important for the advancement of the material science, and device applications, when the new materials of the single crystal and bulk have discovered and exploited. The film growth in vacuum processes has had an even greater impact. Among vacuum processes, evaporation and sputtering methods are well known for the film preparation. However, it is difficult to grow films of complex oxide materials by using evaporation and sputtering methods, because of the partial vapor pressure and sputtering yields of the composition. Therefore, by using a laser, complex oxide materials can be ablated and deposited onto the substrate.

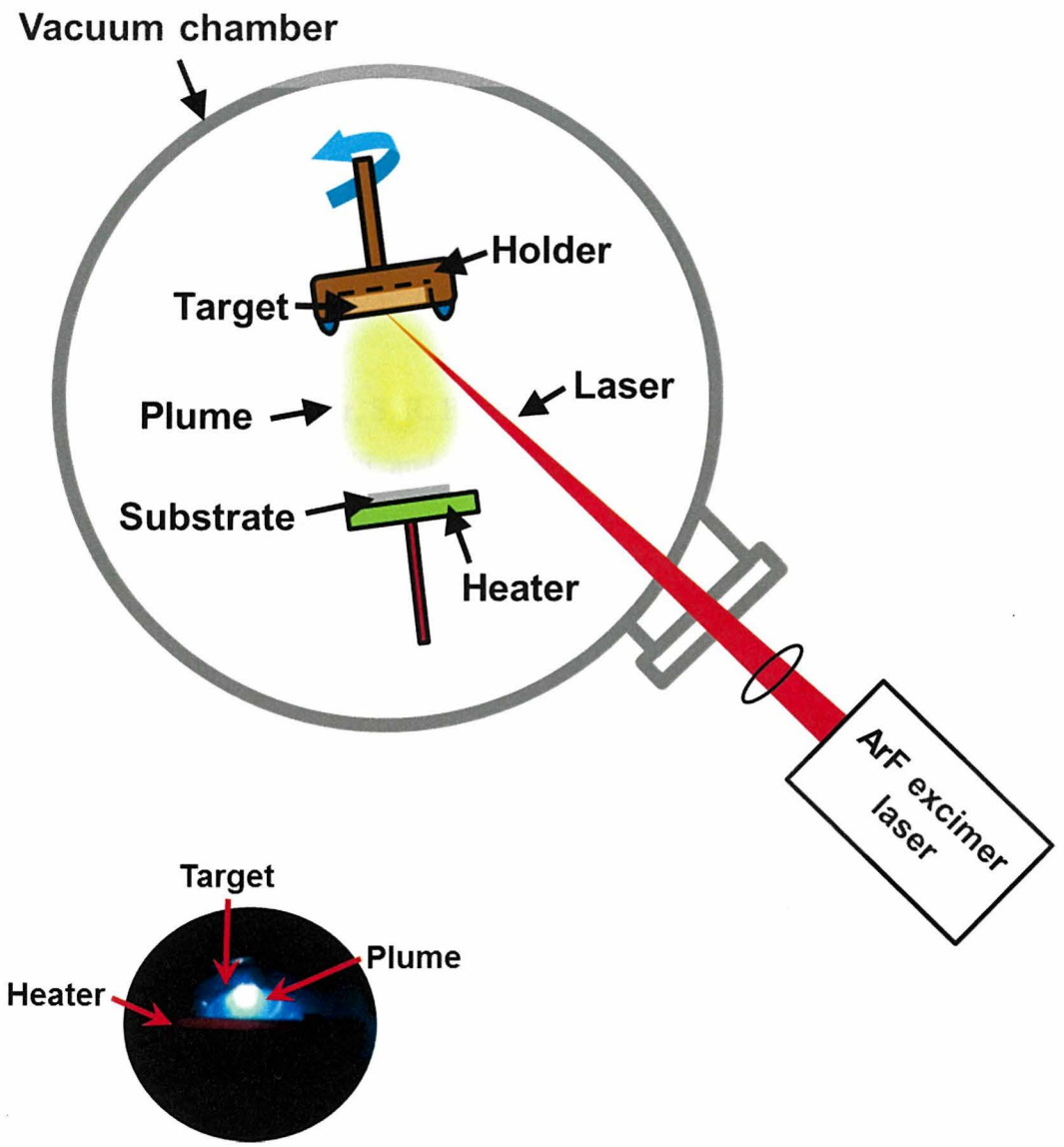

Figure 3.1. Schematic of the conventional pulsed laser deposition method and the plume produced by a laser ablation.

This method is the so-called the pulsed laser deposition method.

Figure 3.1 shows the schematic of the conventional pulsed laser deposition method. This method has attracted more attention after it was used successfully to grow high-temperature superconducting films. [3-5] Recently, the growth of nano-tubes and quantum dots by using a pulsed laser deposition method has been reported, the method was successfully used to prepare polycrystalline films and epitaxial films. [6-9]

The pulsed laser deposition is very simple. A pulse laser produced by an energy source in the outside chamber is focused onto a target. The interaction between the laser and the surface of the target takes place. Absorption and thermal diffusivity occur inside the target, as shown in Figs. 3.2(a) and (b). These phenomena allow the surface to reach a temperature high enough to ablate the target compositions. When a certain laser fluence value of a target is exceeded, naming ablation threshold, a plume is formed on the target surface, while all the components in the target are evaporated as shown in Fig. 3.2(c). After the laser pulse, the temperature around the surface is decreased to the initial temperature. The heated part that has molten is re-solidified as shown in Fig. 3.2(d). In order to keep the stoichiometry of the multi-component target, the fluence used for pulsed laser deposition is always above the threshold as shown in Fig. 3.2(e). Of course, the threshold value depends on the ablated material. The plume produced by a laser ablation above the threshold consists of highly excited and ionized species such as ions, atoms, and clusters. They interact with themselves or with the background gas. Electron excitation gives rise to the colored plume, and characteristic to the charge gas. This is due to the fact that an electrical breakdown in the material is generated by an electric field induced by the laser power density. [10] Next, the evaporated species are deposited on the substrate and this results in a layer (or film) of the re-condensed target material onto the substrate by migration and coalescence. During film growth using the pulsed laser deposition method, various parameters are included such as gas pressure, laser energy, pulse repetition rate (frequency), and distance between the target and the substrate.

The pulsed laser deposition method has some advantages in preparing films as compared with other deposition methods. One of the major advantages in pulsed laser

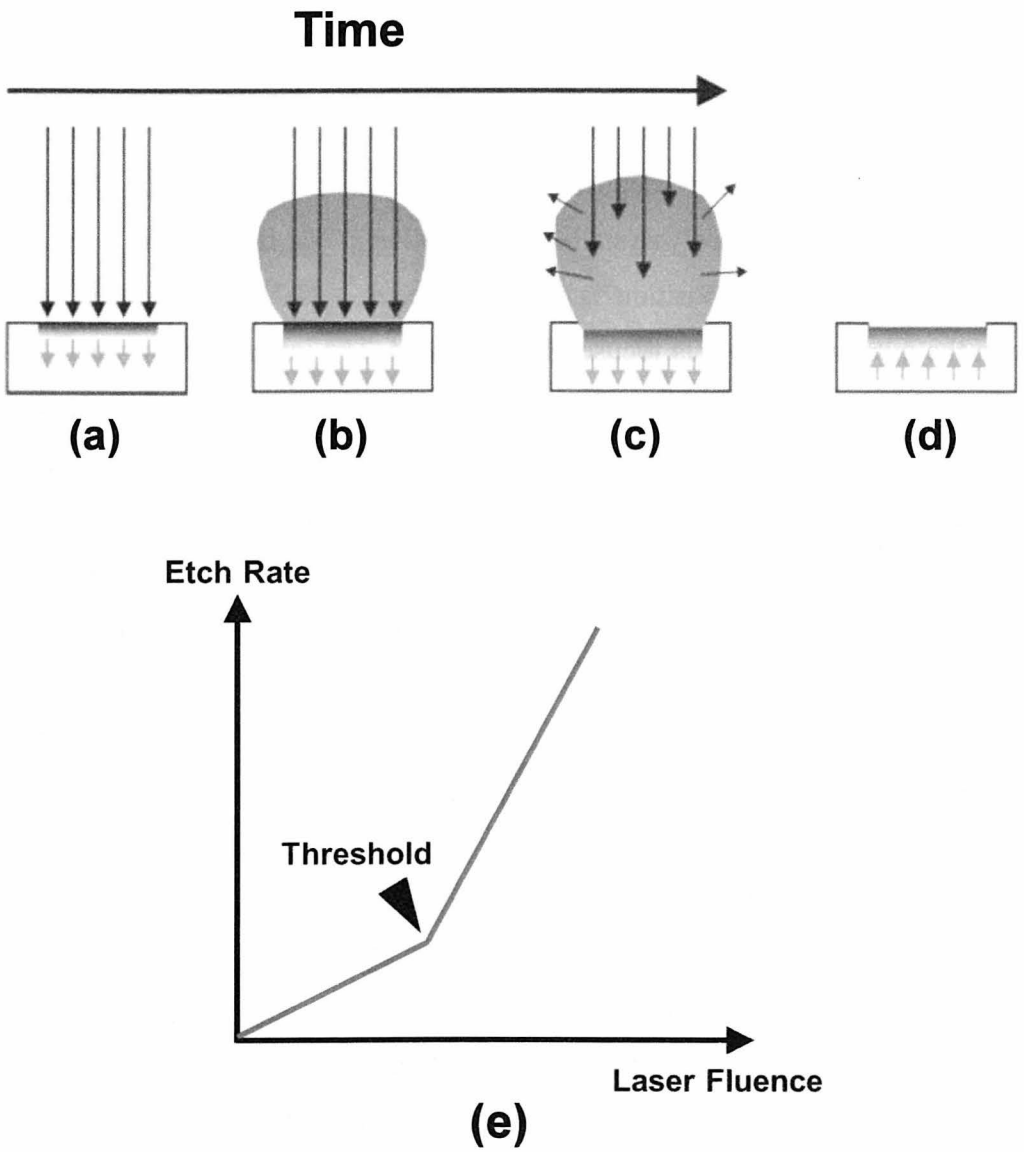

Figure 3.2. Schematic illustrating the principle of laser ablation. (a) Initial absorption of laser radiation represented by long arrows; initiation of melting and vaporization (the shaded area indicates the melted material, and the short arrows represent the motion of diffusivity). (b) Melt front propagates inside the target, vaporization continues and laser-plume interactions start. (c) Absorption of incident laser radiation, and formation of plume. (d) Melt front recedes leading to re-solidification. (e) Laser ablation threshold. [10]

deposition is the fact that a wide range of materials including metals, oxides, and polymers can be deposited, while the target area is smaller, due to the smaller spot size of the laser. Other advantages are being able to maintain the desired target composition in the deposited films and to aid crystallization under a lower substrate temperature due to the high kinetic energy of ions existing in the plume. [2, 11]

In addition, the working pressure for the preparation of films is not limited like in the case of the sputtering method using the plasma. Besides the advantages of the pulsed laser deposition method, there are noticeable some disadvantages. As mentioned above, even though a small target size is required due to the small spot size of the laser, unfortunately, the deposition over lager area is limited, and the distribution of the thickness is not homogeneous. Also, one of the major problems is the splashing, or droplets, associated with the laser ablation onto non smooth and dense targets. [2, 11] The size of a droplet might be as large as a few micrometers and the existence of droplets greatly affects the film growth as well as the electric properties of the films. Recently, it has been suggested that the off-axis and inset of the shadowing mask between the target and the substrate are effective when depositing large areas with uniform distribution of film thickness, and preventing splashing. [12, 13]

3.1.2 Magnetic-field-assisted pulsed laser deposition

Chapter 3.1.1 introduced the conventional pulsed laser deposition method. As mentioned above, the biggest advantage of the pulsed laser deposition method is that it is able to maintain desired target composition in the deposited film. In this study, a magnetic field was applied to the pulsed laser deposition method and this method is called the magnetic-field-assisted pulsed laser deposition. Figure 3.3(a) shows a schematic of the magnetic-field-assisted pulsed laser deposition method. Previously, several groups have attempted the preparation of films though the application of a magnetic field during a laser ablation. [14-16] They used a permanent magnet to apply a magnetic field. The distance affected by the magnetic field is short, due to the characteristics of the permanent magnet. Moreover, most experiments were conducted at low temperature or room temperature, because the magnetic

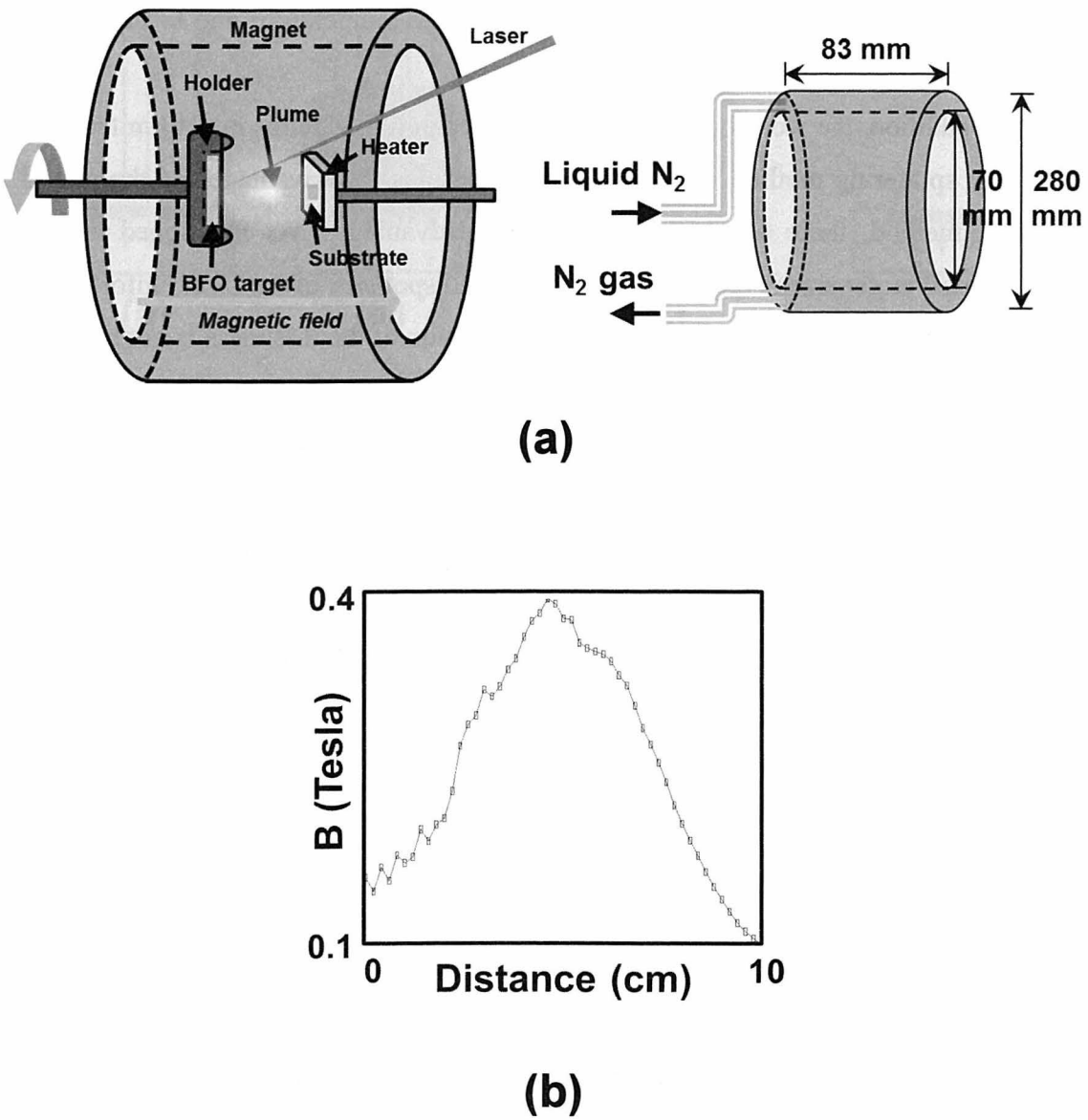

Figure 3.3. (a) Schematic of magnetic-field-assisted pulsed laser deposition method indicating magnet set in a vacuum chamber for applying magnetic field and (b) distribution of magnetic field strength for I = 40 A.

characteristics of a permanent magnet are deprived above 200°C. The best features of the magnetic-field-assisted pulsed laser deposition are the fact that the temperature does not need to be limited depending on the type of films prepared, and that the magnetic field is applied perpendicularly to the substrate during a laser ablation.

To apply a magnetic field, the cylinder magnet is set between the target and the substrate in a vacuum chamber. The magnet consists of a solenoid coil of an oxide-superconductive tape set in a liquid nitrogen container, of which inner diameter, outer diameter, and length are 70, 280, and 83 mm, respectively. Figure 3.3(b) shows the distribution of the magnetic field strength in a magnet for I = 40 A. A maximum magnetic field of 0.4 T can be applied to the substrate perpendicularly during a laser ablation and can be controlled from 0 T to 0.4 T. The use of a magnetic field with a laser-created plume has attracted a lot of attention recently, as the magnetic field can be used to better control the dynamic behavior of the plume. In the absence of the magnetic field, the collimation and stable state of the plume appear. In the presence of the magnetic field during a laser ablation, several interesting physical phenomena occur. It has been reported that the presence of a magnetic field during expansion of the plume causes the conversion of the plasma thermal energy into kinetic energy, plume confinement, ion acceleration, emission enhancement, and plume instability. [17] Other reports have also pointed out that the effect of the magnetic field on the dynamics of the laser-produced plume affects the film preparation. [18] The effective reduction of debris (particulate) by using magnetically guided pulsed laser deposition has also been demonstrated. [19] In these studies, the magnetic field was used to deflect the trajectory of evaporated species to the substrate, and separate only charge species. However, these works are very poor to understand film growth and the evolution of the microstructure and no works related to film growth and the evolution of microstructures under a magnetic field exist.

As mentioned above, the plume under a magnetic field has dynamical behaviors and includes interesting physical phenomena. The plume is an important factor in a pulsed laser deposition and significantly will affect the film growth and the evolution of microstructures. Accordingly, investigation of the effect of a magnetic field on film growth and the evolution of microstructures is very valuable.

In this study, the evolution of the microstructures of $BiFeO_3$ films prepared by magnetic-field-assisted pulsed laser deposition as well as the behavior of the plume under a magnetic field has been investigated in order to understand the effect of a magnetic field on film growth. The results and discussion are detailed in the following chapter.

3.1.3 Deposition of $BiFeO_3$ films

Before depositing $BiFeO_3$ films, the substrates ($Pt/TiO_2/SiO_2/Si$) were cleaned to remove any surface contamination. They were washed in acetone and 2-propanol with an ultrasonic bath and dried by blowing nitrogen. The $Bi_{1.1}FeO_3$ composition (Bi 10 % excess due to Bi loss during film growth) was used as a ceramic target. To deposit $BiFeO_3$ films, an ArF excimer laser with a wavelength of 193 nm was used. The laser repetition rate (f) was 5 Hz, and the laser fluence (J) was 3.7 J/cm^2. The pulse width was about 20 ns. The distance from the target to the substrate was about 5 cm. The base pressure in the vacuum chamber was ~ 5 x 10^{-6} Torr. A suitable oxygen pressure for the deposition of $BiFeO_3$ films was maintained in vacuum chamber. Under optimum deposition conditions, $BiFeO_3$ films were deposited up to the desired thickness. The detailed deposition conditions are presented in the following chapters. After the deposition of $BiFeO_3$ films, the substrate temperature was cooled to around 370°C and maintained for 10 min at suitable oxygen pressure. Then, the substrate temperature was cooled to room temperature (RT).

3.2 Characterization of $BiFeO_3$ Films

3.2.1 X-ray diffraction (XRD) analysis

X-ray diffraction (XRD) is one of the most powerful techniques for qualitative and quantitative analysis of crystalline compounds such as powder, bulk and film. The method can obtain information, including the crystal phase, structure, degree of crystallinity, and

orientation of any crystalline compound.

X-ray reflections from any crystal arise from the parallel planes inside the crystal. The orientation of the planes is defined by three integers, *h, k, l* called miller indices. The *h, k, l* cut the a-axis, b-axis and c-axis of the unit cell in *h, k, l* sections. For example, the 110 plane cuts the a-axis and b-axis in 1, but are parallel to the c-axis. These *h, k, l* induces show the order of diffraction along the unit cell axes a, b and c. When X-ray irradiates on a pair of parallel planes separated by spacing *d*, constructive or destructive interferences are scattered by the crystal plane in crystal, and incident X-rays make an angle with these planes. The diffraction peak is observed from the constructive interference of the X-ray scattered by planes. This condition is given by the equation of Bragg's law.

$$n\lambda = 2d\sin\theta. \tag{3.1}$$

The equation shows the relationship between the wavelength to angle of incidence and the lattice spacing, where n is a numeric constant, λ is the wavelength of the beam, d denotes the distance between lattice planes, and θ represents the angle of the diffracted wave.

In this study, the crystal structure of $BiFeO_3$ films was identified by XRD analysis (Rigaku, RINT 2000) which is a conventional θ-2θ scan. The 2 theta range was from 20° to 80°, and the scan speed was 0.02°/second; the slit was 0.15 mm. The radiation source was Cu K_α. The X-ray generator power was operated at 40 mA and 40 kV.

3.2.2 Scanning electron microscope (SEM)

The scanning electron microscope (SEM) is a well-known tool that facilitates the investigation of solid specimens. The electron microscope uses a scanning beam of electrons to scan the surface of specimens, and it has a greater resolution than the optical microscope. The SEM consists of an electron gun, magnetic lenses and a detector in vacuum column. The basic principle of SEM is the following: A stream of electrons produced by an electron gun in high vacuum is accelerated toward the surface of the specimen;

It is confined and focused by passing through apertures and magnetic lenses. The surface of the specimen is irradiated by the focused beam and an interaction occurs inside the specimen. When the specimen interacts with the electron beam, various species from the specimen are scattered. Among them, secondary electrons are topography associated. The collector serves as a collection of electrons. They are subsequently transformed to an image.

In this study, the surface morphologies and cross-sectional images of $BiFeO_3$ films were observed by SEM (Hitachi, S-4800).

3.2.3 Current density measurement

To measure electric properties such as current density, Pt dots as top electrodes were formed through a shadow mask, using RF sputtering at room temperature (RT) as shown in Fig.3.4. Circular Pt top electrodes are about 200 nm-thick and have a diameter of about 200 μm. In this study, leakage current versus electric field (*J-E*) characteristic was measured with a semiconductor parameter analyzer (Agilent, 4155C). The leakage current characteristic used staircase of waveform involving step and delay time as shown in Fig.3.5. The ramp step and delay time were 0.01 V and 0.1 sec, respectively.

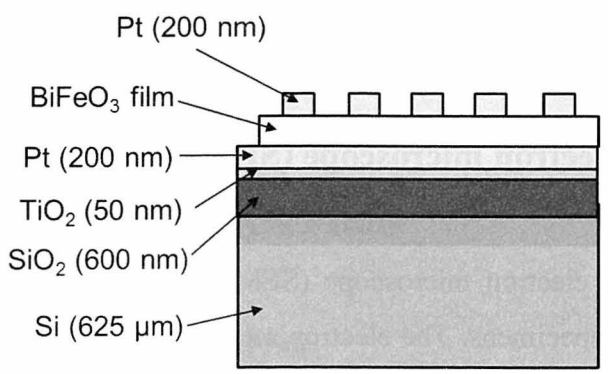

Figure 3.4. Sample structure for measuring the electric and ferroelectric properties of polycrystalline $BiFeO_3$ films.

3.2.4 Ferroelectric properties measurement

The ferroelectric polarization versus electric field (*P-E*) hysteresis loop includes important parameters such as remanant polarization (P_r) and coercive field (E_c), used to characterize ferroelectric materials. The Sawyer and Tower circuit is the most conventional method used in *P-E* hysteresis loop measurements. [20] Unfortunately, this circuit cannot accurately evaluate ferroelectric properties such as polarization and coercive field in the *P-E* hysteresis loop, as the leakage current is superposed on the capacitor current. Recently, the virtual ground QV method has been employed. Because the virtual ground QV circuit has a higher resolution than the Sawyer-Tower method, the ferroelectric properties can be evaluated more accurately as shown in Fig. 3.6. [21]

In this study, the *P-E* hysteresis loops of all $BiFeO_3$ films were measured using the ferroelectric test system (Toyo Co., FCE-1). The used signal was a triangular waveform.

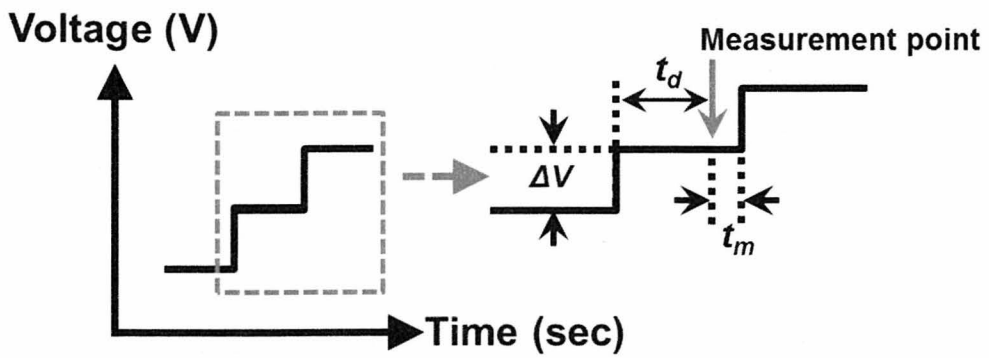

Figure 3.5. DC voltage step of current density measurement, where t_d is the delay time in a staircase DC bias.

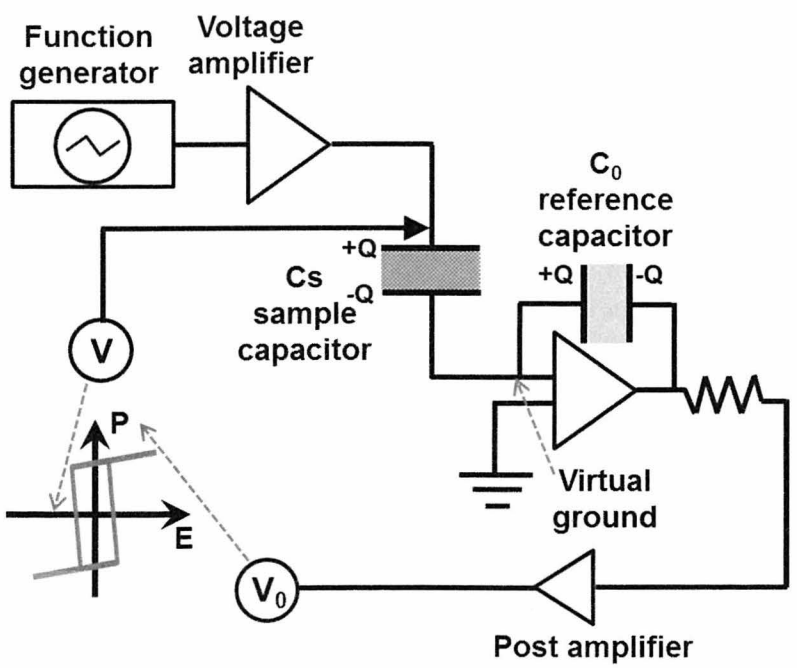

Figure 3.6. Schematic diagram of virtual ground QV method for measuring ferroelectric *P-E* hysteresis loop.

References

[1] H. M. Smith and A. F. Turner, *Appl. Optics* **4**, 147 (1965).

[2] D. B. Shrisey and G. K. Hubler, "Pulsed Laser Deposition of Thin Films", John Wiley, New York, 1994.

[3] J. G. Bednorz and K. A. Muller, *Phys. B* **64**, 198 (1986).

[4] D. K. Fork, F. A. Ponce, J. C. Tramontana, and T. H. Geballe, *Appl. Phys. Lett.* **58**, 2294 (1991).

[5] D. Dijkkamp, T. Venkatesan, X. D. Wu, S. A. Shaheen, N. Jisrawi, Y. H. Lee, W. L. McLean, and M. Croft, *Appl. Phys. Lett.* **51**, 619 (1987).

[6] K. Nagashima, T. Yanagida, H. Tanaka, and T. Kawai, *J. Appl. Phys.* **101**, 124304 (2007).

[7] S. Choopun, H. Tabata, and T. Kawai, *J. Crys. Growth* **274**, 167 (2005).

[8] J. M. Park, S. Nakashima, F. Gotoda, T. Kanashima, and M. Okuyam, *Jpn. J. Appl. Phys.* **48**, 09KB03 (2009).

[9] J. M. Park, T. Kanashima, M. Okuyama, S. Nakashima, K. M. Kim, J. Y. Lee, and H. Y. Lee, *J. Kor. Phys. Soc.* **58**, 674 (2011).

[10] N. R. Ashfold, F. Claeyssens, G. M. Fuge, and S. J. Henley, *Chem. Soc. Rev.* **33**, 23 (2004).

[11] P. R. Willmott and J. R. Huber, *Rev. Mod. Phys.* **72**, 315 (2000).

[12] K. L. Chen, J. H. Chen, H. C. Yang, and H. E. Horng, *Physica C* **372**, 1078 (2002).

[13] K. Kinoshita, H. Ishibashi, and T. Kobayashi, *Jpn. J. Appl. Phys.* **33**, L417 (1994).

[14] X. K. Shen, Y. F. Lu, T. Gebre, H. Ling, and Y. X. Han, *J. Appl. Phys.* **100**, 053303 (2006).

[15] V. N. Rai, J. P. Singh, F. Y. Yueh, and R. L. Cook, *Laser and Particle Beams* **21**, 65 (2003).

[16] C. Pagano, S. Hafeez, and J. G. Lunney, *J. Phys. D: Appl. Phys.* **42**, 155205 (2009).

[17] S. S. Harial, M. S. Tillack, B. O'Shay, C. V. Bindhu, and F. Najmabadi, *Phys. Rev E* **69**, 026413 (2004).

[18] Y. Y. Tsui, H. Minami, and R. Fedosejevs, *J. Vac.Sci. Technol. A* **20**, 744 (2002).

[19] M. Tachiki and T. Kobayashi, *Electrical Engineering in Japan* **130**, 88 (2000).

[20] C. B. Sawyer and C. H. Tower, *Phys. Rev.* **35**, 269 (1930).

[21] Toyo Corp. technical note for ferroelectric test system.

CHAPTER 4

PREPARATION OF POLYCRYSTALLINE $BiFeO_3$ FILMS ON $Pt/TiO_2/SiO_2/Si$ SUBSTRATE

In this chapter, polycrystalline $BiFeO_3$ films on $Pt/TiO_2/SiO_2/Si$ substrate are prepared under optimized deposition conditions by using magnetic-field-assisted pulsed laser deposition. In addition, thick $BiFeO_3$ columnar films and $BiFeO_3$ films prepared by 90° off-axis deposition are characterized.

4.1 Introduction

Polycrystalline $BiFeO_3$ films on $Pt/TiO_2/SiO_2/Si$ substrate have giant polarization values and have been prepared by using various deposition methods. [1] In this study, magnetic-field-assisted pulsed laser deposition as a new deposition method was used for the preparation of $BiFeO_3$ films. In chapter 2, the trajectory of the plume and the evolution of microstructures under a magnetic field were investigated. The preliminary results obtained from simulations were confirmed that under a magnetic field, the evaporated species in the plume reveal conical flux, and the trajectory of the plume is modified and confined.

In addition, the conical flux resulted in dynamic evolution of the microstructure, such as the formation of the columnar structures.

In this chapter, based on the simulated results, the effect of the magnetic field on the plume and the evolution of microstructures is investigated though experiments. Polycrystalline $BiFeO_3$ films on $Pt/TiO_2/SiO_2/Si$ substrate are prepared by using the magnetic- field-assisted pulsed laser deposition under optimized conditions. The effect of the magnetic field on the preparation of polycrystalline $BiFeO_3$ films is investigated, and the microstructure, crystal structure, and electric properties of polycrystalline $BiFeO_3$ films prepared under a magnetic field are characterized.

4.2 Polycrystalline $BiFeO_3$ Films Prepared under Various Magnetic Fields

4.2.1 Preparation of $BiFeO_3$ films

Polycrystalline $BiFeO_3$ films were prepared on a Pt (150 nm) / TiO_2 (50 nm) / SiO_2 (600 nm) / Si (625 μm) substrate using the magnetic-field-assisted pulsed laser deposition method with a $BiFeO_3$ ceramic target (Bi 10% excess because of volatilization of Bi). The films were deposited at 520°C and an oxygen pressure of 0.1 Torr for deposition time of 30 min, using an ArF excimer laser (λ = 193 nm) with an energy of 130 mJ and a frequency of 5 Hz. The deposition conditions are listed as shown in Table 4.1.

Table 4.1. Deposition conditions for the preparation of polycrystalline $BiFeO_3$ films

Material	Temperature	O_2 pressure	Frequency	Magnetic field	Depo. time
$BiFeO_3$	520°C	0.05 Torr	5 Hz	0 T	30 min
$BiFeO_3$	520°C	0.1 Torr	5 Hz	0.1 ~ 0.3 T	30 min

4.2.2 Shape and emission spectrum of the plume under magnetic field

Before the preparation of the polycrystalline $BiFeO_3$ films, the shape of the plume was experimentally observed by using a streak camera (Hamamatsu, C4187) as illustrated in Fig. 4.1. In the measurement, the oxygen pressure in the vacuum chamber was set to 0.05 Torr, and the laser power was set to 130 mJ. The magnetic field was controlled from 0 T to 0.4 T. After laser was irradiated in the vacuum chamber, the exposure time for measuring the shape of the plume was 1 ms, and each image was obtained from a single laser pulse. Figures 4.2(a)-(e) show the shape of the plume under various magnetic fields. Although the color of each image represents the emission intensity, they are not necessarily representative of the total flux, because a part of the plume is not luminescent.

The shape of the plume without a magnetic and under a magnetic field shows several differences. The plume without a magnetic field expands freely, and the split of the plume occurs. This is typical behavior in the case of the straight path of the plume without a magnetic field. The split of the plume is often found due to the existence of both fast components and slow components in the plume emitted from a target. On the other hand, the shape of the plume under a magnetic field is modified. The confinement of the plume was evident with increasing a magnetic field, while the plume expands vertically along the direction of the magnetic field. These results are in agreement with the simulated result on the behavior of the plume under a magnetic field as mentioned in chapter 2.1. The confinement of the plume strongly supports the fact that the plume is made up mainly of charge species deflected by magnetic field. Typically, the angular distribution of the plume is well known that it follows cosine function. [2-5]

$$f(\theta) = \cos^n\theta. \tag{4.1}$$

When n increases in the cosine function, the angular distribution of the plume is confined. This relationship is often found for the plume which exists in various background gas pressures. D. J. Lichtenwainer *et al.*, observed the behavior of the plume over wide range of an oxygen pressures. They reported that the confinement of the plume was observed under

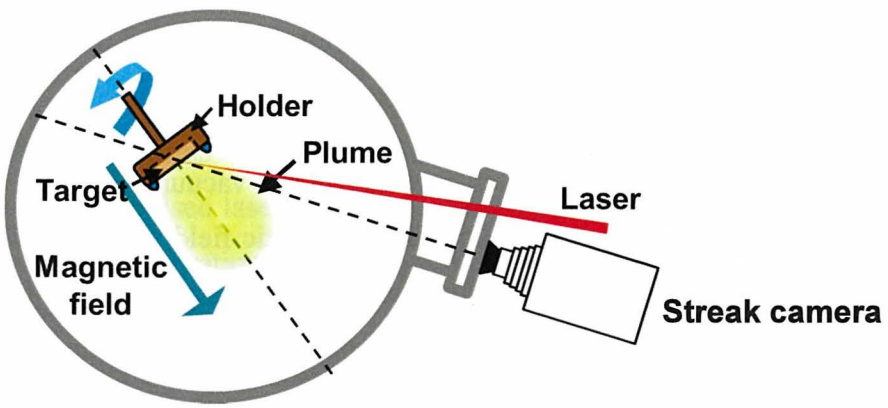

Figure 4.1. Schematic of measurement for observing the shape of a plume under magnetic field by using streak camera.

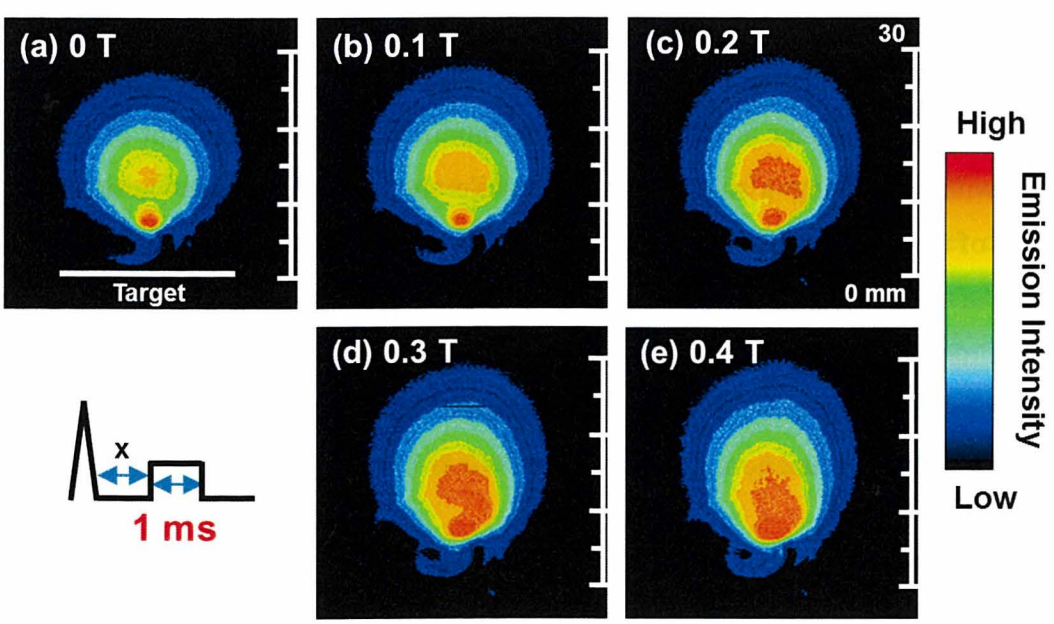

Figure 4.2. Observation of a plume under magnetic fields of (a) 0 T, (b) 0.1 T, (c) 0.2 T, (d) 0.3 T, and (e) 0.4 T.

a high oxygen pressure, and it caused a high deposition rate due to the confined angular distribution. [6] In the present results, while the shape of the plume is controlled by only a magnetic field, the plume could be confined by a magnetic field, regardless of the background gas pressure. The n can be changed by changing the magnetic field strength. While n is increased by increasing a magnetic field, the deposition rate is increased with the confinement of the plume. This result proposes that applying a magnetic field is also useful for the preparation of films under a high deposition rate in a wide range of gas pressures, regardless of the gas pressure, although the background gas pressure is a sensitive factor in the preparation of oxide films.

Figures 4.3(a)-(h) and (i)-(p) show the time-resolved plume images under magnetic field of 0.4 T and 0 T, respectively. The exposure time for the measurement of the plume is 0.07 μs. The plume at 0 T and 0.4 T expands gradually with time. However, the expansion of the plume under a magnetic field has a longer lifetime than that without a magnetic field. This might be due to the dynamic plume confined by a magnetic field. Many authors have already reported the influence of external magnetic field on laser-produced plume. These reports confirmed that the plume is confined by a magnetic field and as a result, the emission intensity of the plume is enhanced, due to the probability of electron-atom/ion collisions. [7-10] In present result, the confinement of the plume was confirmed in the presence of the magnetic field as shown in Fig. 4.2. Based on above fact, the enhancement of the emission intensity can be suggested and as a result, the long lifetime of the plume might be contributed.

Apart from the changes in the shape of the plume under a magnetic field, observing the spectroscopy of the plume under a magnetic field is also important. The information is useful for understanding the dynamics of the plume and preparing films. In order to investigate the spectroscopy of the plume, the optical emission spectrum of the plume without a magnetic field and under a magnetic field was measured. The emission lines were identified based on NIST atomic spectra database. [11] Figure 4.4 shows a comparison of the optical emission spectra for the plume without a magnetic field and under a magnetic field at a given range of the wavelength. The black and red lines represent the emission intensity of the plume without a magnetic field and under a magnetic field of 0.4 T. The emission intensity under a magnetic field of 0.4 T is significantly enhanced in comparison with that without a

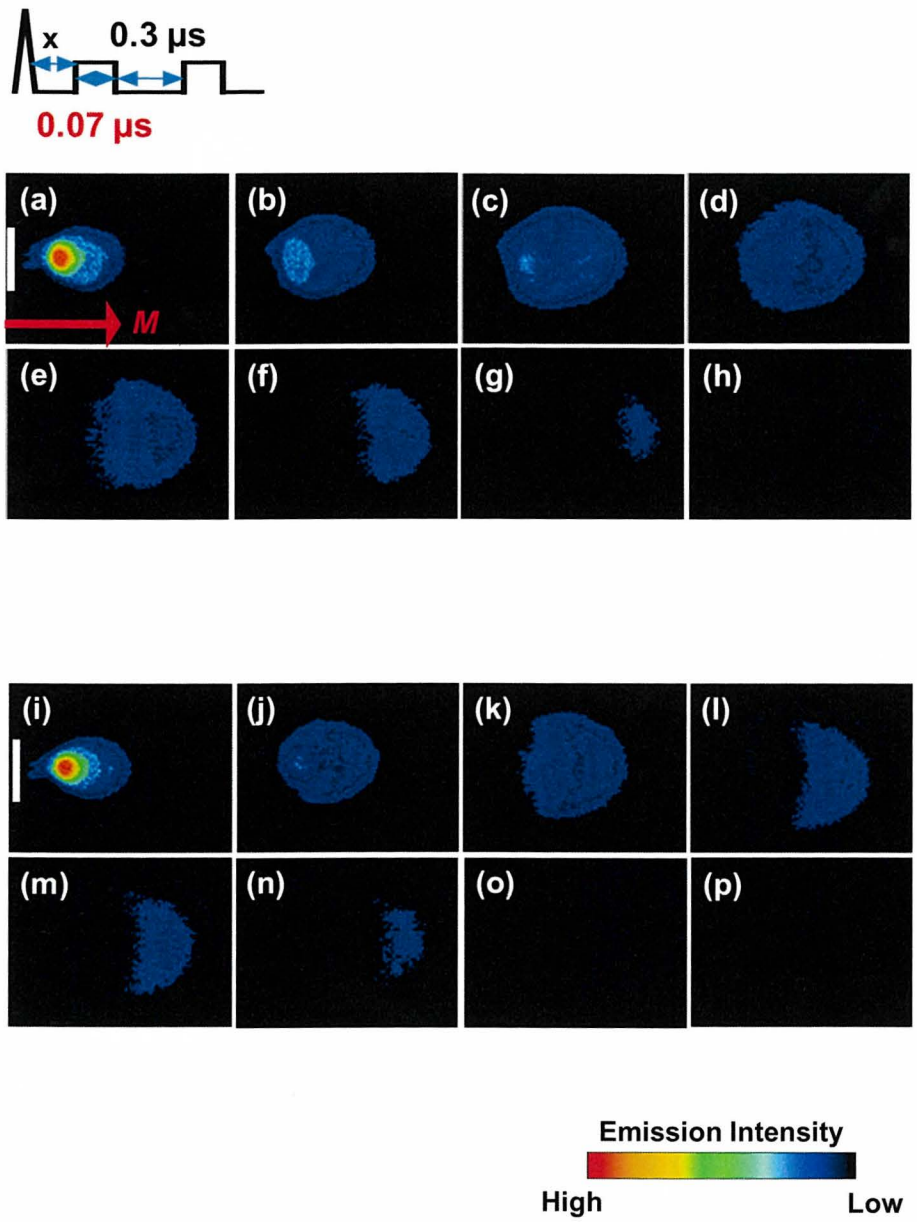

Figure 4.3. The time-resolved plume images for magnetic fields of (a)-(h) 0.4 T and (i)-(p) 0 T.

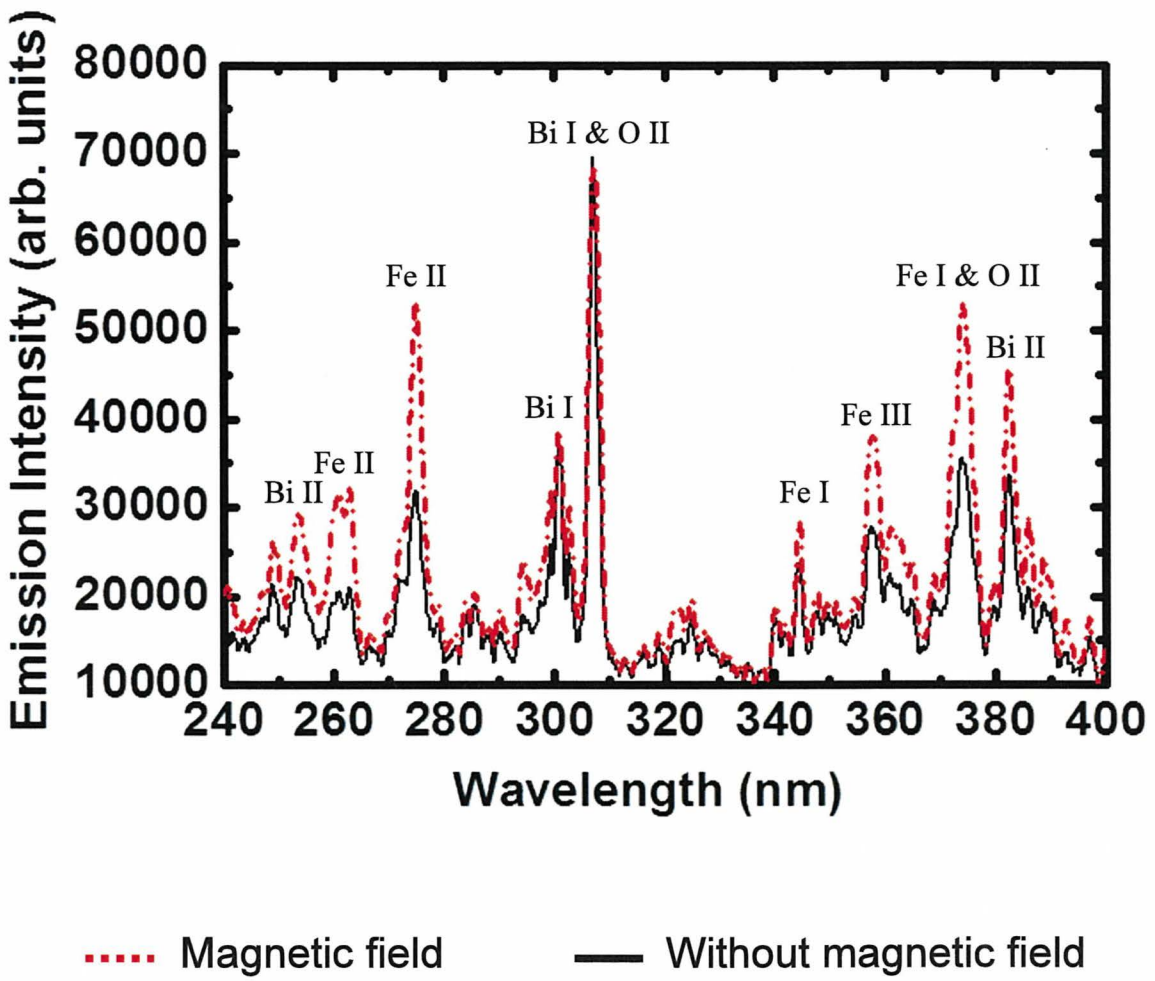

Figure 4.4. Comparison of the emission intensity spectrum for the plume under a magnetic field of 0.4 T and without a magnetic field. The red line represents the emission spectrum for a magnetic field of 0.4 T, and the black line represents the emission spectrum without a magnetic field. (I , II, and III represent ionization stages one, two, and three). [11]

magnetic field. The emission line intensity in the presence of the magneticfield was significantly enhanced, although all emission line intensity under a magnetic field was not enhanced. This supports the fact that the confinement of the plume under a magnetic field causes the enhancement of the emission intensity. Also, this agrees well with results on the optical emission intensity of the plume under a magnetic field. [7, 8, 12, 13] Consequently, in the presence of the magnetic field, the plume is confined, and this can result in the enhancement of emission intensity, whereas the free expansion of the plume appears without a magnetic field.

Based on these results, the preparation of polycrystalline $BiFeO_3$ films was carried out. The phase diagram based on the phases of polycrystalline $BiFeO_3$ films prepared under various deposition conditions. The phase diagrams for polycrystalline $BiFeO_3$ films prepared without a magnetic field and under a magnetic field are shown in Figs. 4.5(a) and (b). At temperatures lower than 500°C, mixed Bi_2O_3 and Fe_2O_3 phases exist in both phase diagrams. In the case of the film preparation without a magnetic field, the pure polycrystalline $BiFeO_3$ phase could be obtained around 520°C and 0.05 Torr. At this regime, when increasing an oxygen pressure, a Bi_2O_3 phase with pure polycrystalline $BiFeO_3$ phase exists. Also, when decreasing an oxygen pressure, a Fe_2O_3 phase with $BiFeO_3$ phase exists. However, above 550°C, regardless of the oxygen pressure, a rich Fe_2O_3 phase with polycrystalline $BiFeO_3$ phase is dominant, due to the Bi and Bi_2O_3 loss in the $BiFeO_3$ film.

On the other hand, the regime of pure polycrystalline $BiFeO_3$ films under a magnetic field was shifted to a high oxygen pressure. The pure polycrystalline $BiFeO_3$ phase could be obtained around 520°C and 0.1 Torr. Also, when increasing a temperature, regardless of the oxygen pressure, a Fe_2O_3 phase with polycrystalline $BiFeO_3$ phase is dominant similar to the case of the film preparation without a magnetic field. The shift in the regime of the pure polycrystalline $BiFeO_3$ phase under a magnetic field is likely to be due to the difference of the plume state. As shown in Fig. 4.4, the emission spectrum of the plume under a magnetic field differs from that without a magnetic field. While the emission intensity of the plume under a magnetic field is increased, the charge species in the plume is significantly enhanced due to the enhancement of the ionization. These facts suggest that the plume under a magnetic field causes dynamically chemical reaction. As a result, the shift in the regime of

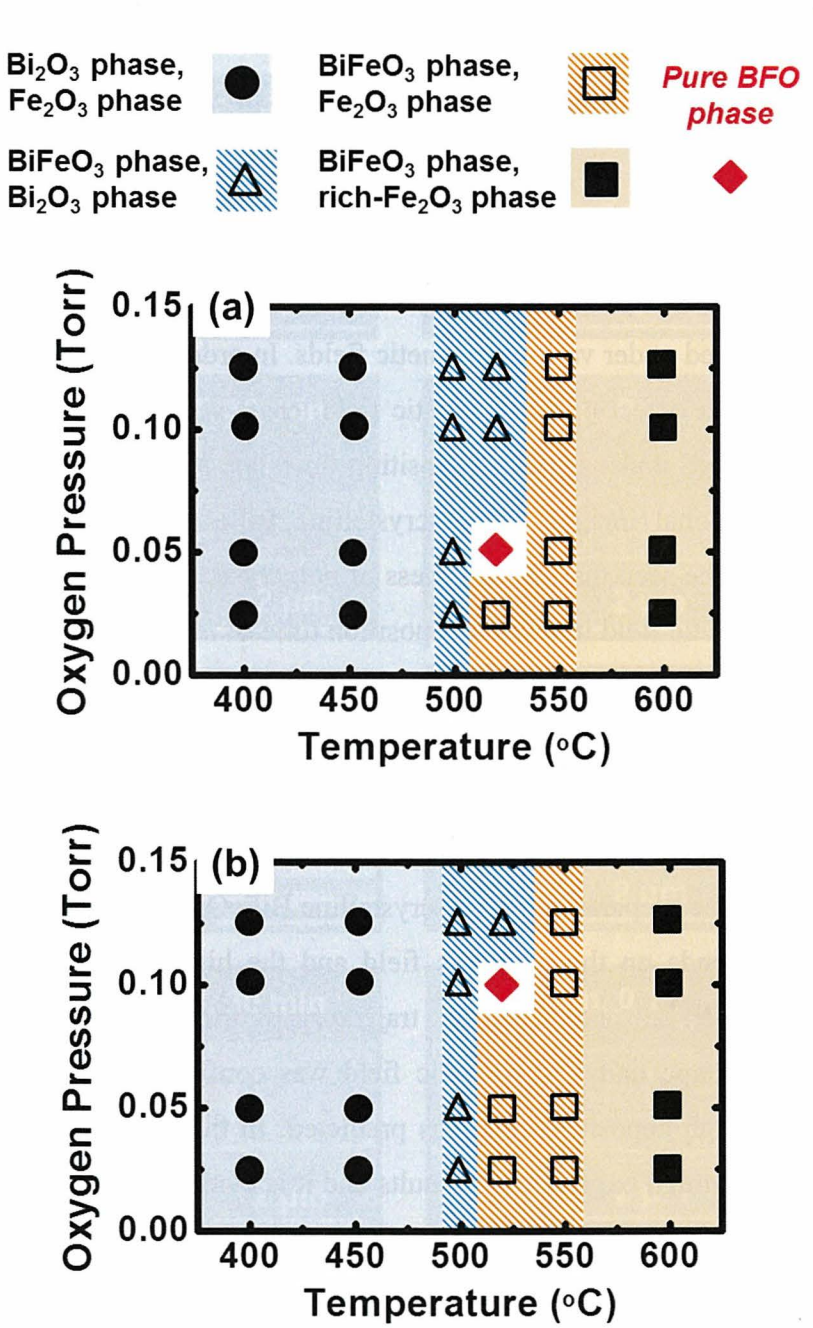

Figure 4.5. Phase diagrams of polycrystalline $BiFeO_3$ films prepared (a) without a magnetic field and (b) under magnetic fields of 0.1 T, 0.2 T, and 0.3 T.

the optimized deposition condition occurs.

4.2.3 Microstructure of $BiFeO_3$ films prepared under various magnetic fields

Figures 4.6(a), (c), (e), and (g) show cross-sectional images of polycrystalline $BiFeO_3$ films prepared under various magnetic fields. In order to investigate the change of the microstructure on the effect of the magnetic field, cross-sectional images of polycrystalline $BiFeO_3$ films prepared under various deposition times are shown in Figs 4.6(b), (d), (f), and (h). The cross-sectional images of polycrystalline $BiFeO_3$ films prepared under various magnetic fields can be seen that the thickness of polycrystalline $BiFeO_3$ films is increased by increasing the magnetic field in a fixed deposition time of 30 min, whereas the film thickness is increased with increasing a deposition time for polycrystalline $BiFeO_3$ films prepared under various deposition times. The film thickness for a magnetic field of 0.3 T and a deposition time of 30 min was about 1.1 μm, whereas the film thickness for a magnetic field of 0 T and a deposition time of 60 min was about 1.2 μm as shown in Figs. 4.6(g) and (h). This means that in the preparation of polycrystalline $BiFeO_3$ films under a magnetic field, the film thickness depends on the magnetic field and the high deposition rate is caused. As mentioned in chapter 2.2 and 4.2.2, the trajectory of the plume was concentrated to the substrate, and its shape under a magnetic field was confined. Based on these results, the possibility of the high deposition rate was predicted. In the present chapter, the predictions are demonstrated through experimental results and it is evident that applying a magnetic field gives rise to the high deposition rate as well as effective reaching of evaporated species.

On the other hand, the microstructure of polycrystalline $BiFeO_3$ films prepared under magnetic fields and the deposition times is notably different. Even though the microstructure of polycrystalline $BiFeO_3$ films prepared under various deposition times is a granular structure, polycrystalline $BiFeO_3$ films prepared under a magnetic field show a columnar structure. The distinct microstructure is thought as consequence of the trajectory of the plume modified under a magnetic field. As discussed in chapter 2, the simulation results were

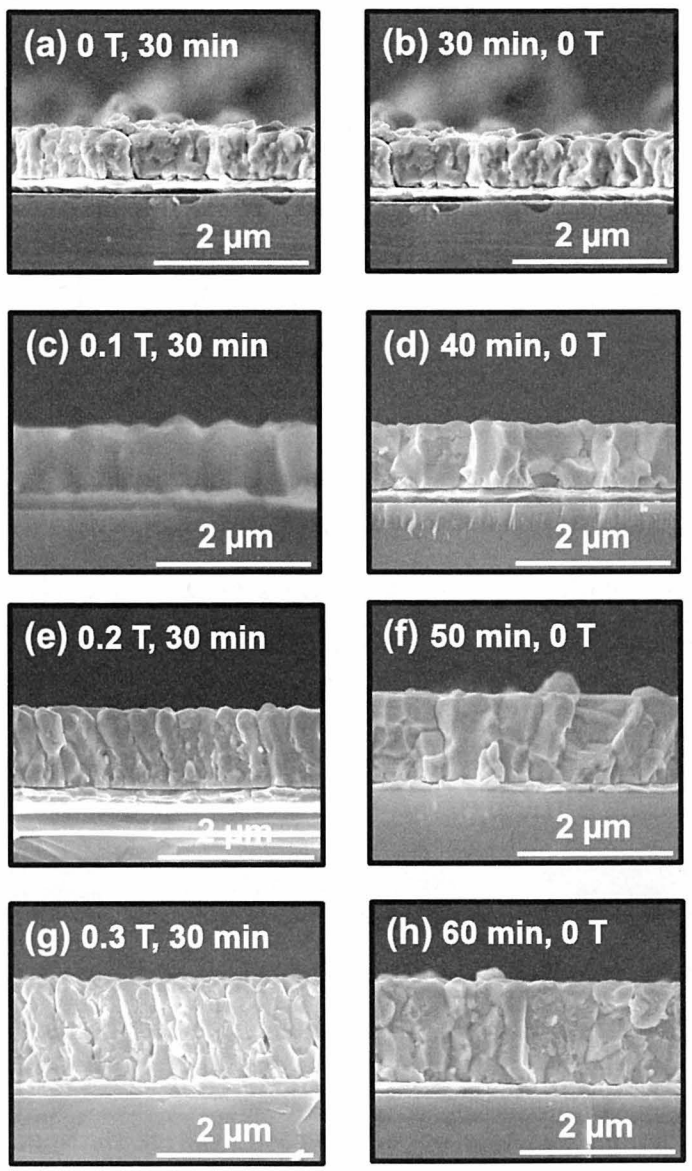

Figure 4.6. Cross-sectional images of polycrystalline $BiFeO_3$ films prepared under magnetic fields of (a) 0 T, (c) 0.1 T, (e) 0.2 T, and (g) 0.3 T for a deposition time of 30 min, and deposition times of (b) 30 min, (d) 40 min, (f) 50 min, and (h) 60 min without a magnetic field.

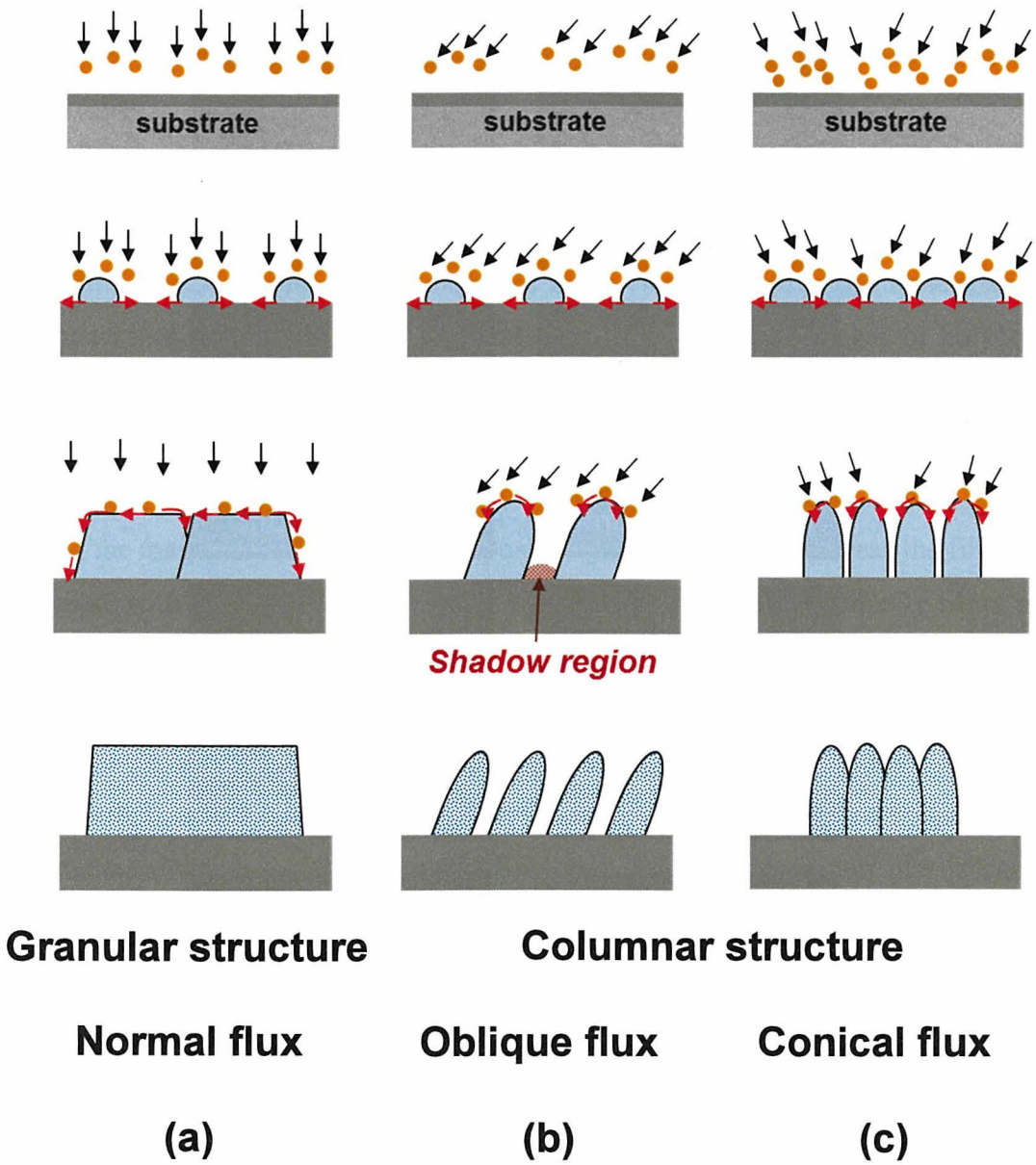

Figure 4.7. Mechanism of the microstructure evolution for (a) normal, (b) oblique, and (c) conical flux.

identified that the flux angle of evaporated species was attributed to the evolution of microstructures. Under the conical flux caused by a magnetic field, the columnar structures appeared as shown in Figs 2.4 and 2.5. Experimentally observed result confirmed the columnar structure for polycrystalline $BiFeO_3$ films prepared under a magnetic field, and demonstrated the predicted results through the simulation.

To help understanding of the present experimental result, the mechanism of the microstructure evolution of polycrystalline $BiFeO_3$ films prepared under a magnetic field is illustrated in Fig. 4.7. In the initial stage, the nucleus is formed by nucleation onto the surface of the substrate for normal, oblique, and conical flux. In the case of the normal flux, after nucleation, island growth and coalescence of islands occur, and a film growth continues. [14, 15] Finally, the growth of the lateral direction is significant while film thickening continues. On the other hand, in comparison with the normal flux, the growth mechanism for the oblique flux and the conical flux is different, because the flux is not parallel to the substrate normal. The oblique flux without a magnetic field and the conical flux under a magnetic field arrive onto the substrate at an incident angle. They predominantly reach the top of the nucleus, rather than the surface of the substrate. [16-18] In the case of the oblique flux from one side, the region behind the nucleus is not reached any evaporated species, because of a shadow effect. [16-18] The evaporated species will only be deposited onto the nucleus, and the columnar structure will develop. The feature for the oblique flux from one side is that columns are tilted along the direction of the oblique angle, and the columnar structure becomes porous, when the oblique angle becomes large. [16-18] In the case of the conical flux from both sides caused by a magnetic field, the mechanism of the evolution of microstructures shows somewhat difference. The growth rate on the top of the nucleus is faster than that of the substrate surface, because the top of nucleus intercepts the evaporated species before they can reach the substrate surface. However, in contrast with the oblique flux from one side, the conical flux arrives from all directions, and this gives rise to dense columnar structure in comparison with the columnar structure formed by the oblique flux from one side. Consequently, the feature of the conical flux under a magnetic field is that the dense columnar structure can be obtained, because of the flux from all directions.

Surface morphologies for polycrystalline $BiFeO_3$ films prepared under various

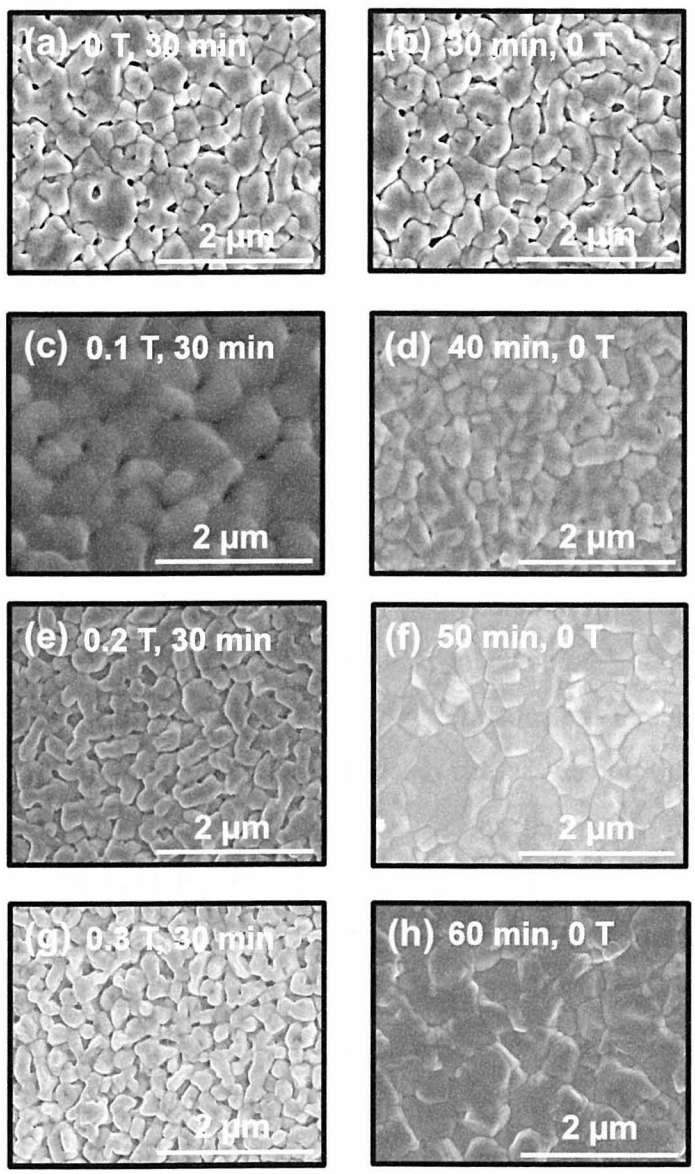

Figure 4.8. Surface morphologies of polycrystalline $BiFeO_3$ films prepared under magnetic fields of (a) 0 T, (c) 0.1 T, (e) 0.2 T, and (g) 0.3 T for a deposition time of 30 min, and deposition times of (b) 30 min, (d) 40 min, (f) 50 min, and (h) 60 min without a magnetic field.

magnetic fields and deposition times show a great difference in grain size as shown in Figs. 4.8(a)-(h). Generally, the grain size of polycrystalline films with film thickening is increased, likely due to the impingement of grains and the stress relaxation. [19] Even though the grain size of polycrystalline $BiFeO_3$ films prepared under various deposition times becomes large with increasing a film thickness, that of polycrystalline $BiFeO_3$ films prepared under various magnetic fields become small with increasing a film thickness. This is originated from the microstructure. As mentioned above, the migration of the grain growth to lateral direction is suppressed, and this results in a small grain size because a formation of the columnar structure is dominant to the growth of the vertical direction.

Based on above results, it can be considered that the plume under a magnetic field has two features. One feature is the modified trajectory of the plume including the conical flux. The other feature is a high deposition rate. As a result, a columnar structure was formed in the preparation of polycrystalline $BiFeO_3$ films by using magnetic-field-assisted pulsed laser deposition. Previously, it was suggested that the formation of columnar structures is due only to the conical flux. Here, we come across the following question. "Is it possible to form a columnar structure under a high deposition rate?" To investigate the microstructure at a high deposition rate without a magnetic field, polycrystalline $BiFeO_3$ films were prepared at a high deposition rate, by using the repetition rate as a kinetic parameter of the pulsed laser deposition.

Figures 4.9(a), (c), (e), and (g) show cross-sectional images of polycrystalline $BiFeO_3$ films prepared under various repetition rates for a deposition time of 30 min and a magnetic field of 0T. The film thickness was increased with increasing the repetition rate, from 5 Hz to 20 Hz, in a fixed deposition time of 30 min. The film thickness is 400 nm and 1.2 μm for 5 Hz and 20 Hz, respectively. Although the repetition rate is 4 times higher, the film thickness is not proportional to the repetition rate. This result is thought to be derived from the interaction between the laser and the target. Generally, the laser irradiates the surface of the target and absorption and thermal diffusivity inside the target are triggered. [20-22] While the heat is accumulated inside the target, it reaches temperature high enough to ablate the target compositions. [23] When the ablation threshold of the target is exceeded, a plume is formed. At a high repetition rate, the interval time between two pulses is not long

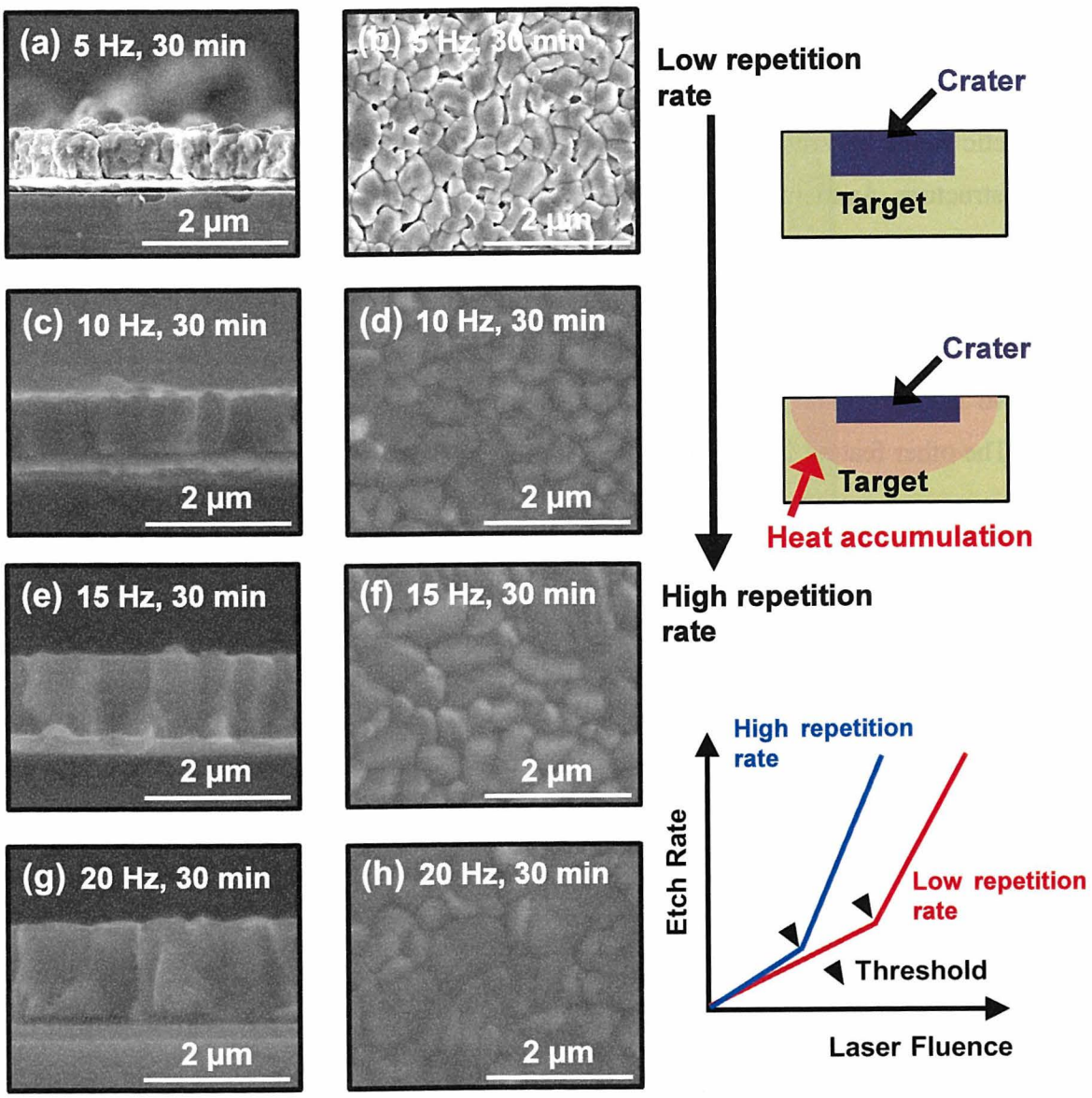

Figure 4.9. Cross-sectional images and surface morphologies of polycrystalline $BiFeO_3$ films prepared under various repetition rates. (a), (b) 5 Hz; (c), (d) 10 Hz; (e), (f) 15 Hz; (g), (h) 20 Hz, for a deposition time of 30 min and a magnetic field of 0 T, respectively.

enough to cool the material down to the initial temperature. [24] The heat accumulation inside the target is due to the big number of pulses caused by the high repletion rate. This ablation threshold at high repetition rate should be lower than that at low repetition rate. A lower ablation threshold causes better ablation efficiency, but the laser fluence is decreased. [23-25] It is suggested that the laser fluence contributes to the evaporation rate of species, and when the deposition time is longer, the film thickness is not proportional to the repetition rate due to the reduction of the evaporation rate. However, applying a magnetic field during a laser ablation is more effective for a high deposition process, because the magnetic field only influences the plume, regardless of the interaction between the laser and the target. In addition, when the repetition.n rate is increased, polycrystalline $BiFeO_3$ films under high deposition rate show a granular structure similar to the microstructure of polycrystalline $BiFeO_3$ films prepared under various deposition times. It is demonstrated that columnar structures are not formed by the high deposition rate, and the flux angle of the evaporated species plays an important role for the formation of the columnar structure.

Figures 4.9(b), (d), (f), and (h) show surface morphologies of polycrystalline $BiFeO_3$ films prepared under various repetition rates for a deposition time of 30 min and a magnetic field of 0 T. This shows that the grain size increases with increasing repetition rate. This result is similar to that obtained in the case of polycrystalline $BiFeO_3$ films prepared under various deposition times. For a normal flux under a high deposition rate, as island density onto the substrate increases, the coalescence of the island becomes more active. [26-28] Grain growth is promoted under active coalescence, because the growth in the lateral direction is promoted. Accordingly, when film thickening continues, larger grain size develops.

4.2.4 Crystal structure of $BiFeO_3$ films prepared under various magnetic fields

Figure 4.10(a) shows the XRD pattern of polycrystalline $BiFeO_3$ films prepared under various magnetic fields. The films observed polycrystalline perovskite single phase

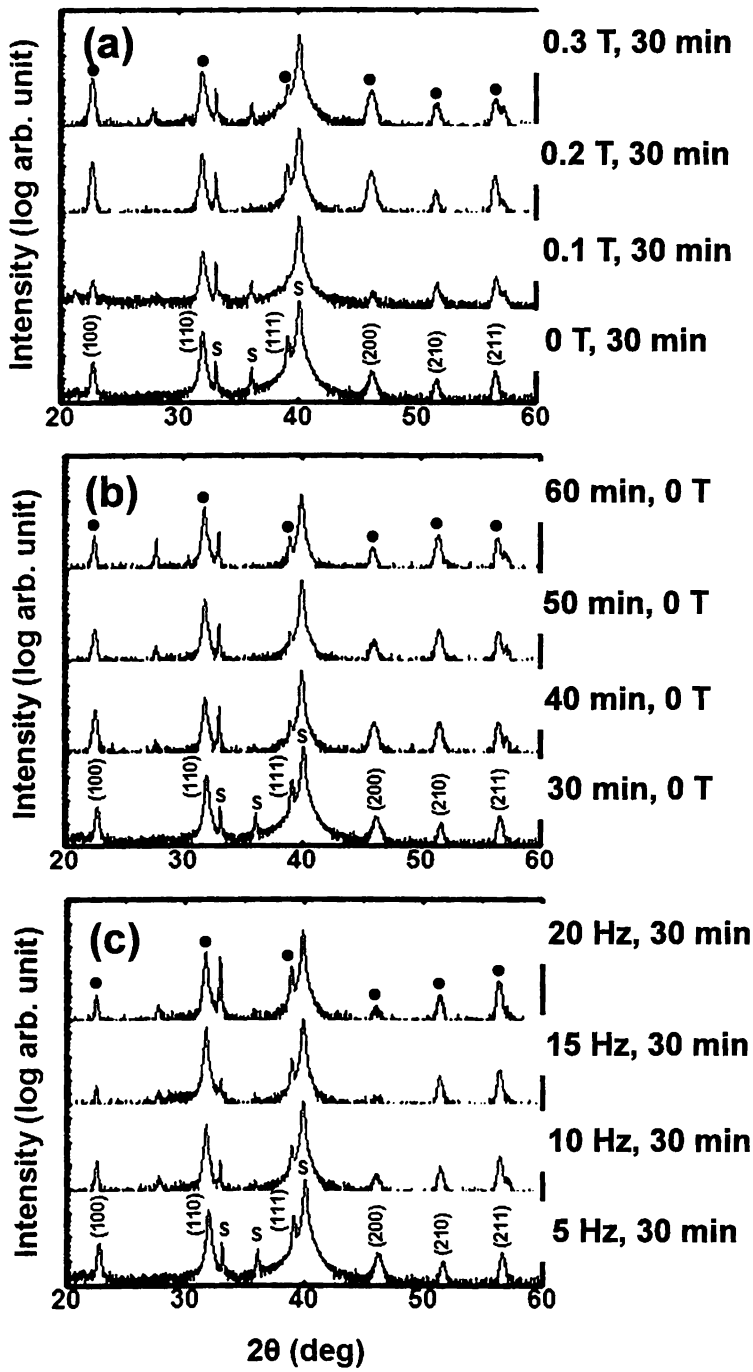

Figure 4.10. XRD patterns of polycrystalline $BiFeO_3$ films prepared under (a) magnetic fields (deposition time of 30 min), (b) deposition times (magnetic field of 0 T), and (c) repetition rates (magnetic field of 0 T). The black circles are the perovskite $BiFeO_3$ phases and S is the substrate.

without secondary phases. The intensity of (100) peaks is increased, while the film thickness is increased by increasing a magnetic field. It is necessary to confirm whether the nature of polycrystalline $BiFeO_3$ films caused by the increase in film thickness or by the application of a magnetic field. In the result of the microstructure, the thickness of polycrystalline $BiFeO_3$ films prepared under various deposition times and repetition rates, was also increased. In order to compare the XRD patterns on the change of the film thickness, XRD patterns of polycrystalline $BiFeO_3$ films prepared under various deposition times and repetition rates are shown in Figs. 4.10(b) and (c). The XRD patterns of polycrystalline $BiFeO_3$ films observed a single-phase perovskite structure. However, the XRD patterns with the increase of the film thickness caused by various deposition times and repetition rates show the distinct tendency in comparison with that under various magnetic fields. The (100) peak intensity of the polycrystalline $BiFeO_3$ film prepared under various magnetic fields was increased with increasing a film thickness, whereas the (110) peak intensity of polycrystalline $BiFeO_3$ films prepared under various deposition times and repetition rates is further increased, in comparison to the (100) peaks. In particular, the (110) peak intensity of the polycrystalline $BiFeO_3$ film prepared under various repetition rates was much stronger than the (100) peak.

To interpret distinct tendency of XRD patterns on film thickness under various parameters (magnetic field, deposition time and repetition rate), the possibility is suggested as illustrated in Fig. 4.11. The microstructure of polycrystalline $BiFeO_3$ films prepared under various deposition times and repetition rates, is granular. The fluxes for the deposition time and repletion rate are parallel to the substrate normal. But, they have different deposition rate. In the initial stage, adatoms of (100) and (110) surfaces exist onto the substrate. Each adatom migrates, because of the minimization of surface energy. In polycrystalline $BiFeO_3$ films grown on a Pt substrate, the adatoms of the (110) surface are likely to have a higher diffusivity than those of the (100) surface. This suggests that the growth of adatoms of the (110) surface is faster in the lateral direction that that of the (100) surface, and this can result in an increase of the (110) peak, as shown in Fig. 4.10. In particular, the growth of adatoms of (110) surface under a high deposition rate caused by the high repetition rate is much faster than that of adatoms of the (100) surface, due to an increase of island density onto the substrate in the case of a high deposition rate. As shown in Fig. 4.10(c), the (110) surface is

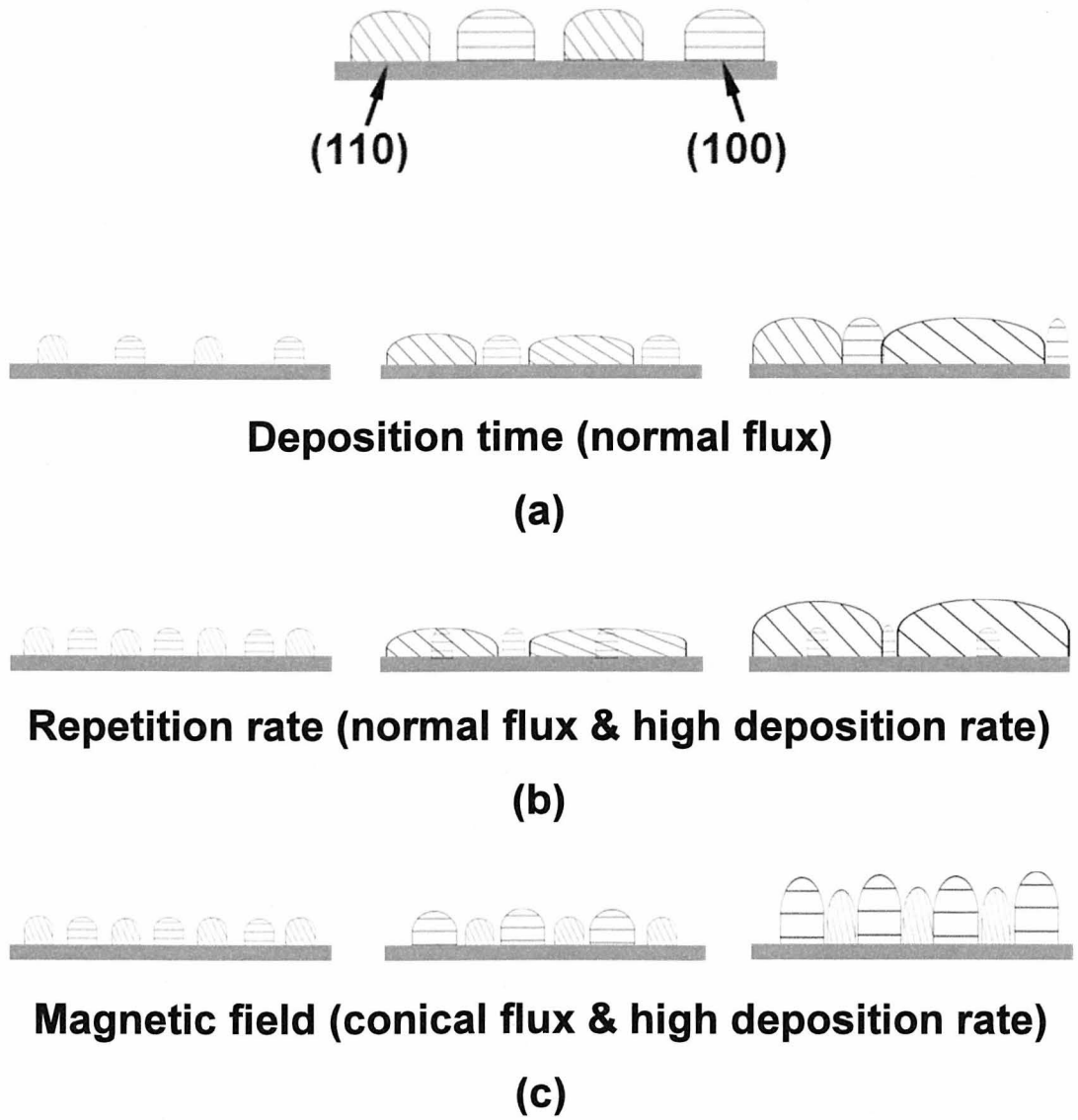

Figure 4.11. Consideration on the tendency of XRD patterns in polycrystalline $BiFeO_3$ films prepared under various parameters of (a) deposition times, (b) repetition rates, and (c) magnetic fields.

predominant, indicating that the intensity of (110) peaks is stronger than that of (100) peaks, because adatoms of the (110) surface cover the substrate with faster growth.

On the other hand, the microstructure of polycrystalline $BiFeO_3$ films prepared under a magnetic field is a columnar structure. The adatoms of the (110) surface also prefer the diffusion in the lateral direction, as they have a high diffusivity in polycrystalline $BiFeO_3$ films grown on a Pt substrate. However, in the case of the columnar structure, the growth rate in the vertical direction is much faster than that in the lateral direction, because the top of nucleus intercepts the evaporated species before they reach the surface of the substrate in the conical flux. The diffusion in the lateral direction is suppressed due to the existence of columns. As a columnar structure is formed, the growth of the (100) surface becomes faster than that of the (110) surface, and as a result, the (100) surface is preferred in columnar $BiFeO_3$ films. This trend is often found in the changes of microstructures from the granular to the columnar structure caused by the modified flux. Consequently, the change in the orientation which occurs when increasing a film thickness in polycrystalline $BiFeO_3$ films prepared under a magnetic field might be related to the microstructure.

4.2.5 Dependence of ferroelectric properties of $BiFeO_3$ films on film thickness

To investigate the ferroelectric properties, the polarization versus electric field (*P-E*) loop of polycrystalline $BiFeO_3$ films prepared under various magnetic fields was measured at 20 kHz and room temperature (RT), as shown in Fig. 4.12(a). In previous experimental studies of polycrystalline $BiFeO_3$ films, the understanding and characterization of the dependence of the ferroelectric properties of $BiFeO_3$ films on film thickness is insufficient. It mostly trends to leaky *P-E* hysteresis loop at RT due to higher leakage current. In this study, the film thickness as well as the high deposition rate and the high plume density could be controlled by magnetic field. As a result, ferroelectric *P-E* hysteresis loops of each $BiFeO_3$ film were obtained at RT, and the dependence of the ferroelectric property on film thickness could be interpreted. For a polycrystalline $BiFeO_3$ film prepared under a magnetic field of 0 T,

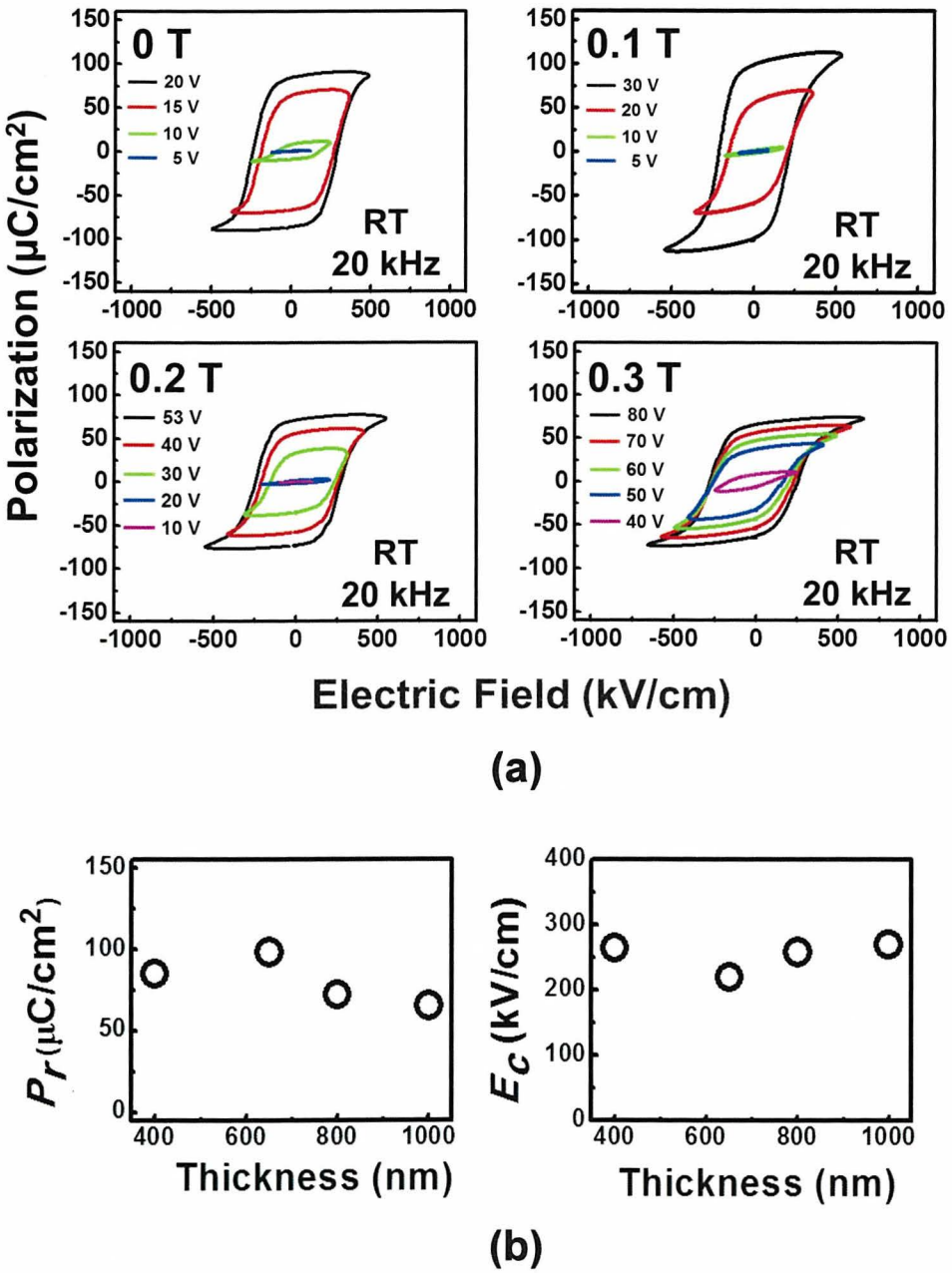

Figure 4.12. (a) Ferroelectric *P-E* hysteresis loops of polycrystalline $BiFeO_3$ films prepared under various magnetic fields and (b) polarization values (P_r), and coercive field (E_c) as a function of thickness.

the polarization value (P_r) and coercive field (E_c) were 85 μC/cm^2 and 264 kV/cm, respectively. The polycrystalline $BiFeO_3$ films prepared under magnetic fields of 0.1 T, 0.2 T, and 0.3 T also obtained *P-E* hysteresis loops at RT. The polarization values and coercive fields for magnetic fields of 0.1 T, 0.2 T, and 0.3 T were 98, 72, and 65 μC/cm^2, and 220, 258, and 270 kV/cm, respectively. Ferroelectric films are well known that ferroelectric properties affect the thickness and grain size. [29-31] Figure 4.12(b) shows the polarization values and coercive fields as a function of film thickness. The polarization value tends to somewhat decrease with increasing a film thickness. This tendency is considered to be a consequence of the change of the orientation in films, because the intensity of the (100) peak of polycrystalline $BiFeO_3$ films prepared under a magnetic field is increased by increasing a film thickness.

In $BiFeO_3$, the polarization axis is along the <111> direction. [32] It is assumed that P_r (111) = $(\sqrt{3}/\sqrt{2})P_r$ (110) = $\sqrt{3}P_r$ (100) in rhombohedral $BiFeO_3$. Thus, the polarization value of the (111)-oriented film is the largest among the (100)-, (110)-, and (111)-oriented films. However, the above assumption for polycrystalline $BiFeO_3$ films is not consistent due to the existence of grains which include each orientation in polycrystalline $BiFeO_3$ films unlike in the case of epitaxial $BiFeO_3$ films. However, from the XRD patterns as shown in Fig. 4.10, as orientation of film is changed from (110) to (100) with increasing film thickness, the volume fraction of (100) grains is increased in polycrystalline $BiFeO_3$ films. Consequently, the polarization value is decreased, due to the projection of easy <111> polarization direction. The change of the coercive field on thickness-dependence is insignificant, excluding the case of the polycrystalline $BiFeO_3$ film under a magnetic field of 0.1 T. The reason is thought to be due to a consequence of the small grain size. A small grain size in polycrystalline films causes an increase of the density of grain boundary, and this is likely to prevent domain switching for the reversal domain. [33-35] The results are often found in polycrystalline films having a small grain size, and applying a high electric field is needed for a domain switching. [33, 35] Accordingly, the behavior of the coercive field in polycrystalline $BiFeO_3$ films prepared under a magnetic field can be attributed to a grain size, rather than a film thickness.

4.2.6 Summary

Polycrystalline $BiFeO_3$ films on $Pt/TiO_2/SiO_2/Si$ substrate have been prepared by using the magnetic-field-assisted pulsed laser deposition method. Under a magnetic field, the shape of the plume was modified and confined. As the plume was modified and confined by a magnetic field, a columnar structure was obtained with the increase in film thickness. From the XRD patterns, a single-phase perovskite structure was identified without secondary phases. Also, the intensity of the (100) peak of polycrystalline $BiFeO_3$ films was increased while film thickness was increased with increasing a magnetic field. A ferroelectric *P-E* hysteresis loop for all polycrystalline $BiFeO_3$ films was obtained at RT. The dependence of the ferroelectric properties of polycrystalline $BiFeO_3$ films on film thickness could be investigated. The ferroelectric properties of polycrystalline $BiFeO_3$ films prepared under magnetic field are affected by their orientation and microstructure.

4.3 Thick $BiFeO_3$ Films with Columnar Structure

In chapter 4.2, it was confirmed that the high deposition rate and the modified microstructure are caused by the magnetic field application during film growth. Also, the preparation and characterization of polycrystalline $BiFeO_3$ films with a thickness of less than 1 μm were carried out. That thickness range can be used for application in memory devices.

On the other hand, the preparation and characterization of thick $BiFeO_3$ films also are required because a thick film above or near 2.0 μm is required for actuator and sensor applications. However, there are significantly fewer studies on thick $BiFeO_3$ films, and their characteristics have not been reported yet. The reason is the difficulty which raises the large leakage current caused by defects arising from the Bi and Bi_2O_3 loss during the fabrication of thick $BiFeO_3$ films with long deposition times, as well as cracking in the film. As the effective solution for overcoming the problem, a high deposition rate and a modified microstructure are proposed to prepare thick $BiFeO_3$ films. The biggest features of the magnetic-field-assisted pulsed laser deposition have the high deposition rate and the formation of the columnar structure.

In this chapter, the preparation of thick $BiFeO_3$ films near to 2.0 μm has been attempted by using the magnetic-field-assisted pulsed laser deposition. The obtained thick $BiFeO_3$ films are characterized.

4.3.1 Preparation of thick $BiFeO_3$ films

To prepare thick $BiFeO_3$ films by using magnetic-field-assisted pulsed laser deposition, a magnetic field of 0.4 T was applied perpendicularly to the substrate during film growth. The thick films were deposited at a 520 °C and 0.1 Torr for deposition time of 30 min by using an ArF excimer laser with an energy of 130 mJ at a frequency of 5 Hz. The deposition conditions are listed as shown in Table 4.1.

Table 4.2 Deposition conditions for the preparation of thick $BiFeO_3$ films.

Material	Temperature	O_2 pressure	Frequency	Magnetic field	Depo. time
$BiFeO_3$	520°C	0.1 Torr	5 Hz	0.4 T	30 min

4.3.2 Microstructure and crystal structure of thick $BiFeO_3$ films

Figures 4.13(a)-(b) show surface and cross-sectional images of the thick polycrystalline $BiFeO_3$ film. The surface morphology of the thick polycrystalline $BiFeO_3$ film showed a compact and dense film with no cracking. The cross-sectional image shows a densely packed columnar structure. The film thickness was about 1.8 μm for a deposition time of 30 min, whereas the thickness of polycrystalline $BiFeO_3$ films prepared by a conventional pulsed laser deposition was a about 400 nm for the deposition time of 30 min, as well as the granular structure as shown in Fig 4.6(a). In order to prepare thick ferroelectric films, the formation of the columnar structure has been previously proposed. For the formation of the columnar structure, the buffer layers on substrate, also the multi-coating method were attempted to prevent films from cracking caused by film thickening. [36, 37] However, the present result proves that the application of the magnetic field during a laser ablation can easily lead to the formation of the columnar structure on the bare substrate with a short deposition time, without a buffer layer and without the multi-coating method, due to the modified trajectory of the plume as mentioned in chapter 4.2.3. In comparison to the granular structure under a normal flux to the substrate, in the conical flux to the substrate, the growth in the vertical direction is dominant, because the evaporated species are intercepted by the nucleus before reaching the surface of the substrate. The advantage of the columnar structure prevents the film cracking caused by the mismatch of the thermal expand coefficient between the film and the substrate. Consequently, even when the film thickness was increased, crack-free thick $BiFeO_3$ films with columnar structures and compact microstructures were successfully obtained.

Figure 4.14(a) shows the XRD pattern of the thick $BiFeO_3$ film identified from the conventional $\theta/2\theta$. In the XRD pattern, a single-phase perovskite structure was observed

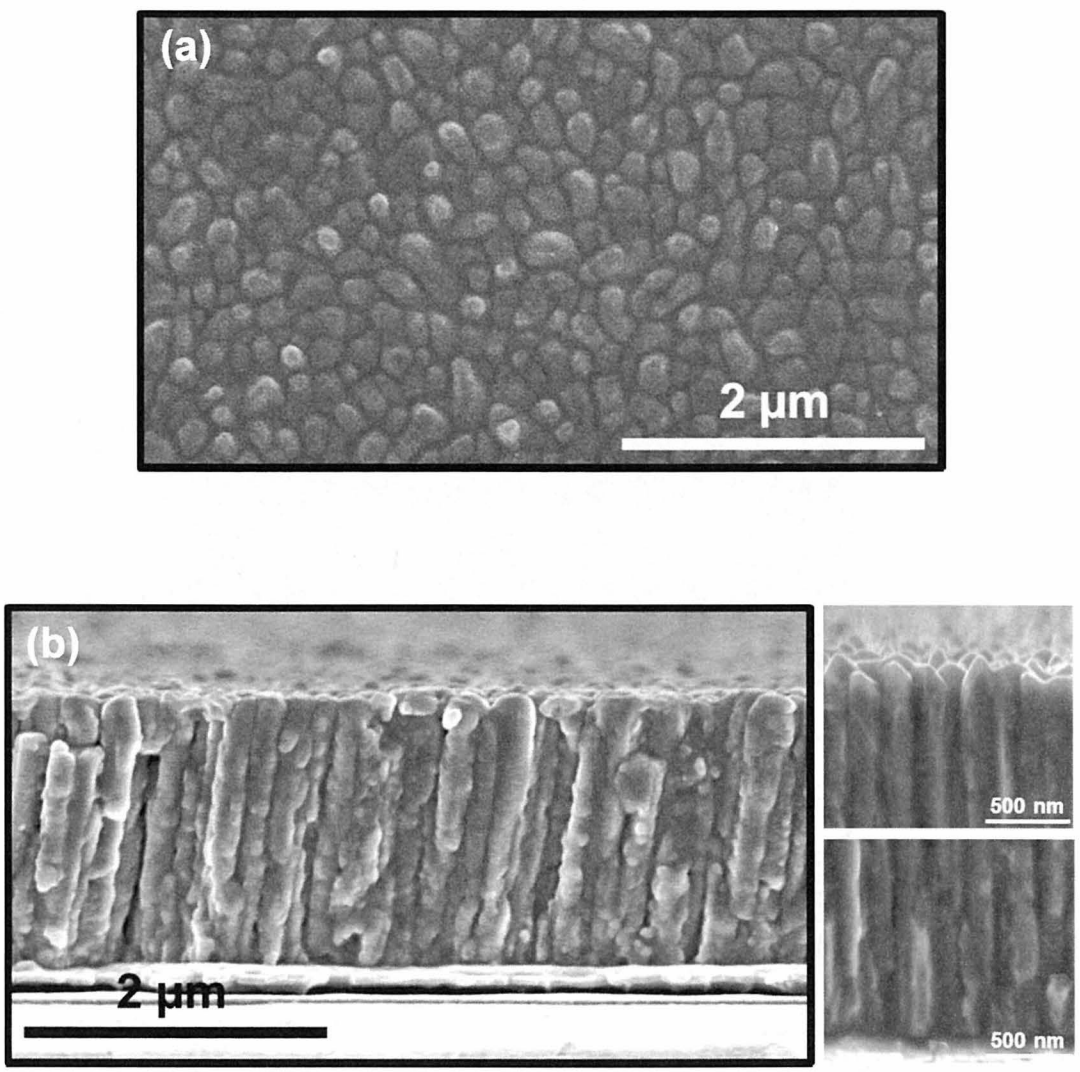

Figure 4.13. (a) Surface and (b) cross-sectional images of thick $BiFeO_3$ films prepared under a magnetic field of 0.4 T for a deposition time of 30 min.

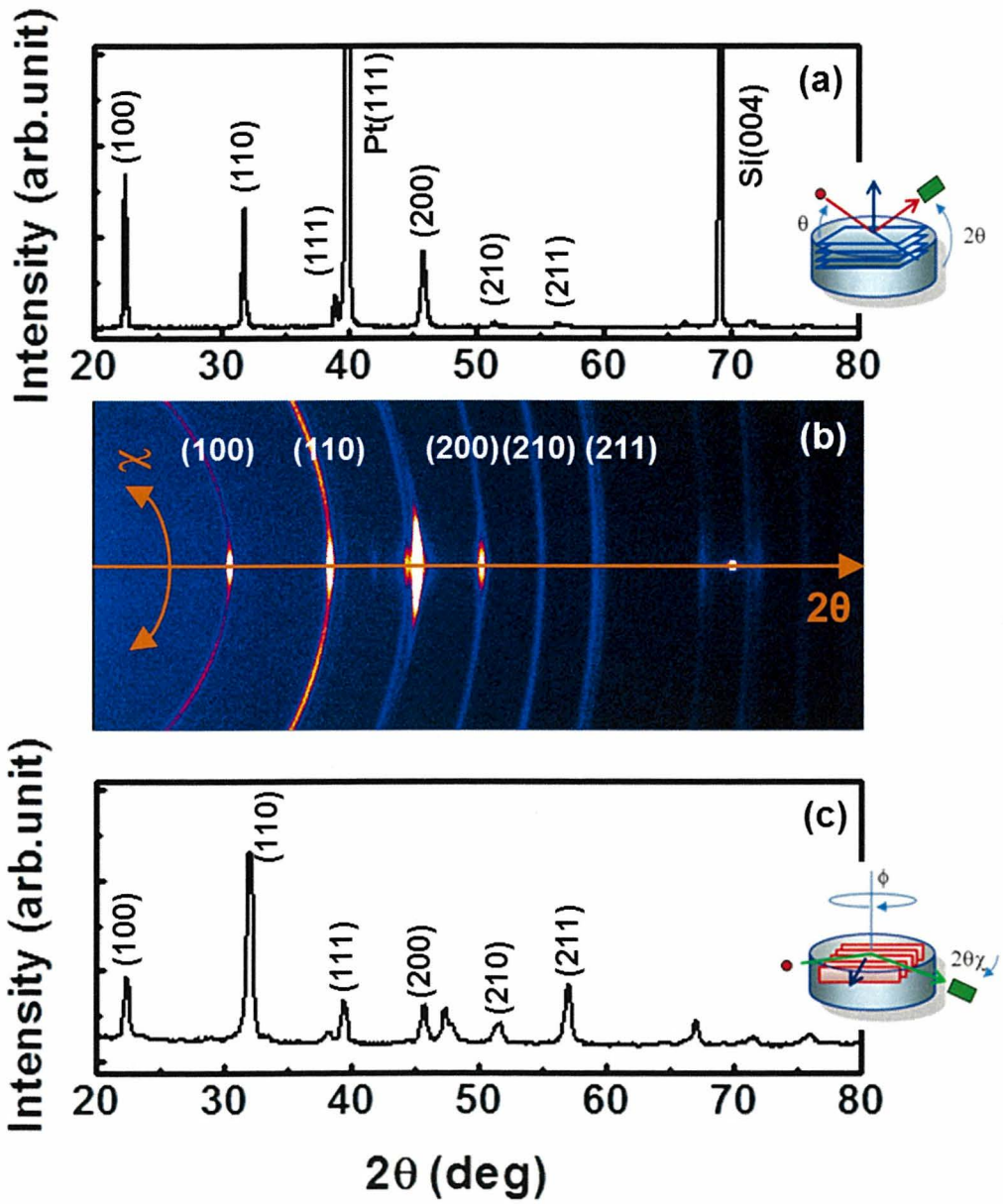

Figure 4.14. (a) Out-plane, (b) 2D-XRD pattern, and (c) in-plane of the XRD pattern for thick $BiFeO_3$ films.

without secondary phases and a strong intensity of the (100) peak was observed. To more investigate the crystal structure, two dimensional XRD (2D-XRD) was conducted. The 2D-XRD pattern shown in Fig. 4.14(b) shows a strong (100)-preferred orientation with the (110) orientation. The Debye-Sherrer ring indicating a polycrystalline structure was observed. This result is in good agreement with the considerations mentioned in Fig. 4.11. The columnar structure is predominant to the growth in the vertical direction. Even though the adatoms of the (110) surface which have a high surface diffusivity, prefer to diffuse the lateral direction, they are suppressed by the column. Consequently, the growth of the preferred (100) surface is promoted, and when film thickening continues, the (100) surface will be preferred. This shows that the intensity of the (100) peak for thick $BiFeO_3$ columnar films prepared under a magnetic field of 0.4 T is higher than that of polycrystalline $BiFeO_3$ films prepared under a magnetic field of 0.3 T. On the other hand, the XRD pattern of the thick $BiFeO_3$ columnar film measured by in-plane scan ($\phi/2\theta\chi$) had a random orientation (JCPDS 72-2112), indicating a strong intensity of only the (110) peak as shown in Fig. 4. 14(c), although the XRD pattern of the out-plane scan ($\theta/2\theta$) was the preferred (100) orientation.

4.3.3 Electric and ferroelectric properties of thick $BiFeO_3$ films

Figure 4.15(a) shows the current density versus electric field (*J-E*) characteristic of the thick $BiFeO_3$ film measured at room temperature (RT). The *J-E* curve at negative and positive biases is symmetric, due to using the same electrode material. At an electric field of 200 kV/cm, the leakage current density was ~ 10^{-3} A/cm^2. To investigate the leakage current mechanism, it was fitted by various current mechanism equations, such as Schottky-emission (SE) conduction, Poole-Frenkel (PF) trap-limited conduction, Fowler-Nordheim (FN) tunneling, and space-charge-limited current (SCLC). [38-40] Among them, the *J-E* characteristic is dominated by the SCLC mechanism.

Figure 4.15(b) shows the fitting of log(*J*) versus log(*E*) plot at negative bias following space-charge-limited current (SCLC). The SCLC is bulk-limited conduction and it can be represented as

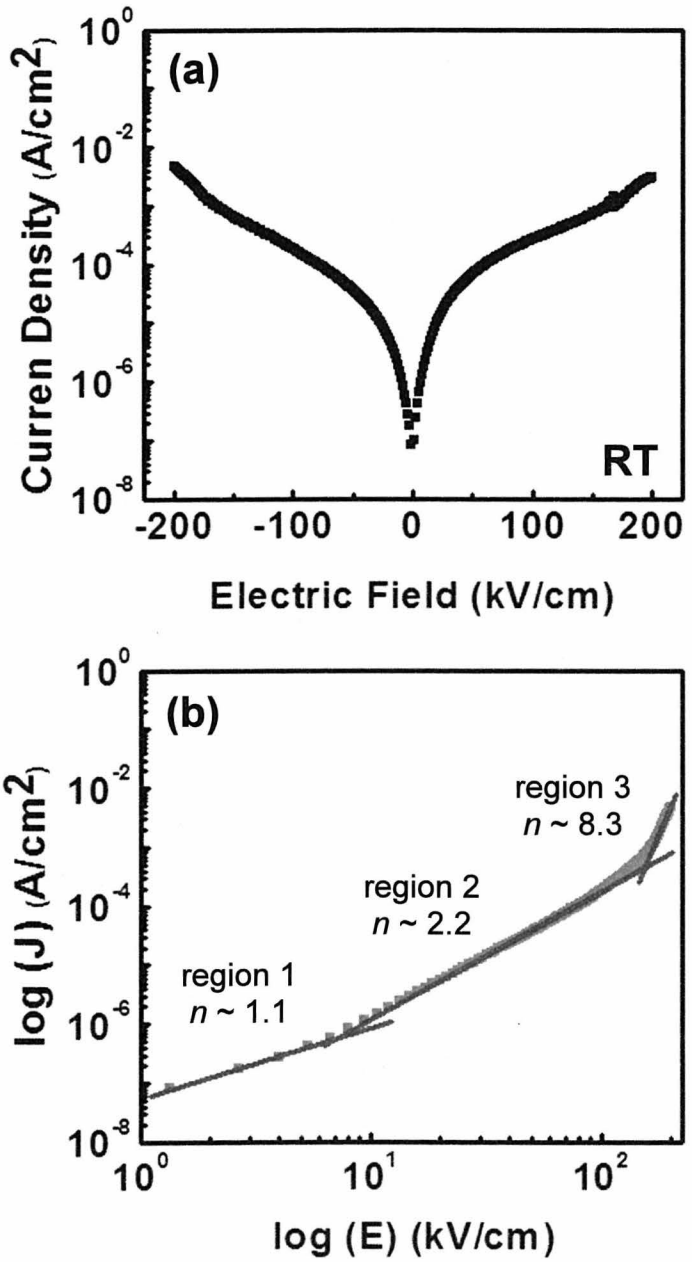

Figure 4.15. (a) Typical *J-E* characteristic of $Pt/BiFeO_3/Pt$ capacitor measured at room temperature and (b) log(*J*) versus log(*E*) plot at negative bias, following space-charge-limited current.

$$J = \frac{9\varepsilon_0\varepsilon_r\mu E^2}{8L^3}, \tag{4.2}$$

where ε_r is the relative dielectric constant of films, ε_o is the permittivity of free space, μ is the charge carrier mobility, and L is the film thickness. It could separate three regions in a given electric field. Region 1 is a linear plot with a slope ~ 1 at low bias, indicating the ohmic contact behavior. Region 2 at above electric field of region 1 also is linear behavior with a slope ~ 2. Region 1 and region 2 are in agreement with the SCLC behavior. However, the slope of the region 3 at high applied field is increased swiftly. This is often found for leakage mechanism of $BiFeO_3$ films or bulk. This behavior is explained by trap-filled-limited (TFL) region.

Figure 4.16(a) shows the polarization versus electric field (*P-E*) hysteresis loop of the thick $BiFeO_3$ film measured at 20 kHz and RT. A saturated *P-E* hysteresis loop was obtained at RT, and the polarization value (P_r) and coercive field (E_c) were 62 μC/cm^2 and 198 kV/cm at a maximum electric field of 490 kV/cm. Previous study has attempted to prepare thick $BiFeO_3$ films above 1.8 μm by aerosol deposition, but the ferroelectric properties proved to be insufficient. [41] Also, polycrystalline $BiFeO_3$ films mainly tend to have the leaky *P-E* hysteresis loop likely due to defects caused by the Bi and Bi_2O_3 loss. Moreover, to fabricate thick $BiFeO_3$ films by conventional deposition methods, a long deposition time is required. In the preparation of thick $BiFeO_3$ films by using magnetic-field-assisted pulsed laser deposition, however, the preparation of thick films in short deposition time is able to be due to the confined plume by a magnetic field. As a result, the problem on the leakage current could be overcome, and the ferroelectric properties of thick $BiFeO_3$ film could be evaluated.

4.3.4 Piezoelectric property of thick $BiFeO_3$ films

To investigate the piezoelectric property of thick $BiFeO_3$ films, atomic force microscopy (AFM) was used. A cantilever is contacted onto the film surface.

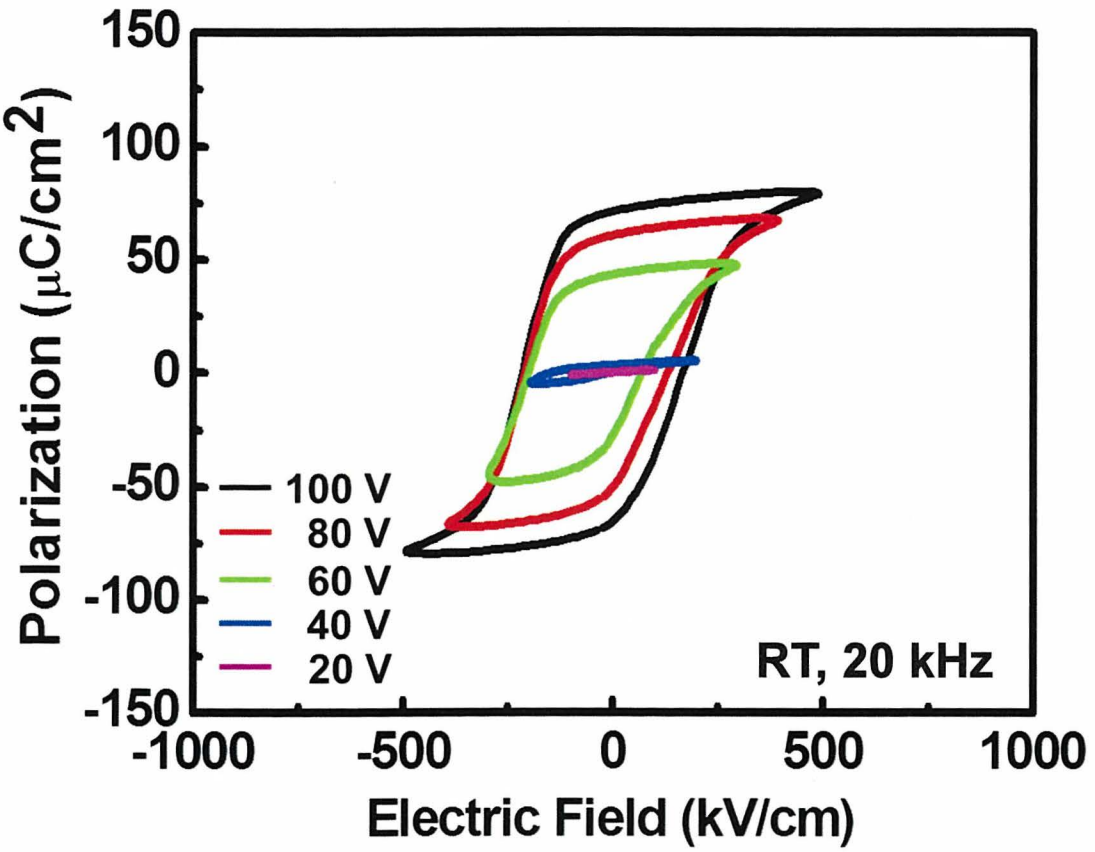

Figure 4.16. *P-E* hysteresis loop of the thick $BiFeO_3$ film prepared under a magnetic field of 0.4 T for a deposition time of 30 min.

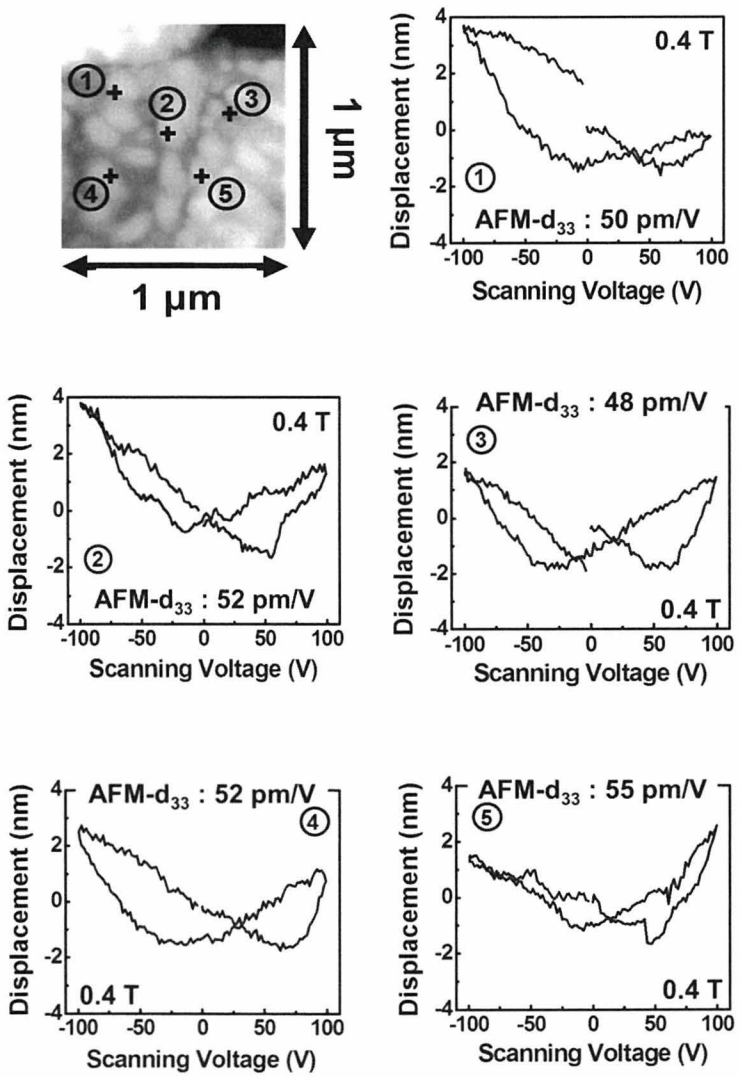

Figure 4.17. Piezoelectric hysteresis loops at given points on thick $BiFeO_3$ film measured by using a scanning probe microscopy.

The voltage is applied through the silicon tip of the cantilever, coated with a Pt/Ir alloy for electric conduction. When voltage is applied between the film surface and the tip, the film is deformed in response to the applied voltage, due to piezoelectric property. The piezoelectric constant can be obtained from the slope of displacement versus applied voltage.

Figure 4.17 shows the piezoelectric response of a thick $BiFeO_3$ film measured at each point. Even though piezoelectric response of each point is slightly different, due to the differences in crystallinity at the measured points, the piezoelectric hysteresis loop shows a butterfly-shaped displacement curve. Piezoelectric coefficient (d_{33}) was about 50 pm/V. This value is comparable to that of an epitaxial $BiFeO_3$ thin film on a (001) $SrTiO_3$ substrate. [42]

4.3.5 Summary

1.8 μm-$BiFeO_3$ columnar films have been successfully obtained under a magnetic field of 0.4 T for a deposition time of 30 min. In comparison with polycrystalline $BiFeO_3$ films prepared without a magnetic field, the deposition rate is 4 times higher together with the compactly and densely packed surface morphology. The XRD pattern showed the preferred (100) orientation. A saturated *P-E* hysteresis loop was obtained at room temperature (RT), and the polarization value and the coercive field were 62 $\mu C/cm^2$ and 198 kV/cm, respectively. The piezoelectric response measured by AFM showed a butterfly-shaped curve, and piezoelectric d_{33} coefficient was about 50 pm/V. So far, there have been no reports on the preparation and characterization of thick $BiFeO_3$ films, because of the limitation in thickness on polycrystalline $BiFeO_3$ films. This study shows that the limitation of the thickness can be overcome using the magnetic-field-assisted pulsed laser deposition as shown in Fig. 4.18. It is suggested that thick $BiFeO_3$ films with columnar structure can be applied to piezoelectric actuator and sensors.

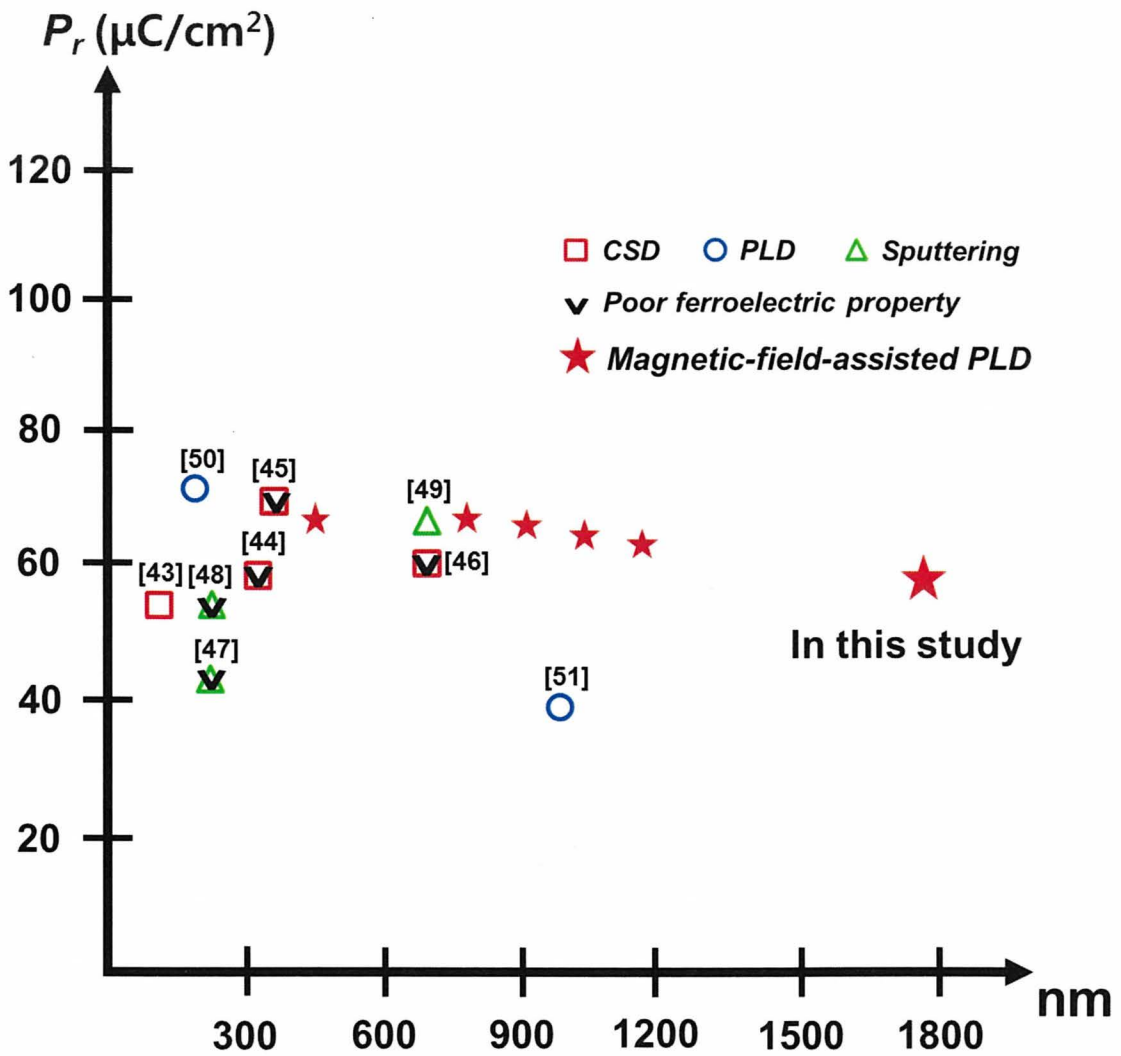

Figure 4.18. Film-thickness versus polarization value for polycrystalline $BiFeO_3$ films prepared by various deposition methods.

4.4 Polycrystalline $BiFeO_3$ Films Prepared by 90° Off-Axis Deposition

The pulsed laser deposition is a useful deposition method for preparing films using complex materials. As mentioned above chapter 3, its biggest advantage is that is can maintain the desired target composition in the deposited film. However, there exist several big problems, such as splashing and droplet, due to the target density and the state of the target surface. [2] These problems cause the degradation of the electric properties, or film properties with undesirable phases. A shadow mask set in front of the substrate, or 90° off-axis deposition has been known to prevent the droplets and the particulates on the film surface. The superconductor films such as $YBa_2Cu_3O_7$ (YBCO) have reported that improved film properties with smooth film surface and suppression of droplets were obtained by using 90° off-axis deposition. [52, 53] Even though a smooth surface without droplets and particulates can be obtained by 90° off-axis deposition, a long deposition time is required to obtain a desired film-thickness. As compared to YBCO films, long deposition times for the preparation of $BiFeO_3$ films are more difficult, due to the fact that Bi and Bi_2O_3 are relatively volatile, which leads to Bi and Bi_2O_3 loss in $BiFeO_3$ films during film-growth. The loss of Bi and Bi_2O_3 leads to the degradation of the electrical characteristics in $BiFeO_3$ films, including a leaky *P-E* hysteresis loop, while undesirable phases which do not have ferroelectric properties are formed.

To prepare polycrystalline $BiFeO_3$ films by 90° off-axis deposition, magnetic-field-assisted pulsed laser deposition is employed. The major feature of this deposition method is the high deposition rate by modified trajectory of plume. Under a high deposition rate, it is proposed that polycrystalline $BiFeO_3$ films by 90° off-axis deposition can be efficiently prepared as well as the suppression of Bi and Bi_2O_3 loss.

In this chapter, the preparation of polycrystalline $BiFeO_3$ films by 90° off-axis deposition has been attempted, and the obtained films are compared to polycrystalline $BiFeO_3$ films prepared by on-axis deposition. They also are characterized on microstructure, crystal structure, ferroelectric properties, and domain switching.

4.4.1 Preparation of $BiFeO_3$ films by 90° off-axis deposition

To prepare $BiFeO_3$ films through 90° off-axis deposition by using a magnetic field assisted PLD, the substrate was titled as shown in Fig 4.19. The magnetic field of 0.4 T was applied parallel to the substrate during a film growth. The films were deposited at 500°C and 0.1 Torr for 30 min by using an ArF excimer laser with an energy of 130 mJ at a frequency of 5 Hz. The deposition conditions are listed as shown in Table 4.3.

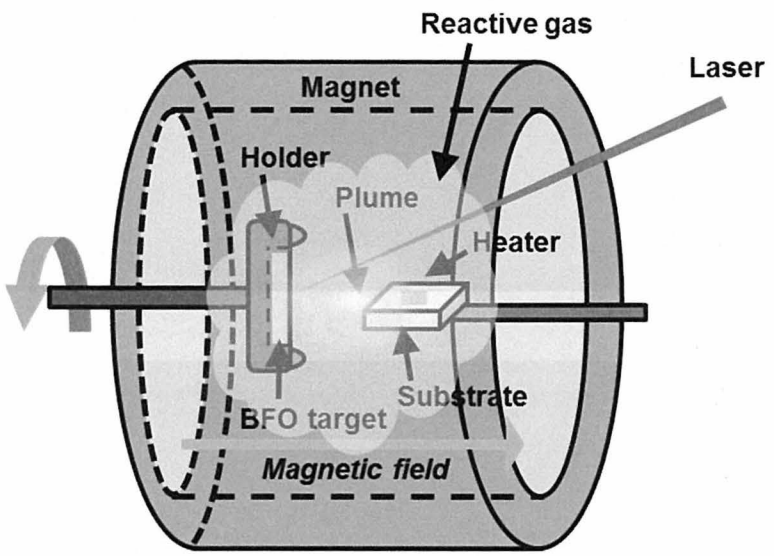

Figure 4.19. Schematic of 90° off-axis deposition.

Table 4.3. Deposition conditions for the preparation of polycrystalline $BiFeO_3$ films by 90° off-axis deposition.

Material	Temperature	O_2 pressure	Frequency	Magnetic field	Depo. time
$BiFeO_3$	500°C	0.1 Torr	5 Hz	0.4 T	30 min

4.4.2 Microstructures of $BiFeO_3$ films prepared by 90° off-axis deposition

Figures 4.20(a)-(b) show the surface morphologies of $BiFeO_3$ films prepared by off-axis and on-off deposition. The surface morphology of polycrystalline $BiFeO_3$ film prepared

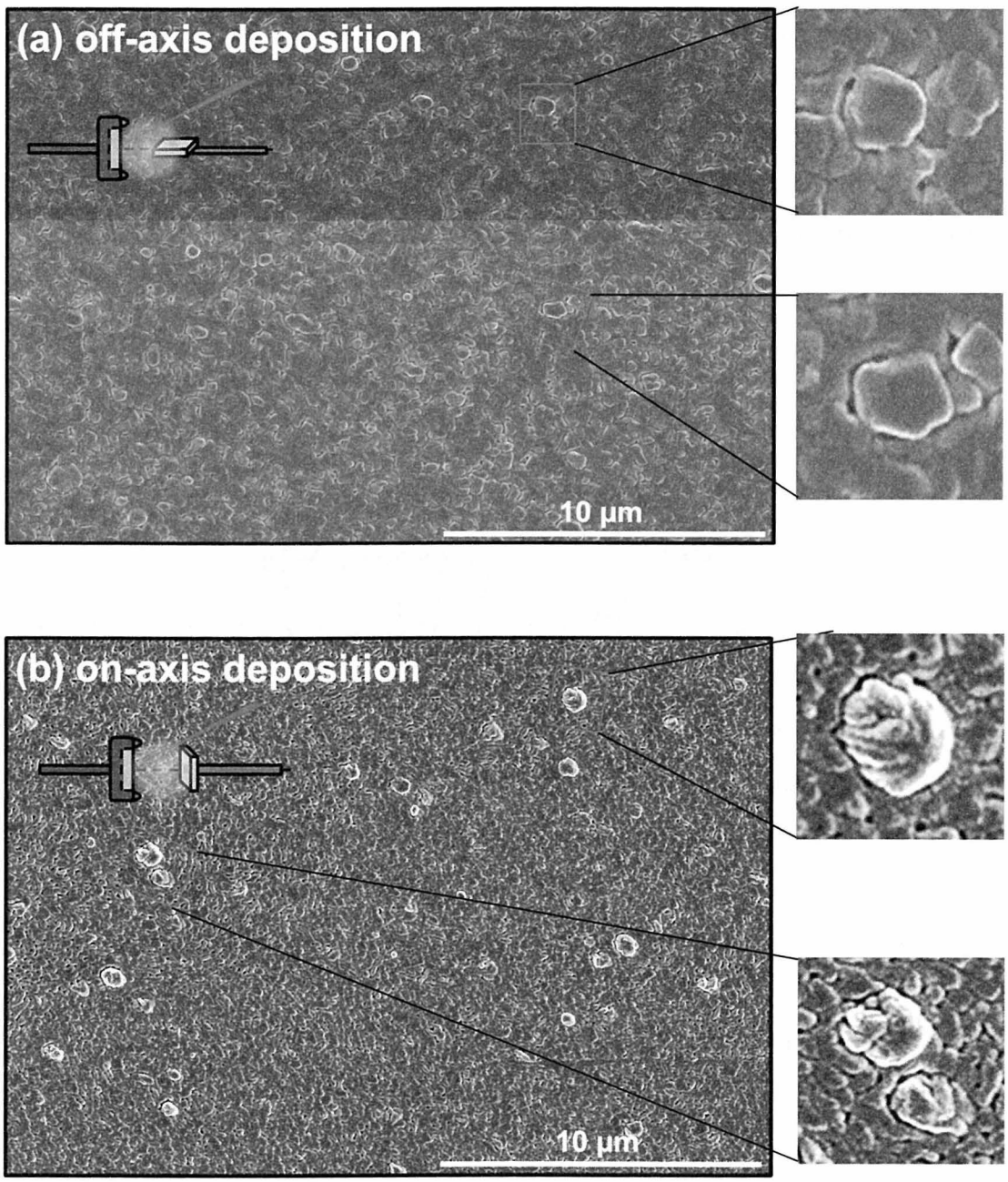

Figure 4.20. Surface morphologies of polycrystalline $BiFeO_3$ films prepared by (a) off-axis deposition and (b) on-axis deposition.

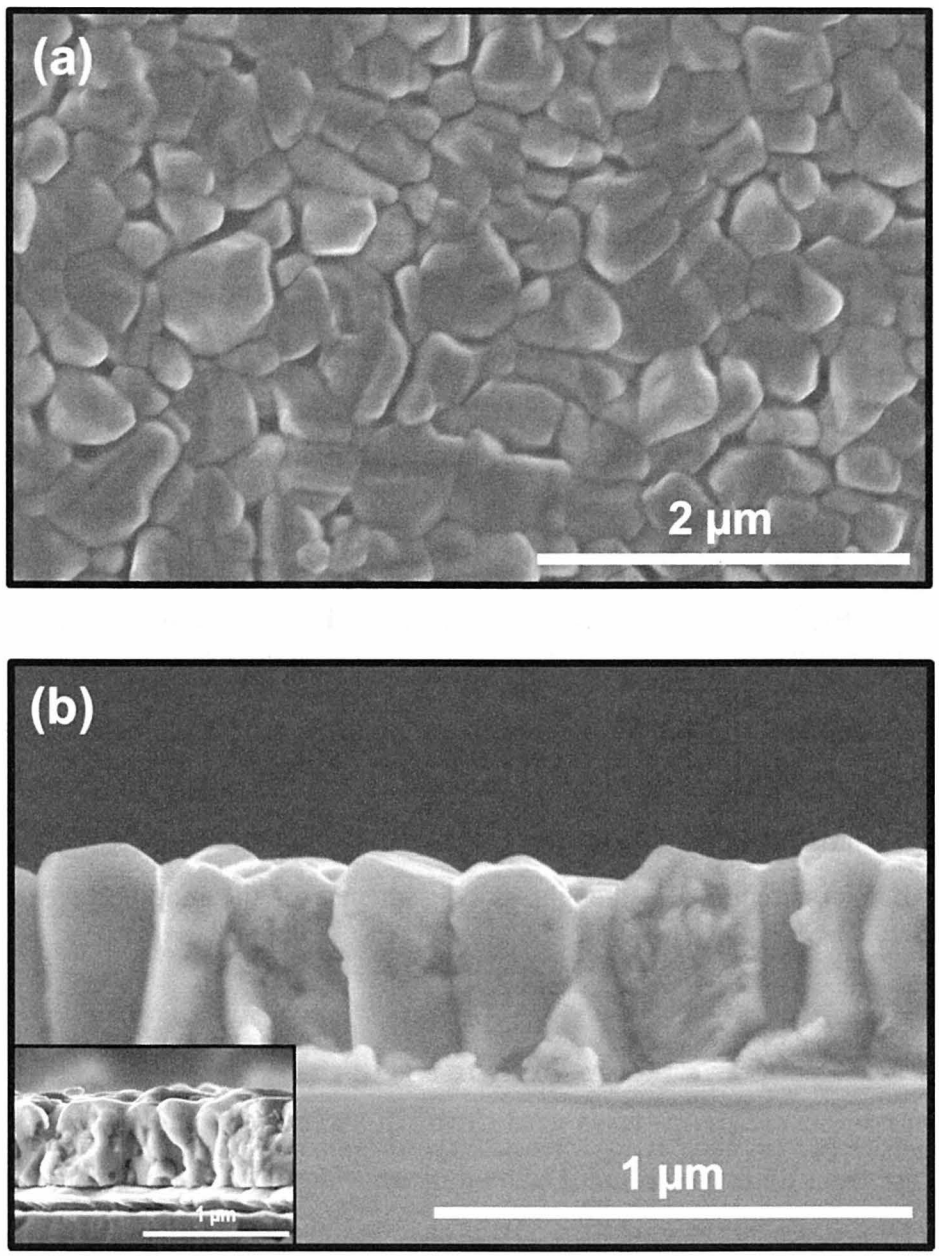

Figure 4.21. (a) Surface morphology and (b) cross-sectional image (the insert is cross-sectional image of polycrystalline $BiFeO_3$ films prepared by on-axis deposition.) of polycrystalline $BiFeO_3$ films prepared by 90° off-axis deposition.

by off-axis deposition shows a smooth surface without droplets and micro-sized particulates. However, the surface morphology of polycrystalline $BiFeO_3$ film prepared by on-axis deposition shows droplet-like particulates which have a bigger size than near grains. This result which is suppressed from droplet and particulates on the film surface is commonly found in superconductor $YBa_2Cu_3O_7$ (YBCO) films prepared by 90° off-axis deposition without magnetic field. [52, 53] However, as compared with 90° off-axis deposition without magnetic field, the magnetic field separates the charge species. An applying a magnetic field deflects the charge species from their primary path by Lorenz force. The charge species travel along the lines of the magnetic field, whereas the neutral species, including heavy and large particulates, are not affected and proceed along a straight path. [54] The charge species can be collected on the substrate to produce films. As a result, this effectively solves the problems, such as droplet and splashing.

Figures 4.21(a) and (b) show the surface morphology and cross-sectional image of polycrystalline $BiFeO_3$ films prepared by 90° off-axis deposition. The large grain and columnar structure appear. 400 nm-$BiFeO_3$ films could be obtained by 90° off-axis deposition under a magnetic field of 0.4 T for a deposition time of 30 min. This result suggests that the reduction of deposition rate in off-axis deposition can be easily compensated by high deposition rate arising from the modified and confined plume by the magnetic field. The difference of microstructures is thought as consequence of the modified trajectory by the magnetic field.

4.4.3 Ferroelectric properties and domain switching in $BiFeO_3$ films

To investigate the ferroelectric properties of polycrystalline $BiFeO_3$ films prepared by 90° off-axis deposition, polarization versus electric field (*P-E*) hysteresis loop was measured at room temperature (RT) and 20 kHz. Figure 4.22 shows the ferroelectric *P-E* hysteresis loop of polycrystalline $BiFeO_3$ films prepared by off-axis deposition. A good *P-E* hysteresis loop was obtained at RT, and the polarization value (P_r) and the coercive field (E_c) were 90 $\mu C/cm^2$ and 178 kV/cm, respectively. The coercive field of the polycrystalline

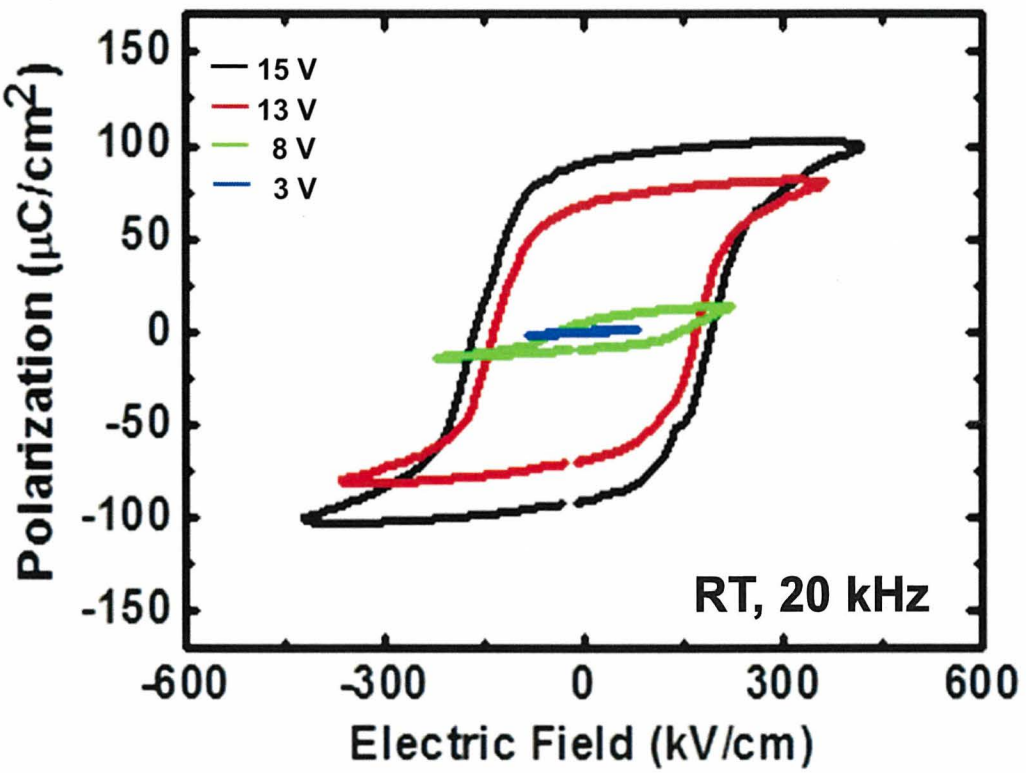

Figure 4.22. Ferroelectric *P-E* hysteresis loop of polycrystalline $BiFeO_3$ films prepared by 90° off-axis deposition.

Table 4.4. Comparison of ferroelectric properties for on-axis and off-axis deposition. (Film thickness for off-axis and on-axis is about 400 nm.)

	P_r	E_c	Maximum applying field (V)
Off-axis deposition	90 μC/cm^2	178 kV/cm	15 V
On-axis deposition	85 μC/cm^2	264 kV/cm	20 V

$BiFeO_3$ film prepared by off-axis deposition is significantly reduced in comparison with polycrystalline $BiFeO_3$ films prepared by on-axis deposition as shown in Table 4.4.

The coercive field is required to reverse domain switching, and domain switching influences the coercive field in ferroelectric films. Figure 4.23 shows the piezoresponse force microscopy (PFM) images measured by atomic force microscopy (AFM), representing the behavior of ferroelectric domain switching as a function of applied scanning voltage on a polycrystalline $BiFeO_3$ film prepared by off-axis deposition. The darkness and brightness in the given images represent the up and down state of polarization. In as-grown, the region of darkness and brightness coexist. By increasing the positive voltage, the region of darkness indicating the up-polarization state expands. When applying a higher negative voltage, the region of brightness indicating down-polarization state expands. This behavior means domain reversal, indicating ferroelectricity. When applying -15 V in the polycrystalline $BiFeO_3$ film, PFM image shows almost the region of brightness that represents down-polarization state. In this case, the applied voltage is consistent with the maximum applied voltage for the measured ferroelectric *P-E* hysteresis loop. Thus, it is considered that one direction is aligned, while polarization is saturated. Again, when the applied positive voltage is increased, the region of darkness gradually expands and domain switching occurs. When applying +15 V, the PFM image shows the region of darkness that represents up-polarization state. In this case, the region of brightness also is observed a little in contrast to the PFM image for applying voltage of -15 V. The difference of PFM images between -15 V and +15 V is thought that the easy polarization for domain switching occurs when applying a negative voltage, whereas the domain switching is difficult when applying a positive voltage. This confirms that the electric field in point 8 is higher than that in point 3. However, the domain switching requires about 5 V, and this value is much smaller in the polycrystalline $BiFeO_3$ films prepared by 90^o off-axis deposition than that of the polycrystalline $BiFeO_3$ film prepared by on-axis deposition. The reduced coercive field of polycrystalline $BiFeO_3$ films prepared by 90^o off-axis deposition is likely to originate from the microstructure. The clamping effect caused between the substrate and the film prevents the domain switching in the ferroelectric film. However, the columnar structure does not influence the clamping effect in comparison with the granular structure. As a result, the easy switching is achieved by releasing the clamped polarization domains.

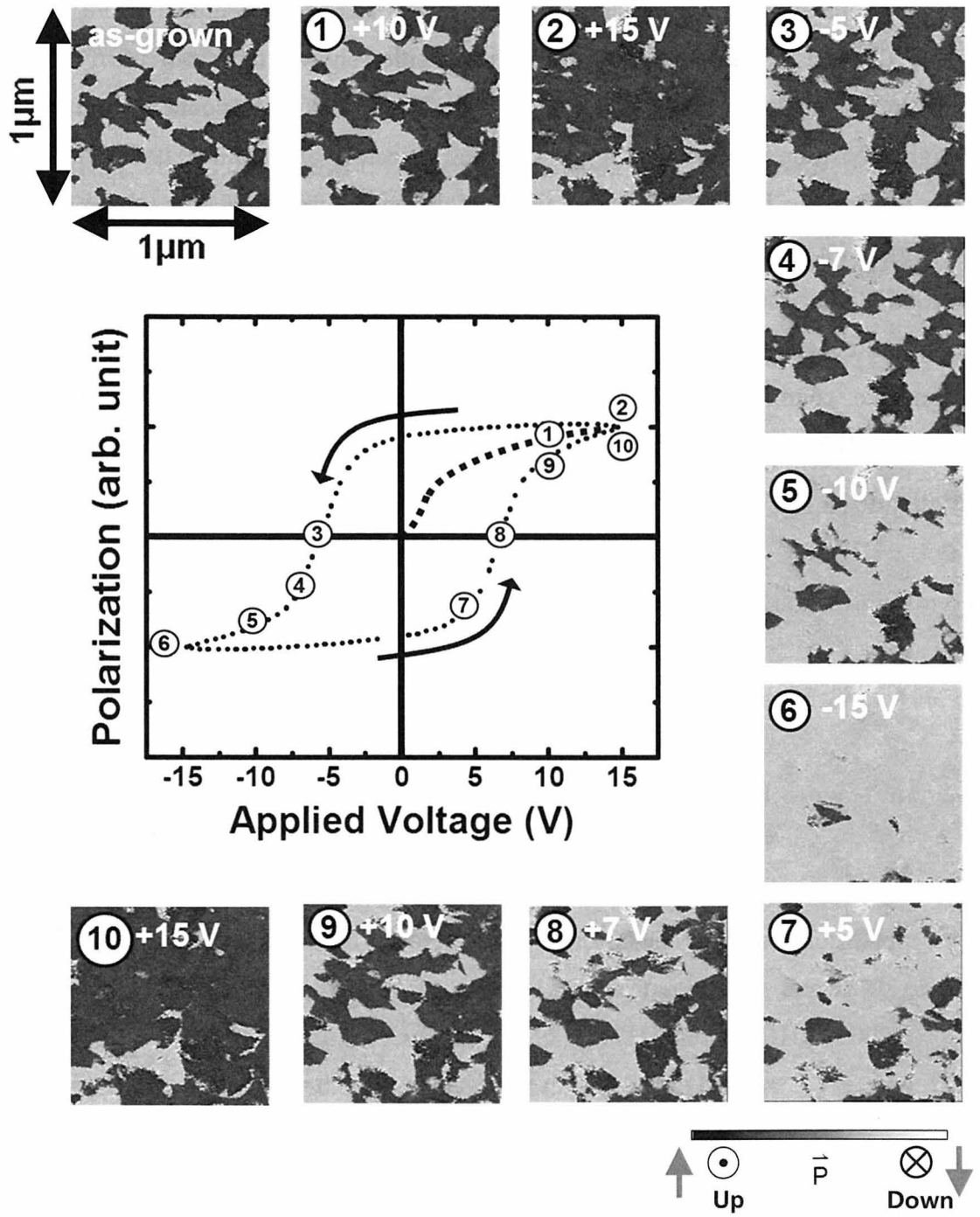

Figure 4.23. Domain switching of polycrystalline $BiFeO_3$ films prepared by 90° off-axis deposition as a function of applied scanning voltage.

4.4.4 Summary

The preparation of polycrystalline $BiFeO_3$ films has been attempted by 90° off-axis deposition. The surface morphology for off-axis deposition showed droplet-free $BiFeO_3$ films. The reduction of the deposition rate caused by 90° off-axis deposition could be compensated by the high deposition rate induced by the modified trajectory of the plume under a magnetic field. For a magnetic field of 0.4 T and with a deposition time of 30 min, about 400 nm-$BiFeO_3$ films with columnar structures were obtained. The ferroelectric polarization versus electric field (*P-E*) hysteresis loop was obtained at room temperature (RT), and polarization value (P_r) and coercive field (E_c) were 90 μC/cm^2 and 178 kV/cm, respectively. In off-axis deposition, the coercive field was significantly reduced in comparison with that of polycrystalline $BiFeO_3$ films prepared by on-axis deposition, likely due to the microstructure of the film.

References

[1] K. Y. Yun, D. Ricinschi, T. Kanashima, M. Noda, and M. Okuyama, *Jpn. J. App. Phys.* **43**, 647 (2004).

[2] D. B. Chrisey, and G. K. Hubler, *"Pulsed Laser Deposition of Thin Film"*, John Wiley & Sons, Inc., New York, 1994.

[3] I. Noorbatcha, R. R. Lucchese, and Y. Zeiri, *J. Chem. Phys.* **86**, 5816 (1987).

[4] R. K. Singh and J. Narayan, *Rhys, Rev. B* **41**, 8843 (1990).

[5] S. I. Anisimov, D. Bauerle, and B. S. Luk'yanchuk, *Rhys, Rev. B* **48**, 12076 (1993).

[6] D. J. Lichtenwainer, O. Auciello, R. Dat, and A. I. Kingon, *J. Appl. Phys.* **74**, 7497 (1993).

[7] S. S. harilal, M. S. Tillack, B. O. Shay, C. V. Bindhu, and F. Najmabadi, *Phys. Rev. B* **69**, 026413 (2004).

[8] X. K. Shen, Y. F. Lu, T. Gebre, H. Ling, and Y. X. Han, *J. Appl. Phys.* **100**, 053303 (2006).

[9] C. Ducruet, N. Kornilov, C. J. Fernandez, and D. Givord, *Appl. Phys. Lett.* **88**, 044102 (2006).

[10] C. Pagano and J. G. Lunney, *J. Phys. D: Appl. Phys.* **43**, 305202 (2010).

[11] NIST Database, http://physics.nist.gov/PhysRefData/ASD/lines_form.html

[12] V. N. Rai, J. P. Singh, F. Y. Yueh, and R. L. Cook, *Laser. Part. Beams* **21**, 65 (2003).

[13] Y. Li, C. Hu, H. Zhang, Z. Jiang, and Z. Li, *Appl. Optics* **48**, B105 (2009).

[14] P. B. Barna and M. Adamik, *Thin Solid Films* **317**, 27 (1998).

[15] C. V. Thompson, *Annu. Rev. Mater. Sci.* **30**, 159 (2000).

[16] M. M. Hawkeye and M. J. Brett, *J. Vac. Sci. Technol. A* **25**, 1317 (2007).

[17] L. Abelmann and C. Lodder, *This Solid Films* **305**, 1 (1997).

[18] H. Kranenburg and Cock Lodder, *Mater. Sci. and Eng. R* **11**, 295 (1994).

[19] X. Tang, J. Dai, X. Zhu, J. Lin, Q. Chang, D. Wu, W. Song, and Y. Sun, *J. Am. Ceram.Soc.* **95**, 538 (2012).

[20] D. H. Lowndes, D. B. Geohegan, A. A. Puretzky, D. P. Norton, and C. M. Rouleau, *Science* **273**, 898 (1996).

[21] P. R. Willmott and J. R. Huber, *Rev. Mod. Phys.* **72**, 315 (2000).

[22] C. Belouet, *Appl. Surf. Sci.* **96**, 630 (1996).

[23] F. Brygo, C. Dutouquet, F. L. Guern, R. Oltra, A. Semerok, and J. M. Weulersse, *Appl. Surf. Sci.* **252**, 2131 (2006).

[24] F. Brygo, A. Semerok, R. Oltra, and J. M. Weulersse, *Appl. Surf. Sci.* **252**, 8314 (2006).

[25] M. Stafe, C. Negutu and I. M. Popescu, *Appl. Surf. Sci.* **253**, 6353 (2007).

[26] Y. Shuai, S. Zhou, S. Streit, H. Reuther, D. Burger, S. Slesazeck, T. Mikolajick, M. Helm, and H. Schmidt, *Appl. Phys. Lett.* **98**, 232901 (2011).

[27] L. Guan, D. Zhang, X. Li, and Z. Li, *Nucl. Instrum. Methods Phys. Res. B* **266**, 57 (2008).

[28] T. Yoshitake, T. Hara, and K. Nagayama, *Diamond and Related Materials* **12**, 306 (2003).

[29] T. Iijima, J. Onagawa, and N. Sanada, *Integ. Ferroelectrics* **20**, 129 (1998).

[30] J. Celinska, V. Joshi, S. Narayan, L. McMillan, and C. Araujo, *Appl. Phys. Lett.* **82**, 3937 (2003).

[31] M. Shimizu, S. Nakashima, K. Kaibara, H. Fujisawa, and H. Niu, *Ferroelectrics* **241**, 183 (2000).

[32] F. Bai, J. Wang, M. Wuttig, J. F. Li, N. Wang, A. P. Pyatakov, A. K. Zvezdin, L. E. Cross, and D. Viehland, *Appl. Phys. Lett.* **86**, 032511 (2005).

[33] S. B. Ren, C. J. Lu, J. S. Liu, H. M. Shen, and Y. N. Wang, *Phys. Rev. B*, **54**, 14337 (1996).

[34] S. H. Hu, G. J. Hu, X. J. Meng, G. S. Wang, J. L. Sun, S. L. Guo, J. H. Chu, and N. Dai, *J. Crys. Growth* **260**, 109 (2004).

[35] S. Choudhury, Y. L. Li, C. K. III, and L. Q. Chen, *Acta Materialia* **55**, 1415 (2007).

[36] C. S. Park, J. W. Lee, G. T. Park, H. E. Kim, and J. J. Kim, *J. Mater. Res.* **22**, 1373 (2007).

[37] C. S. Park, J. W. Lee, G. T. Park, H. E. Kim, and J. J. Kim, *J. Mater. Res.* **22**, 1367 (2007).

[38] G. W. Dietz, W. Antpohler, M. Klee, and R. Waser, *J. Appl. Phys.* **78**, 6113 (1995).

[39] K. H. Ahn, S. S. Kim, and S. G. Baik, *J. Appl. Phys.* **92**, 421 (2002).

[40] C. J. Peng and S. B. Krupanidhi, *J. Master. Res.* **10**, 708 (1995).

[41] J. H. Ryu, C. W. Baek, D. S. Park, and D. Y. Jeong, *Met. Master. Int.* **19**, 639 (2010).

[42] J. Wang, J.B. Neaton, H. Zheng, V. Nagarajan, S.B. Ogale, B. Liu, D. Viehland, V. Vaithyanathan, D.G. Schlom, U.V. Waghmare, N.A. Spaldin, K.M. Rabe, M. Wuttig, and R. Ramesh, *Science* **299**, 1719 (2003).

[43] Y. Nakamura, S. Nakashima, and M. Okuyama, *Integ. Ferro.* **95**, 226 (2007).

[44] R. Zheng, X. Gao, J. Wang, and S. Ramakrishna, *J. Am. Ceram. Soc.* **91**, 463 (2008).

[45] X. Tang, J. Dai, X. Zhu, L. Yin, R. Ang, W. Song, Z. Yang. Y. Sun, and R. Zhang, *J Am. Ceram. Soc.* **93**, 1682 (2008).

[46] X. Tang, J. Dai, X. Zhu, J. Lin, Q. Chang, D. Wu, W. Song, and Y. Sun, *J. Am. Ceram. Soc.* **95**, 538 (2008).

[47] Y. Li, T. Srithanran, S. Zhang, X. He, Y. Liu, and T. Chen, *Appl. Phys. Lett.* **92**, 132908 (2008).

[48] J. Wu, J. Wang, D. Xiao, and J. Zhu, *Appl. Mater. Interfaces* **4**, 1182 (2012).

[49] J. Wu, J. Wang, D. Xiao, and J. Zhu, *Appl. Mater. Interfaces* **3**, 3261 (2011).

[50] K. Y. Yun, D. Ricinschi, T. Kanashima, and M. Okuyama, *Appl. Phys. Lett.* **89**, 192902 (2006).

[51] M. H. Lee, S. S. Kim, D. H. Do, and T. K. Song, *J. Kor. Phys. Soc.* **60**, 288 (2012).

[52] K. L. Chen, J. H. Chan, H. C. Yang, and H. E. Horng, *Physica C* **372**, 1078 (2002).

[53] V. Boffa, T. Petrisor, L. Ciontea, U. Gambardella, and S. Barbanera, *Physica C* **276**, 218 (1997).

[54] R. Jordan, D. Cole, and J. G. Lunney, *Appl. Surf. Sci.* **109**, 403 (1997).

CHAPTER 5

PREPARATION OF EPITAXIAL $BiFeO_3$ FILMS ON La-DOPED $SrTiO_3$ (001) SUBSTRATE

In this chapter, epitaxial $BiFeO_3$ films on La-doped $SrTiO_3$ (001) single crystal substrate are prepared by the magnetic-field-assisted pulsed laser deposition. Epitaxial $BiFeO_3$ films under various magnetic fields are prepared and their crystal structure, microstructure and ferroelectric properties are characterized.

5.1 Introduction

An epitaxial $BiFeO_3$ film on conducting $SrRuO_3$ layer deposited on a (001)-oriented $SrTiO_3$ substrate has a large polarization value of about 50 $\mu C/cm^2$. The fundamental works on crystal structure, domain and ferroelectric properties under an epitaxial stress have been recently conducted. [1] To prepare epitaxial $BiFeO_3$ films on a single crystal substrate, various deposition methods have been used, such as pulsed laser deposition (PLD), metalorganic chemical vapour deposition (MOCVD), sputtering and dual ion-beam sputtering. [1, 2-4] Among many studies on epitaxial $BiFeO_3$ films, Eom's group has reported the preparation and characterization of high-quality epitaxial $BiFeO_3$ films on a single crystal

(001)-oriented $SrTiO_3$ substrate by a high rate off-axis sputtering. [3, 5] They have also used a miscut (001)-oriented $SrTiO_3$ substrate, having the angle, terrace, step, edge, and kink site on the surface. The miscut substrate for preparing epitaxial $BiFeO_3$ films plays an important role. Bi atoms, as a volatile species, have a bond more strongly to the edge and kink site than to a terrace with increasing the miscut angle. As a result, a good hysteresis loop is obtained at room temperature as it is possible to maintain a stoichiometry during a film growth. [6, 7] On the other hand, Shelke *et al.* have reported that an epitaxial $BiFeO_3$ film on a non-miscut $SrTiO_3$ substrate with a good *P-E* hysteresis loop was successfully prepared under a high deposition rate by a kinetic growth parameter, using the pulsed laser deposition method. [8]

In this study, the magnetic-field-assisted pulsed laser deposition method as a new deposition method was employed in the preparation of epitaxial $BiFeO_3$ films. One feature of this deposition method is the high deposition due to the fact that the plume is confined to the substrate as opposed to the plume in a conventional pulsed laser deposition. The high deposition rate arising from the confined plume might induce the suppression of Bi volatilization or deficiency. Also, the deflected trajectory of the evaporated species might influence the effective deposition necessary for preparing the films. As a result, since the stoichiometric composition in epitaxial $BiFeO_3$ film is maintained, a good hysteresis loop can be obtained at room temperature, without a non-miscut substrate. In this chapter, epitaxial $BiFeO_3$ thin films have been prepared on non-miscut La-doped $SrTiO_3$ single crystal substrate by using the magnetic-field-assisted pulsed laser deposition method and the obtained epitaxial $BiFeO_3$ thin films have been characterized crystallographically and electrically.

Table 5.1. Deposition conditions for the preparation of epitaxial $BiFeO_3$ films.

Material	Temperature	O_2 pressure	Frequency	Magnetic field	Depo. time
$BiFeO_3$	700°C	0.02 Torr	5 Hz	0 T	30 min
$BiFeO_3$	700°C	0.04 Torr	5 Hz	0.1 T	25 min
$BiFeO_3$	700°C	0.1 Torr	5 Hz	0.4 T	10 min

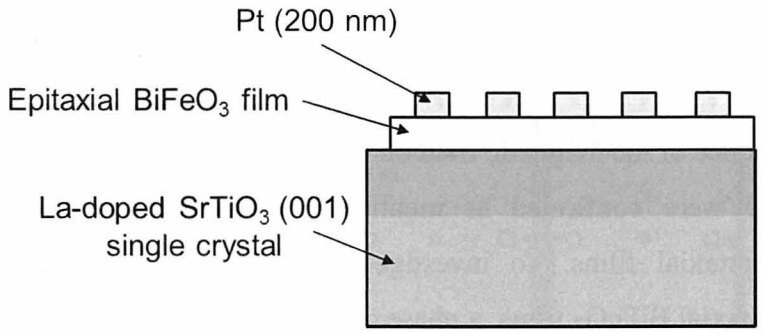

Figure 5.1. Sample structure for measuring ferroelectric properties of epitaxial $BiFeO_3$ films.

5.2 Preparation and Characterization of Epitaxial $BiFeO_3$ Films

La (3.75 wt%)-doped $SrTiO_3$ single crystal was used as the substrate in the preparation of epitaxial $BiFeO_3$ films instead of a $SrRuO_3$-deposited $SrTiO_3$ single-crystal substrate. The La-$SrTiO_3$ substrate is electrically conductive and can be used as a bottom electrode without using the conducting epitaxial $SrRuO_3$ layer. Epitaxial $BiFeO_3$ films on a La-$SrTiO_3$ substrate were prepared by using the magnetic-field-assisted pulsed laser deposition method. The magnetic field was 0, 0.1 and 0.4 T. The epitaxial films were deposited at a substrate temperature of 600 ~ 700 °C under oxygen pressure of 0.01 ~ 0.1 Torr by using an ArF excimer laser (λ = 193 nm) with a pulse energy of 130 mJ and a frequency of 5 Hz. The crystalline structure of the epitaxial films was observed by using X-ray diffraction (XRD) analysis (Rigaku, RINT 2000) and reciprocal space mappings (PANalytical X'Pert, MRD). The microstructure of epitaxial $BiFeO_3$ films was observed by using scanning electron microscopy (SEM), (Hitachi, S-4800). To investigate the electric and ferroelectric properties, circular Pt electrodes of 200 μm were formed on the epitaxial films by using RF sputtering through a shadow mask, as shown in Fig. 5.1. The current density versus electric field (*J-E*) characteristic and ferroelectric polarization versus electric field (*P-E*) were measured by using a semiconductor parameter analyzer (Agilent, 4155C) and a ferroelectric test system (Toyo Co., FCE-1).

5.3 Phase Diagram at Various Magnetic Fields

The influence of the magnetic field on the plume produced by a laser ablation and the dynamical plume were confirmed as mentioned in chapter 4. This should affect the preparation of epitaxial films. To investigate the effect of the magnetic field on the preparation of epitaxial $BiFeO_3$ films, a phase diagram was made. Figures 5.2(a)-(c) show the phase diagrams for a magnetic field of 0 T, 0.1 T, and 0.4 T, respectively. As seen in the figures, the preparation of epitaxial $BiFeO_3$ films under a magnetic field is more sensitive to oxygen pressure than that of polycrystalline $BiFeO_3$ films. These mappings show that the regions of pure $BiFeO_3$ phase were shifted to a high oxygen pressure with an increase in the magnetic field. Fe_2O_3 phases in the epitaxial $BiFeO_3$ films are predominant for the same oxygen pressure for magnetic fields of 0 T, 0.1 T, and 0.4 T, although the temperature is constant. The condition of the species included in the plume modified by a magnetic field might depend on the magnetic field, when increasing a magnetic field, the Fe_2O_3 phases become dominant, and the deposition rate become higher. Therefore, film preparation in a high oxygen pressure might be required.

Figure 5.3 shows the XRD patterns of the epitaxial $BiFeO_3$ films prepared under magnetic fields of 0 T, 0.1 T, and 0.4 T. Only the (00ℓ) diffraction peaks of the epitaxial $BiFeO_3$ films on a La-$SrTiO_3$ substrate prepared under magnetic fields of 0 T, 0.1 T, and 0.4 T were observed without secondary phases under optimized deposition conditions.

5.4 Reciprocal Space Mapping of Epitaxial $BiFeO_3$ Films

To better understand the crystal structure, the reciprocal space mapping (RSM) of epitaxial $BiFeO_3$ films prepared under magnetic fields of 0 T, 0.1 T, and 0.4 T are shown in Figs. 5.4(a)-(f). For a (003) reflection, all epitaxial $BiFeO_3$ films show splitting spots at the central position, and the $BiFeO_3$ planes was not completely parallel to the substrate as shown in Figs. 5.4(a)-(c). This is in agreement with reports in (001)-oriented epitaxial $BiFeO_3$ films

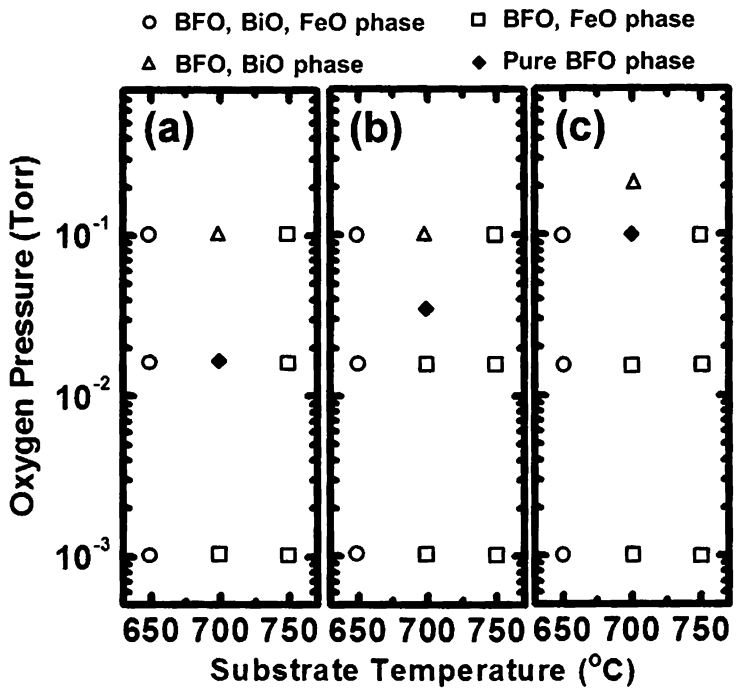

Figure 5.2. Phase diagrams at various magnetic fields of (a) 0 T, (b) 0.1 T, and (c) 0.4 T, respectively.

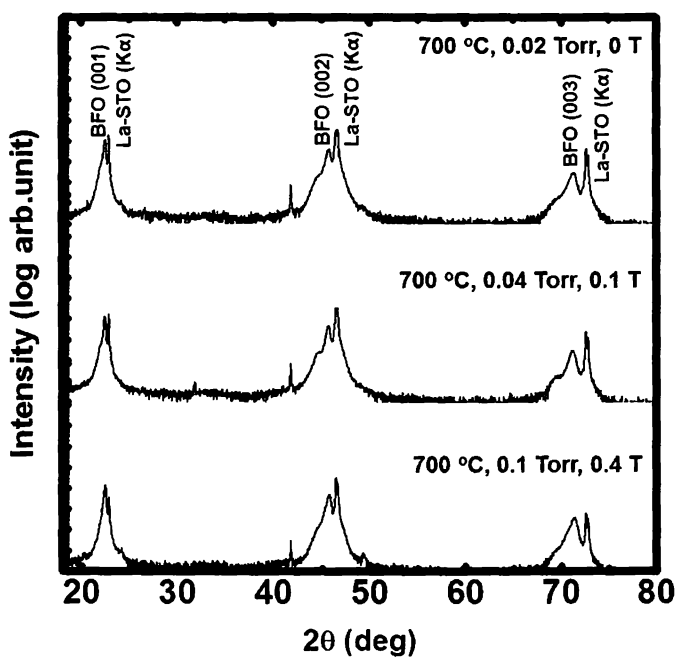

Figure 5.3. XRD patterns of the epitaxial $BiFeO_3$ films on La-$SrTiO_3$ (001) substrate prepared under magnetic fields of 0 T, 0.1 T, and 0.4 T, respectively.

with 720 nm and 1 μm-thick. [9, 10] The splitting spot of (003) is due to the fact that residual strain is relieved by the tilting. [10] The lattice constant of the out-of-plane is 0.396, 0.397, and 0.396 nm for epitaxial $BiFeO_3$ films prepared under magnetic fields of 0 T, 0.1 T, and 0.4 T, respectively. For a (103) reflection, all epitaxial $BiFeO_3$ films show two asymmetric spots, indicating the splitting of (-103) and (103) reflections as shown in Figs. 5.4(d)-(f). However, other reflections such as (013) and (0-13) for 4 variant domains could not be found because the peaks are very close existence and/or the resolution of the XRD optics is limited. The two asymmetric spots of the (013) and (-103) reflections derive from the natural crystal structure of $BiFeO_3$. The crystal structure of $BiFeO_3$ is rhombohedral. Unlike cubic and tetragonal structures, it has different *d*-spacing for the (013) and (-103) planes. [11] Namely, the (013) and (-103) planes of $BiFeO_3$ are tilted at different angles and shifted to both sides of the $SrTiO_3$ spot. The lattice constants of epitaxial $BiFeO_3$ films were calculated. The lattice constants of the in-plane are 0.396, 0.397, and 0.396 nm for the epitaxial $BiFeO_3$ films prepared under magnetic fields of 0 T, 0.1 T, and 0.4 T, respectively. As a result, these results are confirmed that the lattice constants of the in-plane are almost the same as those of the out-of-plane, and the crystal structure of the epitaxial $BiFeO_3$ films in this study is rhombohedral.

5.5 Microstructure of Epitaxial $BiFeO_3$ Films

Figures 5.5(a)-(c) show the cross-sectional microstructure of epitaxial $BiFeO_3$ films prepared under magnetic fields of 0 T, 0.1 T, and 0.4 T, respectively. The film thickness is around 300 ~ 400 nm. The deposition time for obtaining the above mentioned film thickness becomes much shorter by increasing the magnetic field. The cross-sectional images of epitaxial $BiFeO_3$ films prepared under magnetic fields of 0 T and 0.1 T are significantly similar, however the epitaxial $BiFeO_3$ film prepared under a magnetic field of 0.4 T with a high deposition rate showed a columnar structure.

In chapter 4, it was confirmed that a columnar structure was formed in the preparation of polycrystalline $BiFeO_3$ films by using the magnetic-field-assisted pulsed laser deposition. In the case of a polycrystalline film, it is assumed that the formation of the

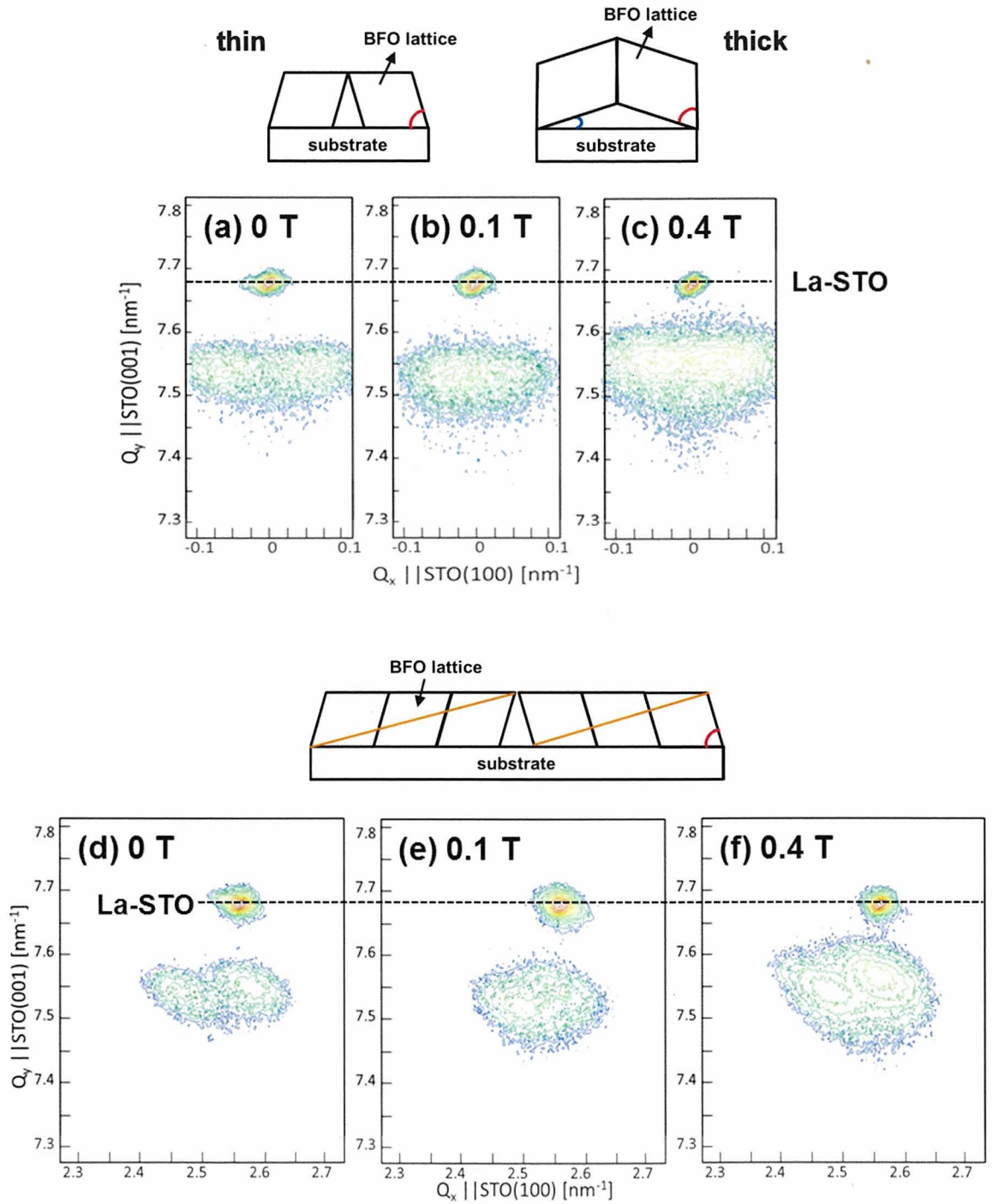

Figure 5.4. Reciprocal space mapping (RSM) for (a)-(c) (003) and (d)-(e) (103) reflections in epitaxial $BiFeO_3$ films prepared under magnetic fields of 0 T, 0.1 T, and 0.4 T, respectively.

columnar structure is due to the conical flux caused by the modified trajectory of the plume under a magnetic field. However, it is difficult to interpret the formation of columnar structures in the preparation of epitaxial films due to the fact that it has a different growth mechanism. In the epitaxial growth mechanism, there are three classical growth modes: The Frank-van der Merwe (FV), Volmer-Weber (VW) and Stranski-Krastonov (SK) modes which refer to step flow, columnar growth, and screw-island growth, respectively. [12, 13] For FV growth mode, a new layer is nucleated only after completely forming the layer below. By repeating this process, the layer spreads over the surface. As shown in Fig. 5.5, the growth mode of epitaxial $BiFeO_3$ films prepared under magnetic fields of 0, 0.1 T is likely to the FV growth mode indicating the step flow. On the other hand, epitaxial $BiFeO_3$ films prepared under a magnetic field of 0.4 T is likely to be in the VW growth mode indicating the columnar structure. The theoretical concept of textbook "epitaxy" is defined to be the formation of a single-crystal film in a layer-by-layer mode on a single-crystal substrate surface. [14] However, $BiFeO_3$ film grown on $SrTiO_3$ single crystal substrate has a lattice mismatch indicating a strained heteroepitaxial growth. When the film thickness is increased above critical thickness, the strain energy will be released through the formation of misfit edge dislocations and twinning, local phase transitions, surface morphology transformations, or a two- or three- dimensional growth transition. [14] Therefore, two possible causes are thought for the formation of columnar structures. First might be derived from lattice mismatch. Typically, the columnar structure for an epitaxial growth is often found in the case of a large mismatch between the film and the substrate. However, the lattice mismatch between the $BiFeO_3$ and the $SrTiO_3$ in this study is small (*compressive strain* ~ -1.4 %). So, this possibility is negligible. The second possibility might be the diffusivity caused by the interfacial energy. For a high deposition rate under a magnetic field of 0.4 T, the migration of adatoms to the lateral direction onto the substrate might be suppressed due to the considerably faster growth of the nucleation onto the substrate. Since the interfacial energy of the film is higher rather than the interfacial energy of the substrate, the tension of the film exceeds that of the substrate. This might result in a columnar structure indicating an island growth.

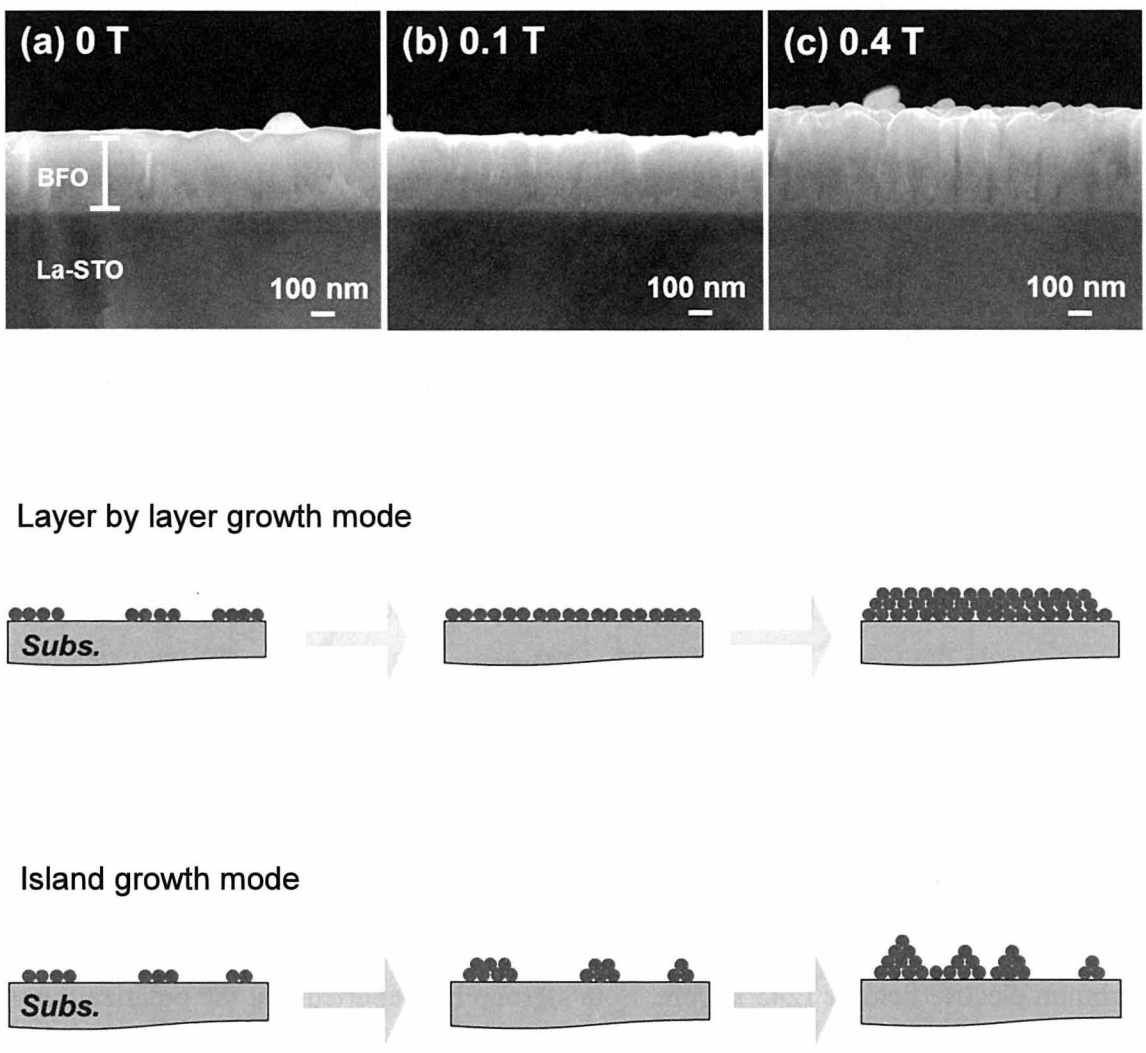

Figure 5.5. Cross-sectional images of epitaxial BFO films prepared under magnetic fields of (a) 0 T, (b) 0.1 T, and (c) 0.4 T, and schematic illustration of epitaxial growth mode.

5.6 Electric and Ferroelectric Properties of Epitaxial $BiFeO_3$ Films

Figure 5.6 shows the current density versus the electric field (*J-E*) characteristic of epitaxial $BiFeO_3$ films prepared under magnetic fields of 0 T, 0.1 T, and 0.4 T measured at room temperature (RT). The epitaxial $BiFeO_3$ film prepared under a magnetic field of 0.1 T shows the lowest current density, while that prepared under a magnetic field of 0.4 T shows the highest current density at an electric field of 285 kV/cm. These behaviors suggest that for a magnetic field of 0.1 T, the epitaxial film is free of Bi deficiency and/or defect, and Bi volatilization is suppressed due to the high deposition rate. However, despite the higher deposition rate, the high leakage current under the magnetic field of 0.4 T is due to the fact that leakage paths are formed among the columns.

To investigate ferroelectric properties of epitaxial $BiFeO_3$ films prepared under various magnetic fields, ferroelectric polarization versus electric field (*P-E*) hysteresis loops were measured by using a triangular waveform at 20 kHz and RT, as shown in Figs. 5.7(a)-(c). An epitaxial $BiFeO_3$ film prepared under a magnetic field of 0.1 T shows a good *P-E* hysteresis loop, unlike the leaky *P-E* hysteresis loops for the epitaxial $BiFeO_3$ films prepared under magnetic fields of 0 T and 0.4 T. The polarization (P_r) and coercive field (E_c) were 46 $\mu C/cm^2$ and 345 kV/cm at maximum electric field of 685 kV/cm, respectively. To investigate the ideal polarization value, excluding the leakage current for an epitaxial $BiFeO_3$ film prepared under a magnetic field of 0.1 T, the *P-E* hysteresis loop was measured at 20 kHz and 80 K. The scanning frequency dependence from 100 Hz to 20 kHz is shown in Fig. 5.7(d). A saturated *P-E* hysteresis loop was obtained at 80 K and 20 kHz and P_r was 47 $\mu C/cm^2$ at the maximum electric field of 1245 kV/cm. Eom's group has reported that the polarization value of an epitaxial $BiFeO_3$ film on a (001) oriented $SrTiO_3$ substrate, having a 4^o miscut toward [100] direction is better than that having a 0.2^o miscut toward [100] direction. [14] The origin of the enhanced polarization value is concluded as the consequence of the domain engineering, where 4-variant domains for a 0.2^o miscut $SrTiO_3$ substrate changes to 2-variant domains for a 4^o miscut $SrTiO_3$ substrate. The P_r value obtained in this study is similar to the P_r value for the 4-variant domains reported by Eom's group. This might be due to the lack of

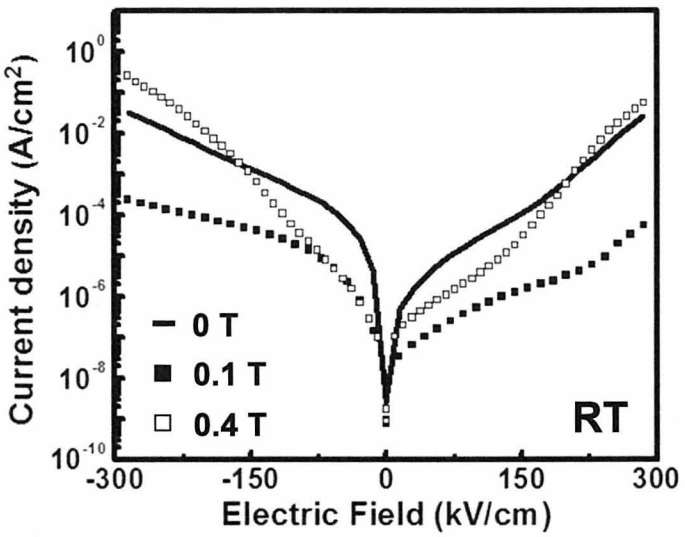

Figure 5.6. *J-E* characteristic of epitaxial $BiFeO_3$ films prepared under magnetic fields of 0 T, 0.1 T, and 0.4 T, measured at room temperature.

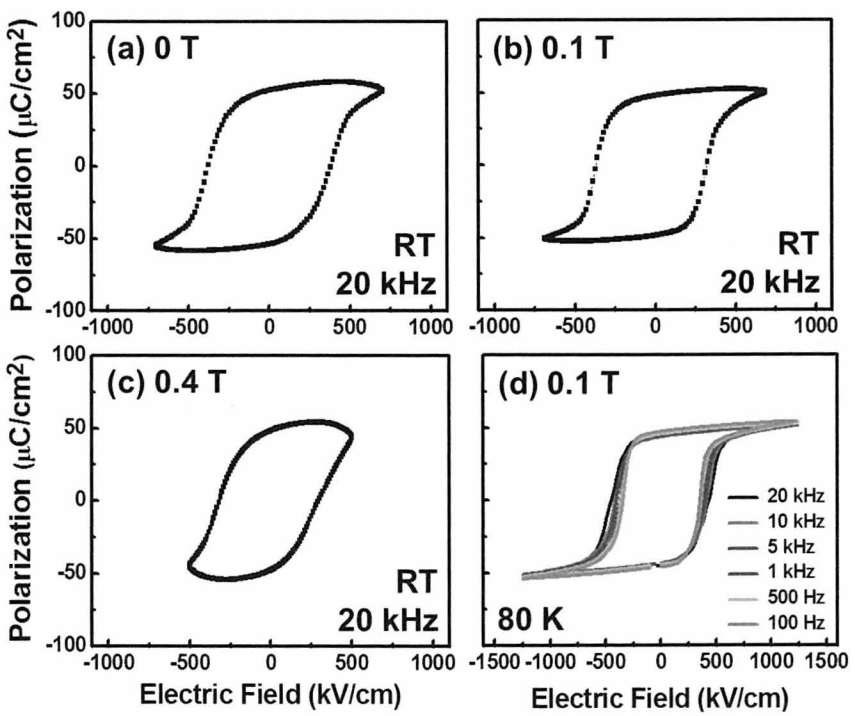

Figure 5.7. *P-E* hysteresis loops of epitaxial $BiFeO_3$ films prepared under magnetic fields of (a) 0 T, (b) 0.1 T, (c) 0.4 T, and (d) scanning frequency dependence of the *P-E* hysteresis loop in epitaxial $BiFeO_3$ films prepared under a magnetic field of 0.1 T, measured at 80 K.

the domain control in the case of non-miscut $SrTiO_3$ substrate. Figure 5.8 illustrates the consideration on the possible directions of the polarization axes by the domain engineering for epitaxial $BiFeO_3$ films grown on various miscut substrates. Also, the coercive field of epitaxial $BiFeO_3$ films on a La-$SrTiO_3$ substrate is much larger than that of epitaxial $BiFeO_3$ films on a $SrRuO_3/SrTiO_3$ substrate. This might be explained from the mechanism caused by the ferroelectric properties of an epitaxial $BiFeO_3$ thin film on a conductive Nb-doped $SrTiO_3$ substrate, as reported by V. Shelke *et al.* [8] They reported that the bonding strength between the film and the electrode and strong bonding between the $BiFeO_3$ and the TiO_2 top layer of the substrate might induce poor switchability in comparison with $BiFeO_3$ and the SrO terminated substrate for $SrRuO_3/BiFeO_3$. Consequently, the coercive field of the epitaxial $BiFeO_3$ films on a La-$SrTiO_3$ substrate might also be larger than epitaxial $BiFeO_3$ films on $SrRuO_3/SrTiO_3$ substrate due to the poor switchability induced by a stronger bond formed between the film and the electrode.

5.7 Summary

Epitaxial $BiFeO_3$ thin films on a La-$SrTiO_3$ substrate by using the magnetic-field-assisted pulsed laser deposition method have been obtained successfully. Although epitaxial $BiFeO_3$ films were prepared under different deposition rates by increasing a magnetic field, only the (00ℓ) diffraction peaks of the epitaxial $BiFeO_3$ films prepared under the optimum condition could be observed without secondary phases. By changing the magnetic field strength, the optimum condition of the pure $BiFeO_3$ phase was shifted to a high oxygen pressure and in magnetic field of 0.4 T, a modified microstructure was observed with highest deposition rate. An epitaxial $BiFeO_3$ film prepared under a magnetic field of 0.1 T shows the lowest current density, and a good ferroelectric polarization versus electric field (*P-E*) hysteresis loop was obtained at room temperature for an epitaxial $BiFeO_3$ film under a magnetic field of 0.1 T. Moreover, a saturated *P-E* hysteresis loop was obtained at 80 K. The polarization (P_r) value was 47 $\mu C/cm^2$ which is almost independent the scanning frequency.

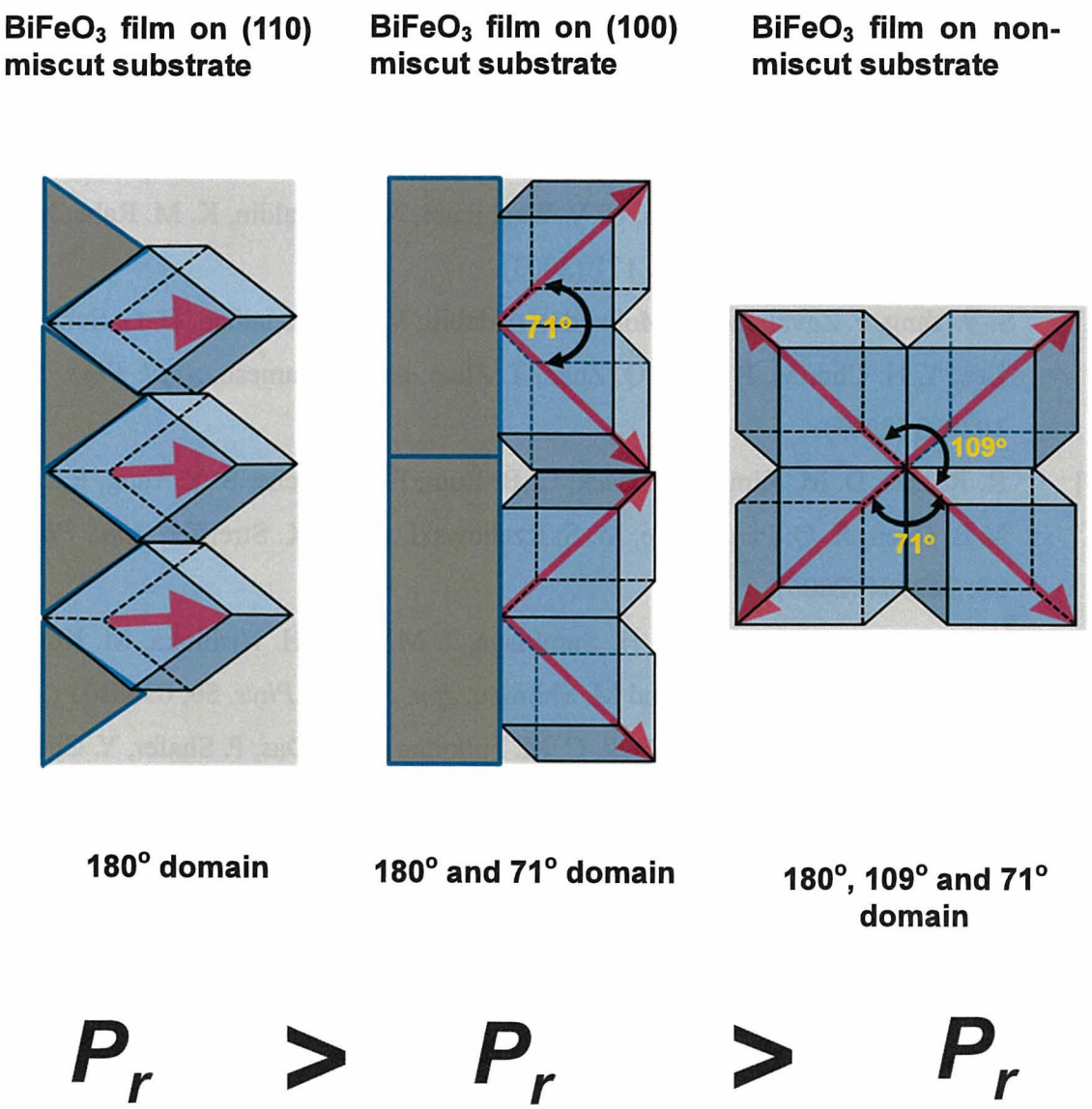

Figure 5.8. Possible directions of the polarization axes by domain engineering for epitaxial $BiFeO_3$ films grown on various miscut substrates.

References

[1] J. Wang, J. B. Neaton, H. Zheng, V. Nagarajan, S. B. Ogale, B. Liu, D. Viehland, V. Vaithyanathan, D. G. Schlom, U. V. Waghmare, N. A. Spaldin, K. M. Rabe, M. Witti, and R. Ramesh, *Science* **299**, 171 (2003).

[2] S. Y. Yang, F. Zavaliche, L. Mohaddes-Ardabili, V. Vaithyanathan, D. G. Schlom, Y. J. Lee, Y. H. Chu, M. P. Cruz, Q. Zhan, T. Zhao, and R. Ramesh, *Appl. Phys. Lett.* **87**, 102903 (2005).

[3] R. R. Das, D. M. Kim, S. H. Baek, C. B. Eom, F. Zavaliche, S. Y. Yang, R. Ramesh, Y. B. Chen, X. Q. Pan, X. Ke, M. S. Rzchowski, and S. K. Streiffer, *Appl. Phys. Lett.* **88**, 242904 (2006).

[4] S. Nakashima, H. Fujisawa, H. Suminaga, J. M. Park, H. Nishioka, M. Kobune, T. Kanashima, M. Okuyama, and M. Shimizu, *Jpn. J. Appl. Phys.* **50**, 09NB01 (2011).

[5] H. W. Jang, D. Ortiz, S. H. Baek, C. M. Folkman, R. R. Das, P. Shafer, Y. Chen, C. T. Nelson, X. Pan, R. Ramesh, and C. B. Eom, *Adv. Mater.* **21**, 817 (2009).

[6] S. D. Bu, M. K. Lee, C. B. Eom, W. Tian, X. Q. Pan, S. K. Streiffer, and J. J. Krajewski, *Appl. Phys. Lett.* **79**, 3482 (2001).

[7] F. Zavaliche, S. Y. Yang, T. Zhao, Y. H. Chu, M. P. Cruz, C. B. Eom, and R. Ramesh, *Phase Transition* **79**, 991 (2006).

[8] V. Shelke, V. N. Harshan, S. Kotru, and A. Gupta, *J. Appl. Phys.* **106**, 104114 (2009).

[9] H. Liu, P. Yang, K. Yao, and J. Wang, App. Phys. Lett. **96**, 012901 (2010).

[10] D. Kan and I. Takeuchi, J. Appl. Phys. **108**, 014104 (2010).

[11] X. Qi, M. Wei, Y. Lin, Q. Jia, D. Zhi, J. H. Dho, Mark. G. Blamire, and J. M. Driscoll, *Appl. Phys. Lett.* **86**, 071913 (2005).

[12] T. Fukuda and H. J. Schell, *"Crystal Growth Technology"* Wiely, New York, 2003.

[13] B. G. Yacobi, "Semiconductor Materials; *"An Introduction to Basic Principle"*. 2003.

[14] R. Eason, "Pulsed Laser Deposition of Thin Films: Application-Led Growth of Function Materials" p.537

[15] J.W Park, S. H. Baek, P. Wu, B. Winchester, C. T. Nelson, X. Q. Pan, L. Q. Chen, T. Tybell, and C. B. Eom, *Appl. Phys. Lett.* **97**, 212904 (2010).

CHAPTER 6

CONCLUSIONS

In this study, magnetic-field-assisted pulsed laser deposition was proposed as a new deposition method. Firstly, the behavior of the plume and film-growth under a magnetic field was observed in simulations. Based on the simulation results, the preparation of polycrystalline thick $BiFeO_3$ films was experimentally attempted by using the magnetic-field-assisted pulsed laser deposition. In addition, polycrystalline $BiFeO_3$ films by 90^o off-axis deposition. Moerover epitaxial $BiFeO_3$ films on a La-doped $SrTiO_3$ (001) substrate were prepared.

The main conclusions can be summarized as follows:

The plume dynamics and microstructure evolution under magnetic field

1) The behavior of the plume under a magnetic field was simulated. Under a magnetic field, the trajectory of the plume was modified. The movement was helical, which is different from the linear movement observed without a magnetic field. In addition, the plume under a magnetic field was confined to the substrate and the confinement of the plume predicted a high deposition rate.

2) The microstructure evolution was also modified, because of the modified trajectory of the plume under a magnetic field. The flux angle affected the microstructure

evolution. The conical flux arising from the modified trajectory of the plume under a magnetic field caused the columnar structure as opposite to the granular structure observed in the case of the normal flux.

Polycrystalline $BiFeO_3$ films on $Pt/TiO_2/SiO_2/Si$ substrate

1) To experimentally demonstrate the plume dynamics and microstructure evolution under a magnetic field obtained from the simulated results, polycrystalline $BiFeO_3$ films on $Pt/TiO_2/SiO_2/Si$ substrate were prepared by using the magnetic-field-assisted pulsed laser deposition. Before preparing the polycrystalline $BiFeO_3$ films, the shape of the plume was measured. The shape of the plume under a magnetic field is confined, as the simulations had shown and this results in a high deposition rate.

2) In a fixed deposition time, the film thickness was increased by increasing magnetic fields from 0 T to 0.3 T. The microstructure of the polycrystalline $BiFeO_3$ films prepared under a magnetic field reveals noticeable difference in comparison with that of a film prepared without a magnetic field. The dependence of ferroelectric properties on film thickness in the case of polycrystalline $BiFeO_3$ films prepared under a magnetic field could be investigated.

3) Under a magnetic field of 0.4 T for a deposition time of 30 min, 1.8 μm-crack-free $BiFeO_3$ columnar films were obtained. A *P-E* hysteresis loop was obtained at 20 kHz and room temperature (RT). The polarization (P_r) and coercive field (E_c) was 62 $\mu C/cm^2$ and 198 kV/cm, respectively. The piezoelectric coefficient (d_{33}) was ~ 50 pm/V.

4) To solve the problem of droplets in pulsed laser deposition, the preparation of polycrystalline $BiFeO_3$ films was attempted by 90° off-axis deposition. Droplet-free $BiFeO_3$ films were successfully obtained with the desired film thickness, due to the high deposition and the modified trajectory of the plume.

Epitaxial $BiFeO_3$ films on La-doped $SrTiO_3$ (001) substrate

1) Epitaxial $BiFeO_3$ films on a La-doped $SrTiO_3$ (001) substrate were prepared

successfully by controlling the magnetic field. Epitaxial $BiFeO_3$ films prepared under magnetic fields of 0 T, 0.1 T and 0.4 T show a rhomhedral structure including two spots, (103) and (-103), with stress-relaxation. An increase of magnetic field caused a high deposition rate, and in epitaxial $BiFeO_3$ films prepared by high deposition rate, the mechanism of epitaxial growth was changed from layer-by-layer mode to island mode. For a magnetic field of 0.1 T, the polarization (P_r) was 46 $\mu C/cm^2$ at 80 K, and a saturated *P-E* hysteresis loop was obtained.

Prospects

In this study, it was found that the magnetic-field-assisted pulsed laser deposition has many advantages. These advantages can be applied in the preparation of films over various materials, including the preparation of $BiFeO_3$ films.

1) Films of the desired thickness can be prepared in a short deposition time while the stoichiometric composition of the target is maintained. Generally, the film preparation of Bi-, Na- and K-based materials is difficult, due to the volatility of Bi, Na and K elements. Loss of those elements in films can result in degradation of film properties. To solve this problem, magnetic-field-assisted pulsed laser deposition proves to be useful.

2) Although preparation of thin film by using pulsed laser deposition is useful, it is difficult to prepare thicker films. A modified microstructure is required to solve the cracking arising from the mismatch of the thermal stress between the film and the substrate. Using magnetic-field-assisted pulsed laser deposition is possible to obtain dynamic structures, such as columnar structure because of the conical flux arising from the modified trajectory of the plume under a magnetic field

3) Droplets are a well-known problem of the pulsed laser deposition. Magnetic-field-assisted pulsed laser deposition can be used for the preparation of films under 90° off-axis deposition, which can solve the droplet and particulate problem.

Future work

In this study, the thickness limitation of polycrystalline $BiFeO_3$ films was solved by

using magnetic-field-assisted pulsed laser deposition. While polycrystalline $BiFeO_3$ films can be prepared over a broad range of thicknesses, the large polarization and piezoelectric coefficient might provide many opportunities for future applications. The thickness of less than 600 nm is required for the application of polycrystalline $BiFeO_3$ films in memory devices. A thickness more than 2 μm is required for the application in actuators and sensors. The crack-free thick $BiFeO_3$ films with columnar structure obtained in this study might provide the way for application in piezoelectric actuators or sensors. The polycrystalline thick $BiFeO_3$ films on silicon cantilever structure can be used for energy convertor from vibration to electricity, and is part of my future work. The results obtained from this investigation could provide useful information for the energy harvesting.

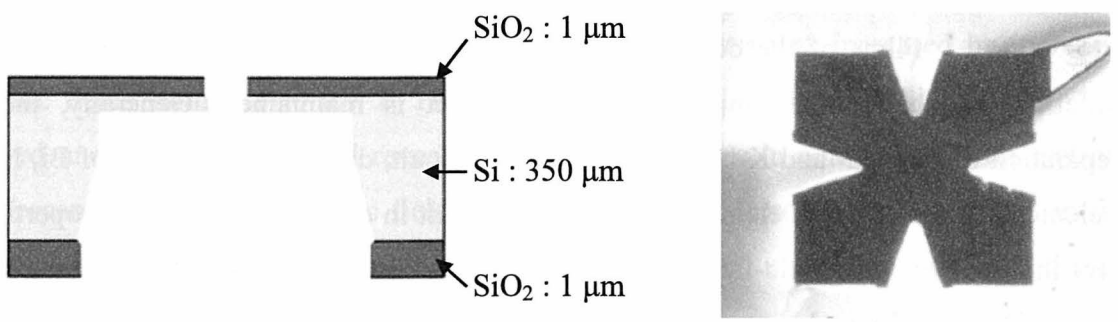

VITA

JungMin Park

Jung Min Park was born in Daegu, Republic of Korea on January 21, 1980. He received the undergraduate study at Yeungnam University, Gyeosang Gyeobuk, Republic of Korea, where he earned a Bachelor of Engineering degree in School of Material Science and Engineering in August 2005. He then received his master of engineering degree in School of Material Science and Engineering at Yeungnam University in August 2007. He entered Graduate School of Engineering Science, Osaka University, Japan in April 2008. He is a member of Japan Society of Applied Physics. Most of his works are related with electric and ferroelectric properties of ferroelectric films and preparation of oxide films by using pulsed laser deposition.

LIST OF PUBLICATIONS

Papers

1) **J. M. Park**, S. Nakashima, M. Sohgawa, T. Kanashima, M. Okuyama
"Repetition Rate Dependence of Ferroelectric Properties on Polycrystalline $BiFeO_3$ Films Prepared by Using Pulsed Laser Deposition Method"
Ferroelectrics, (2012) (in review).

2) **J. M. Park**, S. Nakashima, M. Sohgawa, T. Kanashima, M. Okuyama
"Preparation of Epitaxial $BiFeO_3$ Thin Films on La-$SrTiO_3$ Substrate by Using Magnetic-Field-Assisted Pulsed Laser Deposition Method"
Journal of the Korea Physical Society, (2012) (in review).

3) **J. M. Park**, S. Nakashima, M. Sohgawa, T. Kanashima, M. Okuyama
"Ferroelectric and Piezoelectric Properties of Polycrystalline $BiFeO_3$ thin films prepared by Pulsed Laser Deposition under Magnetic Field"
Japanese Journal of Applied Physics, ***51*** *09MD05 (2012).*

4) S. Nakashima, H. Fujisawa, H. Suminaga, **J. M. Park**, H. Nishioka, M. Kobune, T. Kanashima, M. Okuyama, M. Shimizu
"Preparation of $BiFeO_3$ Thin Films on $SrRuO_3/SrTiO_3(001)$ Substrate by Dual Ion Beam Sputtering Process"
Japanese Journal of Applied Physics, ***50*** *09NB01 (2011).*

5) **J. M. Park**, F. Gotoda, S. Nakashima, M. Sohgawa, T. Kanashima, M. Okuyama
"Preparation of $BiFe_{0.9}Co_{0.1}O_3$ Films by Pulsed Laser Deposition under Magnetic Field"
Japanese Journal of Applied Physics, ***50*** *09NB03 (2011).*

6) **J. M. Park**, F. Gotoda, S. Nakashima, T. Kanashima, M. Okuyama
"Preparation and Characterization of $BiFeO_3$ Thin Films on ITO Substrate by Pulsed Laser Deposition"
Journal of the Korea Physical Society, ***59*** *2537(2011).*

7) **J. M. Park**, F. Gotoda, S. Nakashima, T. Kanashima, M. Okuyama
"Multiferroic Properties of Polycrystalline Zn-substituted $BiFeO_3$ Thin Films Prepared by Pulsed Laser Deposition"
Current Applied Physics, ***11*** *S270 (2011).*

8) S. Nakashima, O. Sakata, **J. M. Park**, H. Fujisawa, T. Yamada, H. Funakubo, T. Kanashima, M. Okuyama, and M. Shimizu
"X-ray Diffraction Study of Electric-field-induced Strains in Polycrystalline $BiFeO_3$ Thin Films at Low Temperature Using Synchrotron Radiation"
Journal of the Korea Physical Society, ***59*** *2556 (2011).*

9) S. Nakashima, Y. Tsujita, S. Kayahara, H. Fujisawa, **J. M. Park,** T. Kanashima, M. Okuyama, and M. Shimizu
"Characterization of Epitaxial $BiFeO_3$ Thin Films Prepared by Ion Beam Sputtering"
Current Applied Physics, ***11*** *S244 (2011).*

10) **J. M. Park,** F. Gotoda, S. Nakashima, T. Kanashima, M. Okuyama
"Mutiferroic Properties of Polycrystalline Sr-substituted $BiFeO_3$ Thin Films Prepared by Pulsed Laser Deposition"
Ferroelectric, ***416*** *119 (2011).*

11) **J. M. Park**, T. Kanashima, M. Okuyama, S. Nakashima, K. M. Kim, J.-Y. Lee, H. Y. Lee
"Multiferroic Properties of Epitaxial $0.7BiFeO_3$-$0.3BaTiO_3$ Solid Solution Thin Films on La-Doped $SrTiO_3$ (001) Substrate"

*Journal of the Korea Physical Society, **58** 674 (2011).*

12) S. Nakashima, H. Fujisawa, S. Ichikawa, **J. M. Park**, T. Kanashima, M. Okuyama, and M. Shimizu
"Structural and ferroelectric properties of epitaxial $Bi_5Ti_3FeO_{15}$ and natural-superlattice-structured $Bi_4Ti_3O_{12}$-$Bi_5Ti_3FeO_{15}$ thin films"
*Journal of Applied Physics, **108** 074106 (2010).*

13) S. Nakashima, D. Ricinschi, **J. M. Park**, T. Kanashima, H. Fujisawa, M. Shimizu, M. Okuyama
"Ferroelectric and Structural Properties of Stress-Constrained and Stress-Relaxed Polycrystalline $BiFeO_3$ Thin Films"
*Journal of Applied Physics, **105** 061617 (2009).*

14) **J. M. Park**, S. Nakashima, F. Gotoda, T. Kanashima, M. Okuyama
"Pulsed Laser Deposition and Characterization of Sr and Zn co-substituted $BiFeO_3$ Thin Films"
*Japanese Journal of Applied Physics, **48** 09KB03 (2009).*

Unrelated to this thesis

15) **J. M. Park**, H. Y. Lee, J. J. Kim, E. T. Park, and Y. K. Chung
"Dielectric Properties of Ni-coated $BaTiO_3$-PMMA Composite"
*IEEE Transactions on Ultrasonics, Ferroelectrics, and Frequency Control, **55** 1038 (2008).*

16) **J. M. Park**, J.-Y. Lee, H. Y. Lee, and J. B. Park
"The Effect of Ion-Beam Treatment on TiO_2 Coatings Deposited on Polycarbonate Substrate"
*Transactions on Electrical and Electronic Materials, **11** 266 (2010).*

Presentations in International Conferences

1) **(INVITED TALK)** M. Okuyama, **J. M. Park**, T. Kanashima, D. Ricinschi
"Preparation of $BiFeO_3$ Films by Using Magnetic Field Assisted PLD and Their Characterization"
The 8th Asian Meeting on Ferroelectrics (AMF-8), December 9-14, 2012, Pattaya, Thailand, INV-26

2) **J. M. Park**, S. Nakashima, M. Sohgawa, T. Kanashima, M. Okuyama
"Preparation of Epitaxial $BiFeO_3$ Thin Films on La-$SrTiO_3$ Substrate by Magnetic Field Assisted Pulsed Laser Deposition"
The 9th Korea-Japan Conference on Ferroelectrics (2012/08/07-08/10), Ulsan Univ., Korea, P-11

3) **(INVITED TALK)** M. Okuyama, **J. M. Park**, S. Nakashima, T. Kanashima
"Preparation of $BiFeO_3$ Films by Using Magnetic Field Assisted PLD and Dual Ion Beam Sputtering Methods and Their Characterization"
International Symposium on Integrated Functionalities 2012, June 18-21, 2012, Hong Kong, China, I305.

4) **J. M. Park**, S. Nakashima, M. Sohgawa, T. Kanashima, M. Okuyama
"Ferroelectric Properties and Microstructure Evolution of Polycrystalline $BiFeO_3$ Films Prepared by Pulsed Laser Deposition under Magnetic Field"
International Conference on Advanced Electromaterials 2011, November 7-10, 2011, Jeju, Korea, FM1144.

5) **J. M. Park**, S. Nakashima, T. Kanashima, M. Okuyama
"Ferroelectric and Piezoelectric Properties of Polycrystalline $BiFeO_3$ Thin Films Prepared Pulsed Laser Deposition under Magnetic Field"
The 20th IEEE International Symposium on Application of Ferroelectrics
International Symposium on Piezoresponse Force Microscopy & Nanoscale Phenomena in Polar Materials, July 24-27, 2011, Vancouver, Canada, p94, AR524.

6) **J. M. Park**, S. Nakashima, T. Kanashima, M. Okuyama
"Ferroelectric and Piezoelectric Properties of Polycrystalline $BiFeO_3$ Thin Films Prepared Pulsed Laser Deposition under Magnetic Field"
The 20th IEEE International Symposium on Application of Ferroelectrics
International Symposium on Piezoresponse Force Microscopy & Nanoscale Phenomena in Polar Materials, July 24-27, 2011, Vancouver, Canada, p94, AR524

7) **J. M. Park**, F. Gotoda, S. Nakashima, T. Kanashima, M. Okuyama
"Preparation of $BiFeO_3$ Thin Films by Pulsed Laser Deposition under Magnetic Field"
The Materials Research Society 2011 Spring Meeting (San Francisco, U.S.A, WW11.37).

8) **J. M. Park**, F. Gotoda, S. Nakashima, T. Kanashima, M. Okuyama
"Preparation of Polycrystalline $BiFeO_3$ Thin Films by Pulsed Laser Deposition under Magnetic Field"
The 20th Symposium on Dielectric and Advanced Matter Physics & The 12th Workshop on High Dielectric and Ferroelectric Device and Materials in Muju, Korea, P-93.

9) **J. M. Park**, F. Gotoda, S. Nakashima, T. Kanashima, M. Okuyama
"Preparation and Characterization of $BiFeO_3$ Thin Film on ITO Substrate by Pulsed Laser Deposition"
The 8th Japan-Korea Conference on Ferroelectrics (2010/08/03-08/06) in Himeji, Japan, P2-082.

10) **J. M. Park**, F. Gotoda, S. Nakashima, T. Kanashima, M. Okuyama
"Current Suppression and Magnetic Enhancement by Zn-substitution in $BiFeO_3$ thin film Prepared by Pulsed Laser Deposition"
7th Asian Meeting on Ferroelectricity and 7th Asian Meeting on ElectroCeramics (2010/06/28-07/01) in Jeju, Korea, 1-b-P20.

11) **J. M. Park**, F. Gotoda, S. Nakashima, T. Kanashima, M. Okuyama
"Characterization of Polycrystalline Sr-Substituted $BiFeO_3$ Thin Films Prepared by Pulsed Laser Deposition"
The 10th Russia/CIS/Baltic/Japan Symposium on Ferroelectricity (2010/06/20) in Yokohama, Japan, P2g-09

12) **J. M. Park**, K. M. Kim, S. Nakashima, T. Kanashima, M. Okuyama, J.-Y. Lee, H. Y. Lee
"Multiferroic Properties of Epitaxial $0.7BiFeO_3$-$0.3BaTiO_3$ Solid Solution Thin Films on La Doped $SrTiO_3$ (001) substrate"
The 19th Symposium on Dielectric and Advanced Matter Physics & The 11th Workshop on High Dielectric and Ferroelectric Device and Materials (2010/02/07) in Muju, Korea, P-54

Presentations in Domestic Conferences

1) 金島 岳、朴 正敏、 奥山 雅則
"磁場印加PLDで作製した$BiFeO_3$薄膜の柱状構造成長過程の検討"
The 60th Spring Meeting, 2012; The Japan Society of Applied Physics and Related Societies (2013/03/27~30, 神奈川工科大学)

2) 朴 正敏、中嶋 誠二、寒川 雅之、金島 岳、奥山 雅則
"磁場中90° off-axis PLD法による多結晶$BiFeO_3$薄膜の作製と評価"
The 73th Autumn Meeting, 2012; The Japan Society of Applied Physics and Related Societies (2012/9/11~14, 愛媛大学、松山大学) 13p-C10-6.

3) 朴 正敏、中嶋 誠二、寒川 雅之、金島 岳、奥山 雅則
"磁場中PLD法によるエピタキシャル$BiFeO_3$薄膜の作製と評価"
The 59th Spring Meeting, 2012; The Japan Society of Applied Physics and Related Societies (2012/03/15~18, 早稲田大学) 18p-F5-5.

4) 朴 正敏、中嶋 誠二、寒川 雅之、金島 岳、奥山 雅則

“磁場中PLD法による$BiFeO_3$薄膜の微細構造と強誘電特性”

The 72th Autumn Meeting, 2011; The Japan Society of Applied Physics and Related Societies (2011/08/29~09/02, 山形大学 小白川キャンパス) 31a-C-1.

5) 朴 正敏、後藤田 文也、中嶋 誠二、金島 岳、奥山 雅則

“磁場中PLD法のよる$BiFeO_3$薄膜の作製”

The 58th Spring Meeting, 2011; The Japan Society of Applied Physics and Related Societies (2011/03/24~27, 神奈川工科大学) 24a-BE-5.

6) 朴 正敏、後藤田 文也、 中嶋 誠二、金島 岳、奥山 雅則

“PLD法によるITO基板上に$BiFeO_3$薄膜の作製と評価”

The 57th Spring Meeting, 2010; The Japan Society of Applied Physics and Related Societies (2010/03/17~20, 東海大学湘南キャンパス) 17p-TR-4.

7) 朴 正敏、中嶋 誠二、後藤田 文也、金島 岳、奥山 雅則

“PLD preparation and characterization of Sr and Zn co-substituted $BiFeO_3$ thin films”

第26回強誘電体応用会議（2009年5/27～30日 コープイン京都）29-L-1, pp. 143.

8) 朴 正敏、中嶋 誠二、後藤田 文也、金島 岳、奥山 雅則

“Sr, Zn共置換した$BiFeO_3$薄膜の磁気特性”

The 56th Spring Meeting, 2009; The Japan Society of Applied Physics and Related Societies. (2009/03/30~04/02, 筑波大学) 30p-ZH-4.

9) 朴 正敏、中嶋 誠二、後藤田 文也、金島 岳、奥山 雅則

“Zn - doped $BiFeO_3$薄膜のPLDによる製作と評価”

The 70th Autumn Meeting, 2009; The Japan Society of Applied Physics and Related Societies.(2009/09/08~11, 富山大学) 10p-L-14.

10) 朴 正敏, 中嶋 誠二, 金島 岳, 奥山 雅則

"Sr, Zn置換したBiFeO$_3$薄膜のPLDによる作製と評価"

The 69th Autumn Meeting, 2008; The Japan Society of Applied Physics and Related Societies.(2008/09/02~05, 中部大学) 2p-K-6.

Awards

- The presentation entitled "*Preparation of Polycrystalline $BiFeO_3$ Thin Films by Pulsed Laser Deposition under Magnetic Field*" was awarded for '**Best Poster Presentation Award**' at the 20th Symposium on Dielectric and Advanced Matter Physics & The 12th Workshop on High Dielectric and Ferroelectric Device and Material in Muju, Korea (2011).

- The presentation entitled "*Ferroelectric Properties and Microstructure Evolution of Polycrystalline $BiFeO_3$ Films Prepared by Pulsed Laser Deposition under Magnetic Field*" was awarded for '**Outstanding Paper**' at the International Conference on Advanced Electromaterials (ICAE 2011), November 7-101, 2011, Jeju, Korea.

- The presentation entitled "*Preparation of Epitaxial $BiFeO_3$ Thin Films on La-$SrTiO_3$ Substrate by Magnetic-Field-Assisted Pulsed Laser Deposition*" was awarded for '**Poster Presentation Award**' at the 9th Korea-Japan Conference on Ferroelectrics (2012/08/07-08/10), Ulsan Univ., Korea.